Fatigue Analysis of Overhead Sign and Signal Structures

Physical Research Report No. 115

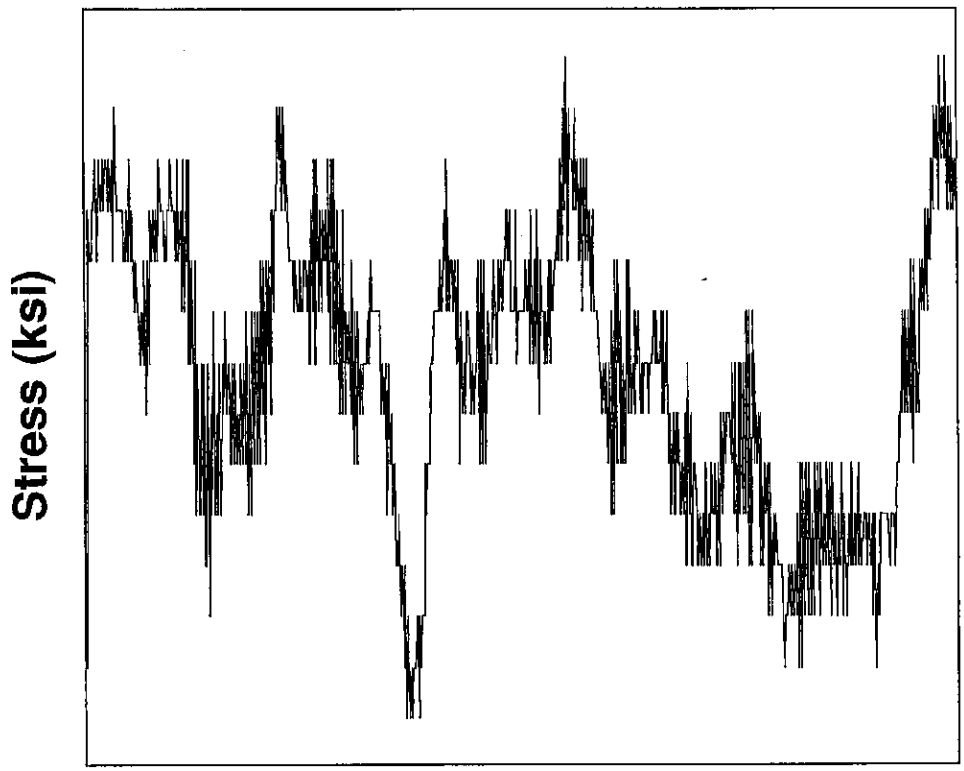

Illinois Department of Transportation
Bureau of Materials and Physical Research

TECHNICAL REPORT STANDARD TITLE PAGE

1. Report No.	2. Government Accession No.	3. Recipient's Catalog No.
FHWA/IL/PR-115		

4. Title and Subtitle	5. Report Date
FATIGUE ANALYSIS OF OVERHEAD SIGN AND SIGNAL STRUCTURES	May 1994
	6. Performing Organization Code

7. Author(s)	8. Performing Organization Report No.
Jeffrey M. South, P.E.	PRR-115

9. Performing Organization Name and Address	10. Work Unit No.
Illinois Department of Transportation Bureau of Materials and Physical Research 126 East Ash Street Springfield, Illinois 62704-4706	11. Contract or Grant No. IHR-319
	13. Type of Report and Period Covered Interim Report: July 1990 through May 1994
12. Sponsoring Agency Name and Address Illinois Department of Transportation Bureau of Materials and Physical Research 126 East Ash Street Springfield, Illinois 62704-4706	14. Sponsoring Agency Code

15. Supplementary Notes

Study conducted in cooperation with the U.S. Department of Transportation, Federal Highway Administration.

16. Abstract This report documents methods of fatigue analysis for overhead sign and signal structures. The main purpose of this report is to combine pertinent wind loading and vibration theory, fatigue damage theory, and experimental data into a useable fatigue analysis method for overhead sign and signal structures. Vibrations and forces induced by vortex shedding were studied analytically and measured experimentally. Analytical models were extracted from the literature. Drag coefficients, generally assumed to be constants or simple functions of Reynolds number, actually depend on the amplitude of vortex shedding vibration. The amplification of drag coefficients can have a significant effect on resulting forces. Fatigue and the concept of fatigue damage quantification were discussed. Fatigue was described as a failure mode which results from cyclic application of stresses which may be much lower than the yield stress. Fatigue damage was quantified using the Palmgren-Miner linear damage equation. Available stress cycles for each applied stress range are calculated by expressing published S-N fatigue data for welds or anchor bolts as N-S equations, where number of available cycles (N) is the dependent variable, instead of stress range. The use and limitations of fracture mechanics methods were discussed. Stress concentrations were discussed as a vital parameter in fatigue analysis. Methods for estimating K_t for fillet welds and anchor bolt threads were extracted from the literature. Experimental data were collected for a representative traffic signal structure. This data included stress range and frequency response for ambient wind loadings, dead load stresses, strain as a function of vertical tip deflection, vibration frequency due to ambient winds, and strain response due to controlled-speed wind loads. The instrumented details were tube to base plate circumferential fillet welds and anchor bolts. Wind speed data were collected at a traffic signal site in Springfield, Illinois for seventeen months. Factor of safety equations for use with welded details were discussed. Sample fatigue life calculations using both strain gage-derived and analytically estimated stress range-frequency histograms were performed as examples to the reader. Calculations using static conditions were also performed. The results differed significantly from the other solutions.

17. Key Words	18. Distribution Statement
Fatigue, wind forces, safety factors, strain gages, histogram-linear damage rule.	No restrictions. This document is available to the public through the National Technical Information Service, Springfield, Virginia 22161.

19. Security Classif. (of this report)	20. Security Classif. (of this page)	21. No. of Pages	22. Price
Unclassified	Unclassified	118	

Form DOT F 1700.7 (8-69)

FATIGUE ANALYSIS OF OVERHEAD SIGN AND SIGNAL STRUCTURES

Jeffrey M. South, P. E.
Engineer of Technical Services

Physical Research Report Number 115
Illinois Department of Transportation
Bureau of Materials and Physical Research

May 1994

FOREWORD

This report should be of interest to engineers involved in structural design, planning, maintenance and inspection; consultants, and other technical personnel concerned with the fatigue life of structures.

NOTICE

The contents of this report reflect the views of the author who is responsible for the facts and the accuracy of the data presented herein. The contents do not necessarily reflect the official views or policy of the Federal Highway Administration or the Illinois Department of Transportation. This report does not constitute a standard, specification, or regulation.

Neither the United States Government nor the State of Illinois endorses products or manufacturers. Trade or manufacturers' names appear herein solely because they are considered essential to the object of this report.

ACKNOWLEDGMENTS

The author gratefully acknowledges the kind assistance and support of:

Mr. Christopher Hahin, Engineer of Bridge Investigations; Ms. Mary Milcic, Research Engineer; Mssrs. Dave Bernardin, Tom Courtney, Russ Gotschall, Harry Smith, Ken Wyatt, and Brian Zimmerman. The typing efforts of Ms. Bev Buhrmester are gratefully acknowledged.

TABLE OF CONTENTS

LIST OF FIGURES

LIST OF FIGURES (CONTINUED)

LIST OF FIGURES (CONTINUED)

LIST OF FIGURES (CONTINUED)

LIST OF TABLES

1. INTRODUCTION

The unexpected failure of an overhead sign or signal structure could result in serious injuries, property damage, and/or increased traffic congestion and accidents.

Overhead structures intended to support signs or traffic signals are designed to resist dead loads, live loads, ice loads, and wind loads.[1] Dead loads include the weight of the member, signs, traffic signals, or other attachments. Live loads are defined as walkways and service platforms. Ice loads are used in areas of the country where winter ice buildup is expected. The wind load is idealized as a maximum pressure based on mean recurrence intervals of a maximum wind speed for the location of service, member shape, and height above ground of the member being loaded. All loads are considered to be static for design purposes.

However, overhead sign and signal structures are subjected to varying wind loads every day. In addition, vortex shedding induces cyclic loads. The variability of these forces from day to day and even from instant to instant implies that these structures are sustaining some amount of cumulative fatigue damage. The cyclic nature of the actual stresses experienced, and therefore, the potential for fatigue damage and failure is not accounted for in the design process. A need exists for rational methods to evaluate the expected fatigue life of overhead sign and signal structures and for methods to assess the fatigue susceptibility of new structures while in the design phase.

The number of overhead sign and signal structures in service is surprising. These structures occur at nearly every modern urban intersection with three or more lanes. Large overhead sign structures are found both before and at nearly every interchange on the interstate system

and on other divided highways. The large number of these structures and the cost to build or replace them requires some study of their fatigue behavior.

There are many types of overhead structures in service. Traffic signal structures in particular show wide variety. Popular cantilevered signal structures include straight and arced tapered single arm and plane frame mastarms. Tubular cross-sections in use include circular, hexdecagonal (16-sided), dodecagonal (12-sided), octagonal, square, and elliptical. Materials used include steel and aluminum. Sign structures include cantilevered space frames with rectangular gross cross-sections and simply supported space frames with both rectangular and triangular cross-sections. The most common components used in overhead sign structure applications are circular tubes, although plane frame structures with rectangular tube or I-shaped cross-sections are becoming popular for new construction.

Fatigue is a failure mode that involves repeated loading at stress levels which may be only a small fraction of the tensile strength of a particular material. Because fatigue failures result from repeated loadings, it is characterized as a progressive failure mode that proceeds by the initiation and propagation of cracks to an unstable size. Each stress cycle causes a certain amount of damage. Depending on applied stress levels and material properties, component fatigue lives can range from a few hundred to more than 10^8 cycles to failure. The most common sites of fatigue failures in components are at areas of stress concentrations. Welds, notches, holes, and material impurities such as

slag inclusions are examples of stress concentrations. Not surprisingly, common fatigue cracking areas in overhead sign and signal structures are at welds and anchor bolts (threads are sharp notches).

The fatigue life of a component may be thought of in two phases. Crack initiation life is that portion of fatigue life which occurs before a crack forms. Crack propagation life is the portion of fatigue life which occurs between crack formation and unstable crack growth. Typically, for the steels used in sign and signal structures, the initiation life for a weld detail is far longer than the propagation life. This implies that once a crack appears, especially in a nonredundant structure, the fatigue life of that detail is effectively used up, and the component could rupture relatively quickly.

The purposes of this report are to combine pertinent existing wind loading and vibration theory, fatigue damage theory, and experimental data into a usable fatigue analysis method for overhead sign and signal structures and to outline factor of safety equations for estimation of weld detail fatigue susceptibility.

2. WIND-INDUCED FORCES AND VIBRATIONS

This chapter discusses theoretical aspects of vortex-induced vibration. The purpose of this chapter is to illustrate the complexity of actual wind loading and to outline methods for estimating the forces caused by winds. It is not intended to cover the subject in depth. Much of the discussion in this chapter is condensed from the work of Blevins.[2]

The study of wind-induced forces and vibrations begins with a look at aerodynamics. In aerodynamics, fluid flow is characterized by the Mach number. The Mach number is a nondimensional number which is defined as the ratio of free stream fluid velocity to the local speed of sound. The local speed of sound in air is a square-root function of the local air temperature. The magnitude of the Mach number is a measure of the tendency of the fluid to compress as it approaches an object. For wind speeds and air temperatures generally encountered by overhead sign and signal structures in the United States the Mach number is less than 0.3, and compressibility of the fluid does not influence vibrations. This implies that the density of air is relatively constant. A Mach number of 0.3 corresponds to a wind speed of 202 mph (325 km/hr) at an air temperature of 70 degrees Fahrenheit (21.1 degrees Celsius).

Observation of long traffic signal mastarms during windy periods reveals that the general motion of the tip of the mastarm is fairly complex. Vortex shedding causes primarily vertical oscillations, while drag forces move the tip horizontally. The combined motion describes an approximate figure eight shape. The long axis of the figure eight rotates under influence of the direction of the wind. The size of the figure eight depends on wind speed.

Vortex Shedding

Vortex shedding is a phenomenon which occurs in subsonic flow past structures. Vortices are shed from one side of a member and then the other. As this continues, oscillating surface pressures are imposed on the structure. The oscillating pressures cause elastic structures to vibrate. A description of the process of vortex shedding is given by Blevins.[3]

> "As a fluid particle flows toward the leading edge of a cylinder, the pressure in the fluid particle rises from the free stream pressure to the stagnation pressure. The high fluid pressure near the leading edge impels flow about the cylinder as boundary layers develop about both sides. However, the high pressure is not sufficient to force the flow about the back of the cylinder at high Reynolds numbers. Near the widest section of the cylinder, the boundary layers separate from each side of the cylinder surface and form two shear layers that trail aft in the flow and bound the wake. Since the innermost portion of the shear layers, which is in contact with the cylinder, moves much more slowly than the outermost portion, the shear layers roll into the near wake, where they fold on each other and coalesce into discrete swirling vortices. A regular pattern of vortices, called a vortex street, trails aft in the wake. The vortices interact with the cylinder and they are the source of the effects called vortex-induced vibration."

A representation of the vortex shedding process is shown in Figure 1. Vortex shedding from smooth, circular cylinders with steady subsonic flow is a function of the Reynolds number. The Reynolds number is given by:

$$Re = \frac{UD}{\nu} \qquad (1)$$

where U = free stream velocity,
D = cylinder diameter,
ν = kinematic viscosity of the fluid,
= 1.564×10^{-4} ft^2/sec (1.681×10^{-3}m^2/sec) for air.

The Reynolds number is the ratio of the inertia force and the friction force on a body. The Reynolds number is a parameter used to indicate dynamic similarity. Two flows are dynamically similar when the Reynolds number is equal for both flows.

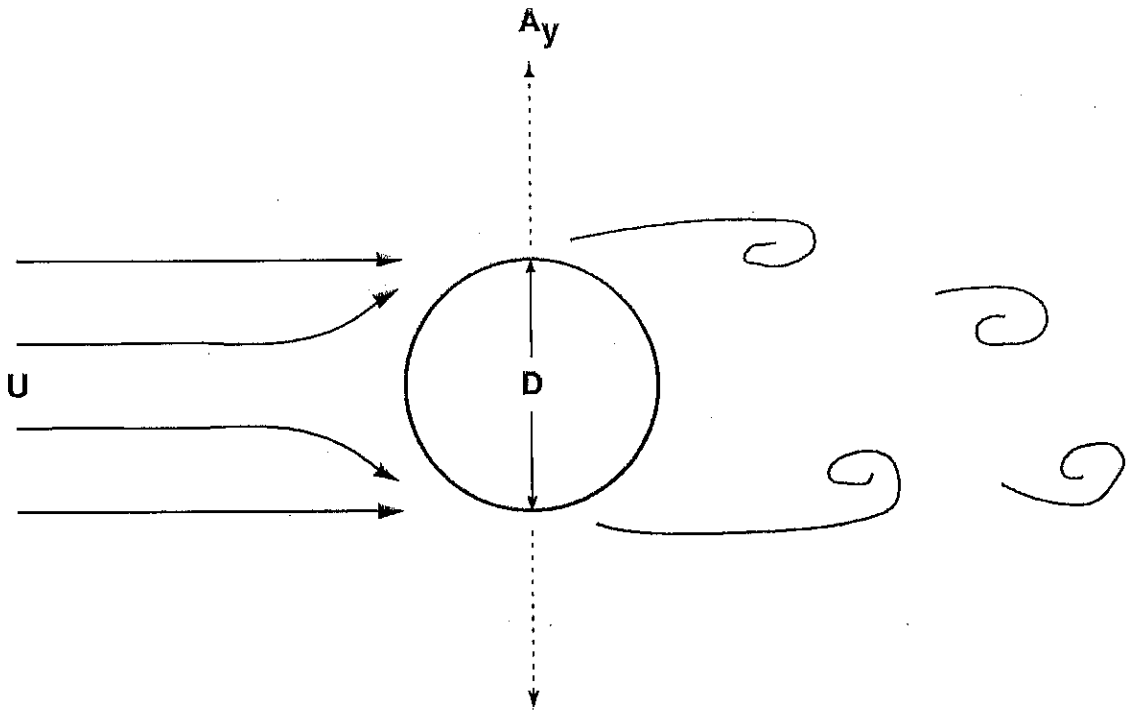

Figure 1. Representation of the vortex sheeding process. U is the windspeed. D is cylinder diameter. A_y is transverse deflection due to vortex shedding.

The primary Reynolds number regimes of vortex shedding from smooth, circular cylinders are given in Table I.

The range of Reynolds numbers between 300 and 1.5×10^5 is called subcritical. In the subcritical range vortex shedding is strong and periodic. The transitional range is between Reynolds numbers of 1.5×10^5 and 3.5×10^6. In the transitional range, the boundary layer becomes turbulent, separation is delayed, and the cylinder drag coefficient drops to 0.3. Also, laminar separation bubbles and three-dimensional affects disrupt the regular shedding process and broadens the shedding frequency spectrum for smooth circular cylinders. The supercritical range (Reynolds number greater than 3.5×10^6) is characterized by re-established regular vortex shedding with a turbulent cylinder boundary layer.[4]

TABLE I

Reynolds Number Regimes For Vortex Shedding From Smooth Circular Cylinders

Reynolds Number Range	Description of Regime[5]
0–5	Flow is unseparated.
5–40	Fixed pair of Föppl vortices in wake.
40–90 & 90–150	Two regimes in which vortex street is laminar.
150–300	Transition range to turbulence in vortex.
$300–3 \times 10^5$	Vortex street is fully turbulent.
$3 \times 10^5–3.5 \times 10^6$	Laminar boundary layer has undergone turbulent transition and wake is narrower and disorganized.
greater than 3.5×10^6	Turbulent vortex street is re-established.

The Strouhal number is the dimensionless proportionality constant which relates the predominant vortex shedding frequency, the free stream velocity, and the cylinder width. It is given by:

$$S = f_S D/U \qquad (2)$$

where f_S = vortex shedding frequency, Hertz (cycles/second),
U = free stream velocity,
D = cylinder diameter.

Vortex-induced vibration of cylinders generally occurs at $S \sim 0.2$ in the transitional Reynolds number regime. An interesting experimental result is that lift oscillations occur at the vortex shedding frequency, while drag oscillations occur at twice the vortex shedding frequency due to the geometry of the vortex street.

Previous discussions were centered on circular cross sections. However, noncircular sections also shed vortices. The vortex street wake is formed by the interaction of two free shear layers that trail behind a structure. Roshko,[6,7] Griffin,[8] and Sarpkaya[9] suggest that it is possible to define a "universal" Strouhal number for any section based on the separation distance between the free shear layers. Therefore, if the characteristic distance D in the Strouhal equation (2) is defined as the distance between separation points, then the Strouhal number is approximately 0.2 over wide ranges of Reynolds number regardless of the section geometry.[10]

Vortex shedding causes transverse (perpendicular to free stream flow) vibration of the affected body. Increased amplitude of transverse cylinder vibration (A_y) can increase the ability of the vibration to lock-in, or synchronize, the shedding frequency. The range of frequencies over which cylinder vibration controls the shedding frequency is known as

the lock-in band. Large amplitude cylinder vibration (A_y/D from 0.3 to 0.5) can shift the vortex shedding frequency by as much as $\pm$ 40% from the stationary cylinder shedding frequency.[11]

The steady drag force per unit length on a cylinder is given by:

$$F_D = (1/2)\rho U^2 D C_D \qquad (3)$$

where ρ = fluid density,
= 0.002378 slug/ft^3 (9.85 x 10^{-4} kg/m^3) for air,
U = free stream velocity,
D = cylinder diameter,
C_D = drag coefficient.

The amplitude of cylinder vibration affects the drag coefficient. Increasing amplitude (A_y) causes the drag coefficient to increase, sometimes substantially. One expression for relating the increase in drag coefficient to vibration amplitude is:

$$C'_D = C_D\,[1 + 2.1(A_y/D)] \qquad (4)$$

where C'_D = Amplitude-influenced drag coefficient,
C_D = steady flow drag coefficient,
A_y = cylinder vibration amplitude,
D = cylinder diameter.

Other, more involved equations are also given by Blevins, but the expressions are within 15% of each other at resonance, and (4) is the easiest to use directly. The synchronization effect also occurs with square, triangular, D sections, and other sections that have sharp separation points. Blevins states that probably all noncircular sections, in addition to circular sections, that shed vortices will synchronize and increase drag with resonant transverse vibration.[12] Large amplitude vibrations can result from synchronization of the vortex shedding frequency with the structure frequency. In other words, when the flow

velocity reaches a value such that the shedding frequency approaches the natural frequency (or a harmonic or subharmonic) of a structure, the structure will resonate. This occurs when:

$$f_n \sim f_s = SU/D, \quad \text{or} \quad U/f_n D \sim U/f_s D = 1/S \qquad (5)$$

where f_s = vortex shedding frequency,
f_n = natural frequency,
U = free stream velocity,
D = diameter,
S = Strouhal number.

Therefore, a combination of $U/fD \sim 5$ can cause synchronization in a structure for an assumed fixed Strouhal number of 0.2.[13]

Analytical Models for Vortex Shedding Response

The purpose of this section is to overview and discuss two analytical models for vortex induced vibration of circular cylindrical structures. The first case is a simple linear harmonic model; the second case is a nonlinear, self-excited oscillator model.

Since vortex shedding is observed to be an approximately sinusoidal process (recall the figure eight discussion), a simple way to model the transverse vortex shedding force is as a harmonic in time at the shedding frequency. This lifting force is given by:

$$F_L(t) = (1/2)\rho U^2 D C_L \sin(\omega_s t) \qquad (6)$$

where F_L = lift force (transverse to mean flow) per unit length of cylinder,
ρ = fluid density,
U = free stream velocity,
D = cylinder diameter,
C_L = lift coefficient, dimensionless
$\omega_s = 2\pi f_s$ = circular vortex shedding frequency, radians/sec, where f_s is given by (2),
t = time, sec.

The lift force is applied as a forcing function to the equation of motion for an elastically supported, damped, rigid cylinder which may only move perpendicularly to the flow. The steady-state solution for the deflection y(t) is assumed to be a sinusoidal response in which A_y is the amplitude of vibration. Substitution back into the equation of motion gives an expression for y/D. The response reaches a maximum at resonance, and the resulting resonant amplitude is:

$$A_y/D = C_L/4\pi S^2\delta_r \qquad (7)$$

Where C_L = lift coefficient,
S = Strouhal number,
δ_r = reduced damping.

The reduced damping term, δ_r, is defined as the mass ratio times the structural damping factor and is given by:

$$\delta_r = 2m(2\pi\xi)/\rho D^2 \qquad (8)$$

Where m = mass per unit length including added mass,
ξ = damping factor,
ρ = density of surrounding fluid,
D = diameter of cylinder.

The mass ratio, $m/\rho D^2$, mentioned above, is a measure of the relative importance of bouyancy and added mass effects on the model. It is used to measure the susceptibility of lightweight structures to flow-induced vibration. The likelihood of flow-induced vibration increases with increasing mass ratio. The damping factor, ξ, characterizes the energy dissipated by a vibrating structure. The damping factor is expressed as a fraction of 1, which is the critical damping factor. For linear, viscously damped structures, $2\pi\xi$, is the natural logarithm of the ratio of the amplitudes of any two successive cycles of

a lightly damped structure in free decay. Many real structures are lightly damped and so have damping factors on the order of 0.01. The amplitude of flow-induced vibration usually decreases with increasing reduced damping.

Note that the right-hand side of (7) implies that the peak amplitude is independent of flow velocity. This occurs because fixing the Strouhal number fixes the relationship between cylinder and fluid frequencies.

Blevins[14] mentions that actual cylinder response is limited because the resonant cylinder motion feeds back into the vortex shedding process to influence the lift coefficient. That is, C_L is a function of A_y for resonating cylinders. The Blevins and Burton model is a three term polynomial curve fit to experimental data which relates C_L to A_y/D:

$$C_{Le} = 0.35 + 0.60(A_y/D) - 0.93(A_y/D)^2 \qquad (9)$$

This model was developed for vortex-induced vibration of circular cylinders in the subcritical Reynolds number range (Re=300 to 1.5×10^5).[15] One drawback for using the harmonic model is that the calculation of A_y/D in (7) requires a prior estimate of the lift coefficient C_L.

The second analytical model is a nonlinear oscillator with self-excitation properties. This is known as the wake oscillator model. The basic assumptions are:

1) Inviscid flow provides a good approximation for the flow field outside the near wake.

2) A well-formed, two-dimensional vortex street with a well-defined shedding frequency exists.

3) The force exerted on the cylinder by the flow depends on the velocity and acceleration of the flow relative to the cylinder.

The characteristics of this model are such that cylinder motion is fed back into the response at synchronization. This response is limited by the nonlinear term. The maximum resonant displacement amplitude is predicted in terms of reduced damping (δ_r) and is given by:

$$A_y/D = \frac{0.07\gamma}{(1.9+\delta_r)S^2}\left[0.3 + \frac{0.72}{(1.9+\delta_r)S}\right]^{1/2} \qquad (10)$$

where δ_r = reduced damping (see Eq 8),
S = Strouhal Number, and
γ = dimensionless mode factor (see Table 2).

Table 2 gives examples of the mode factor for some structural elements and natural frequencies.

TABLE 2

Dimensionless Mode Factors (γ) For Some Structural Elements and Natural Frequencies[16]

Structural Element	Natural Frequency*	γ
Rigid Cylinder	$\sqrt{k/m}$	1.000
Uniform Pivoted Rod	$\sqrt{3k_\theta/mL^3}$	1.291
Taut String or Cable	$n\sqrt{T/mL^2}$	1.155 for n = 1,2,3...
Simply Supported Uniform Beam	$n^2\pi^2\sqrt{EI/mL^4}$	1.155 for n = 1,2,3...
Cantilevered Uniform Beam	$\omega_1 = 3.52\sqrt{EI/mL^4}$	$\gamma_1 = 1.305$
	$\omega_2 = 22.03\sqrt{EI/mL^4}$	$\gamma_2 = 1.499$
	$\omega_3 = 61.70\sqrt{EI/mL^4}$	$\gamma_3 = 1.537$

*Where m = mass/unit length,
E = modulus of elasticity,
I = area moment of inertia of section,
L = spanwise length,
K = linear spring constant,
K_θ = torsional spring constant,
T = tension force in cable.

Calculation of Lift and Drag Forces

Note that the lift and drag forces, F_L and F_D, respectively, are functions of the lift and drag coefficients, C_L and C_D, which were shown to be functions of the vertical deflection amplitude, A_y. The drag forces increase with increasing A_y, while lift forces increase to a maximum value, then decrease with increasing A_y. The maximum value of A_y/D for increasing C_{Le} is estimated to be 0.323. This estimate was calculated by differentiating (9) with respect to A_y/D and setting it equal to zero. The corresponding value of C_{Le} is 0.447. This behavior is in contrast to the method currently used for calculation of wind forces for design of overhead sign and signal structures, in which C_D is a function of wind velocity and diameter (Reynolds Number) for cylindrical, hexdecogonal, dodecagonal, and elliptical shapes, and a constant for other shapes.[17] Lift forces are not considered in current design procedures.

The question of whether the amplitudes are significant or not is important. Obviously, if the amplitude of vibration is less than a certain level, force calculations become simplified because C_L and C_D are easier to identify. Blevins defines the amplitude criteria as a function of both reduced damping and frequency ratio. If δ_r is less than 64 and f_n/f_s is between 0.6 and 1.4, then significant amplitudes will result.[18]

The calculation procedures for F_L and F_D resulting from the previous discussions are complex and require calculation of several nondimensional parameters as well as estimates of natural frequencies and structural damping.

Figure 2 provides a flow-chart for estimating amplitude and drag in vortex-induced vibration. Figure 3 shows an additional flow-chart for estimating lift. Tapered tubes may be treated by dividing the tube into several stepped uniform members of reasonable length for force calculations or by using a uniform tube of equivalent stiffness. Thus, both lift and drag forces induced by vortex shedding may be calculated given the various input parameters. Stresses at welds or other points in the structure are then calculated by conventional methods, taking applicable stress concentration effects into account.

The American Association of State Highway and Transportation Officials (AASHTO) publishes "Standard Specifications for Structural Supports for Highway Signs, Luminaires, and Traffic Signals," which presents a formula for calculating the wind pressure on a structure:[19]

$$P = 0.00256(1.3V)^2 C_D C_h \qquad (11)$$

Where P = wind pressure, lbs/ft^2,
V = wind velocity, mph,
C_D = drag coefficient, and
C_h = height coefficient.

This formula is similar to (3) with a thirty percent gust factor and a coefficient to account for height above ground. One difference between (3) and (11) is in the intended use. Equation (11) is intended for calculating static pressures using an isotach chart to predict maximum wind speed. The gust factor is intended to account for the dynamic effects of gusts and to provide a large factor of safety. The drag coefficient does not reflect the effects of vortex shedding. The amplification of drag force due to vortex shedding heavily influences fatigue life estimates of structures subjected to wind loads.

Closure

The preceding discussions illustrated the complexity of analyzing the actual forces being applied to overhead sign and signal structures by wind loads. The force calculation methods must be regarded as estimates because of their reliance on estimates of important parameters such as structural damping, natural frequency, and stationary lift and drag coefficients. Also, these methods depend on experimental results which may not apply to other Reynolds number regimes. However, the methods do provide a more reasonable picture of the real behavior of overhead sign and signal structures than the force calculation methods used in current design specifications, and therefore would be expected to give a more accurate account of the cyclic loading of these structures.

The most accurate method available for determining the stresses induced by wind loads on overhead sign and signal structures is to install strain gages at the points of fatigue interest and to then monitor the wind-induced stresses over an extended period of time. This method is discussed in more detail in subsequent chapters.

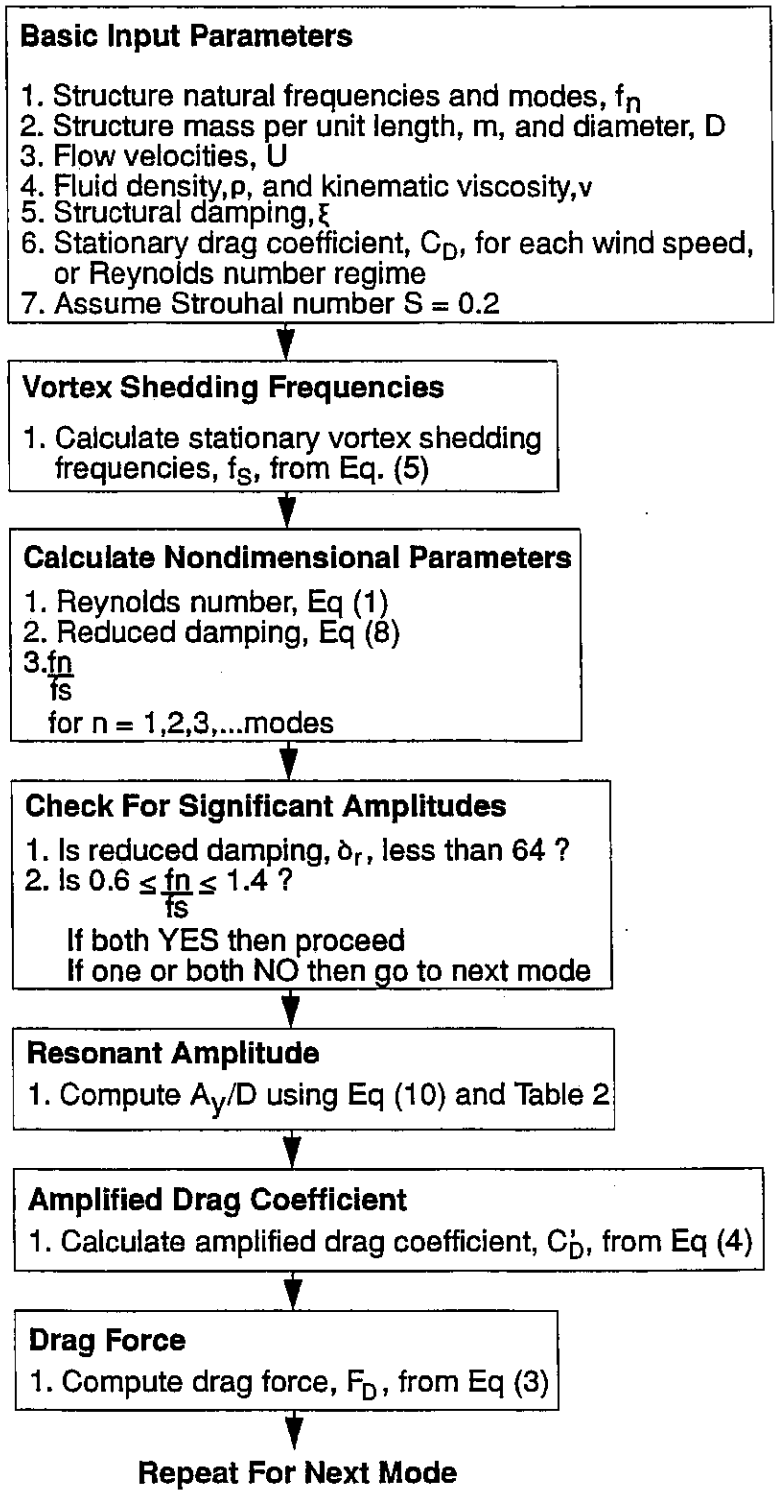

Figure 2. A flow-chart for estimating amplitude and drag for vortex-induced vibration (adapted from Blevins, page 76).

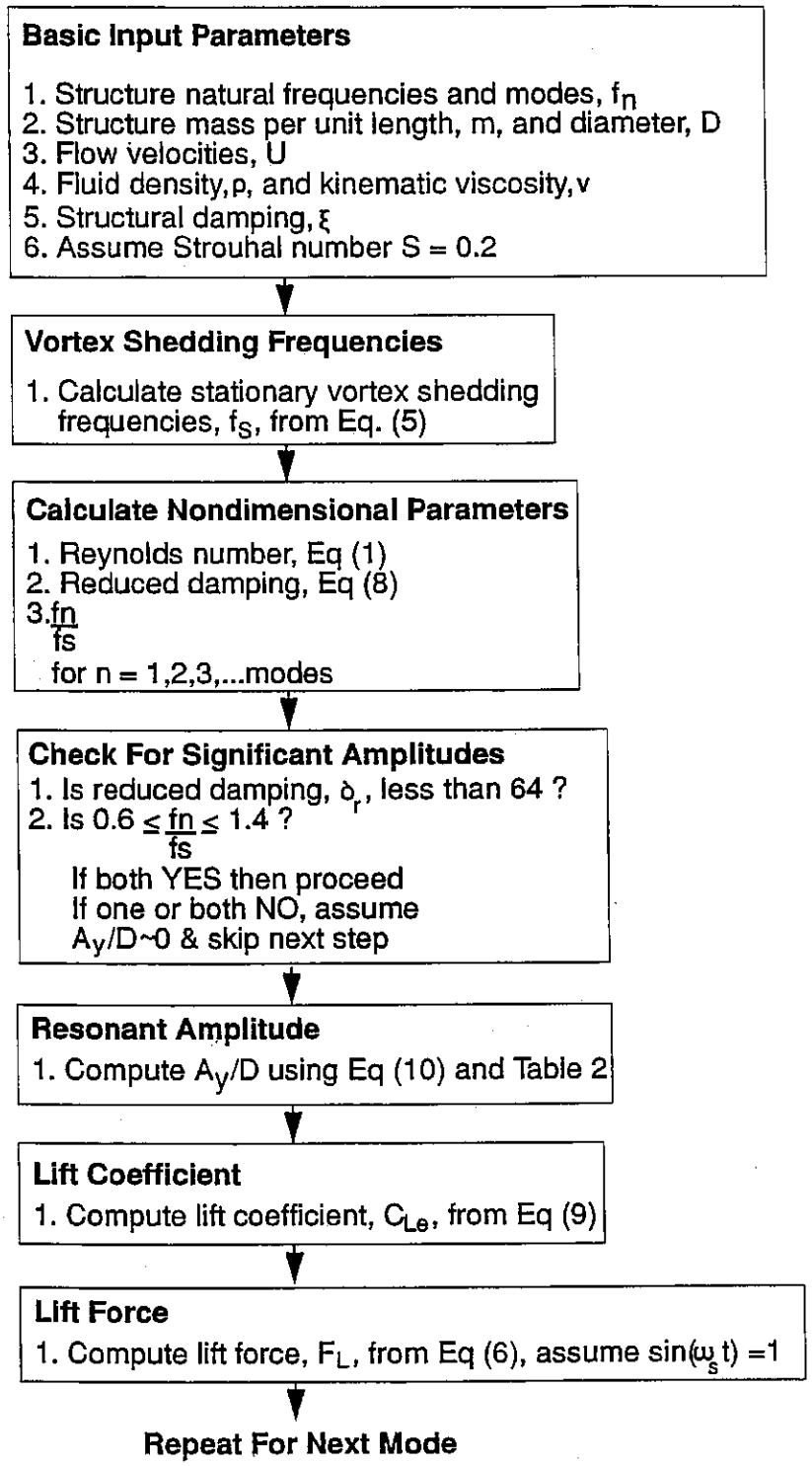

Figure 3. A flow-chart for estimating lift forces for vortex-induced vibration.

3. WIND SPEED DATA

This chapter presents and discusses wind speed data gathered from an instrumented traffic signal structure during the course of the project.

Instrumentation

The instruments used to collect wind speed data included a Model 05103 wind monitor (R.M. Young Company, Traverse City, Michigan) and a Model EL-824-GC Easylogger Field Unit (Omnidata International, Inc., Logan, Utah). The wind monitor was mounted to a pole which rose approximately four feet above the top of the traffic signal anchor pole. This arrangement resulted in a height above ground of about 25 feet (7.62 m). Data were collected at one minute intervals and stored in removable data storage packs. Data collection began on August 7, 1991 and ended January 25, 1993. The traffic signal was located at the intersection of Illinois Route 54 (Wabash Avenue) and White Oaks Drive in Springfield, Illinois. This location is at the extreme west edge of the city. The surrounding terrain is generally flat and nearly treeless. Primary land uses are for residential and shopping area. Nearby building structures range from one to three stories in height. The nearest building structure is approximately 200 feet (60.96 m) due east of the signal structure and is two stories high .

Collected Wind Speed Data

The collected wind speed data for calendar year 1992 were compiled into histogram format. The wind speed-frequency histogram data are presented in Table 3, and are shown graphically in Figure 4. Inspection of Figure 4 shows that the greatest concentration of wind speeds are

clustered between zero and about fifteen miles per hour (mph) (24.14 kilometers per hour [km/hr]), and show a reasonably smooth exponential decay starting at about five mph (8.05 km/hr). The distribution is obviously not Gaussian. In general, the histogram is in agreement with official National Oceanic and Atmospheric Administration (NOAA) data on wind speeds; that is, a large block of data in the lower speed ranges, with decreasing frequencies in the higher speed ranges. Table 3 reveals that only one 60 mph (96.56 km/hr) event was recorded at this location in 1992, while 91.7 percent of the wind speeds measured were at or below 15 mph (24.14 km/hr).

In contrast to the smooth appearance of the histogram, the variation of wind speeds during a particular day shows that wind forces are variable and cyclic. One day for each month of 1992 was selected at random to illustrate the variable amplitude, cyclic behavior of actual wind loadings. This data is presented in Figures 5 through 16. Inspection of these figures shows that the signal structure was almost continuously loaded by wind speeds of variable magnitude. The implication is that sign and signal structures are continuously experiencing fatigue-type load applications and are subject to cumulative fatigue damage.

Closure

The data presented in this chapter showed that structures are subjected to constantly varying winds. Although this observation may seem naive in light of the complexity of the force calculation methods, the effort was made to reinforce the point that use of isotach charts or maximum predicted wind speeds based on empirical formulas will not account for the variations in wind speeds and applied stresses which affect the fatigue life of a structure.

TABLE 3

Wind Speed Histogram Data for Signal Structure at I1-54 at White Oaks Drive for CY 1993.

Wind speed (mph)*	Frequency	Percent	Cumulative Frequency
0	16637	3.3	16637
1	41716	0.9	21353
2	23456	4.7	44809
3	33908	6.8	78717
4	41894	8.4	120611
5	45747	9.2	166358
6	45643	9.1	212001
7	43292	8.7	255293
8	40516	8.1	295809
9	35955	7.2	331764
10	30863	6.2	362627
11	26867	5.4	389494
12	22254	4.5	411748
13	18273	3.7	430021
14	15136	3.0	445157
15	12183	2.4	457340
16	9835	2.0	467175
17	7622	1.5	474797
18	5994	1.2	480791
19	4656	0.9	485447
20	3393	0.7	488840
21	2569	0.5	491409
22	1928	0.4	493337
23	1391	0.3	494728
24	1073	0.2	495801
25	768	0.2	496569
26	607	0.1	497176
27	443	0.1	497619
28	356	0.1	497975
29	277	0.1	498252
30	178	<0.1	498430
31	128	<0.1	498558
32	99	<0.1	498657
33	82	<0.1	498739
34	65	<0.1	498804
35	45	<0.1	498849
36	22	<0.1	498871
37	15	<0.1	498886
38	13	<0.1	498899
39	8	<0.1	498907
40	3	<0.1	498910
41	5	<0.1	498915
42	3	<0.1	498918
43	2	<0.1	498920
44	3	<0.1	498923
45	1	<0.1	498924
46	1	<0.1	498925
48	1	<0.1	498926
60	1	<0.1	498927

*To convert mph to km/hr, multiply by 1.67.

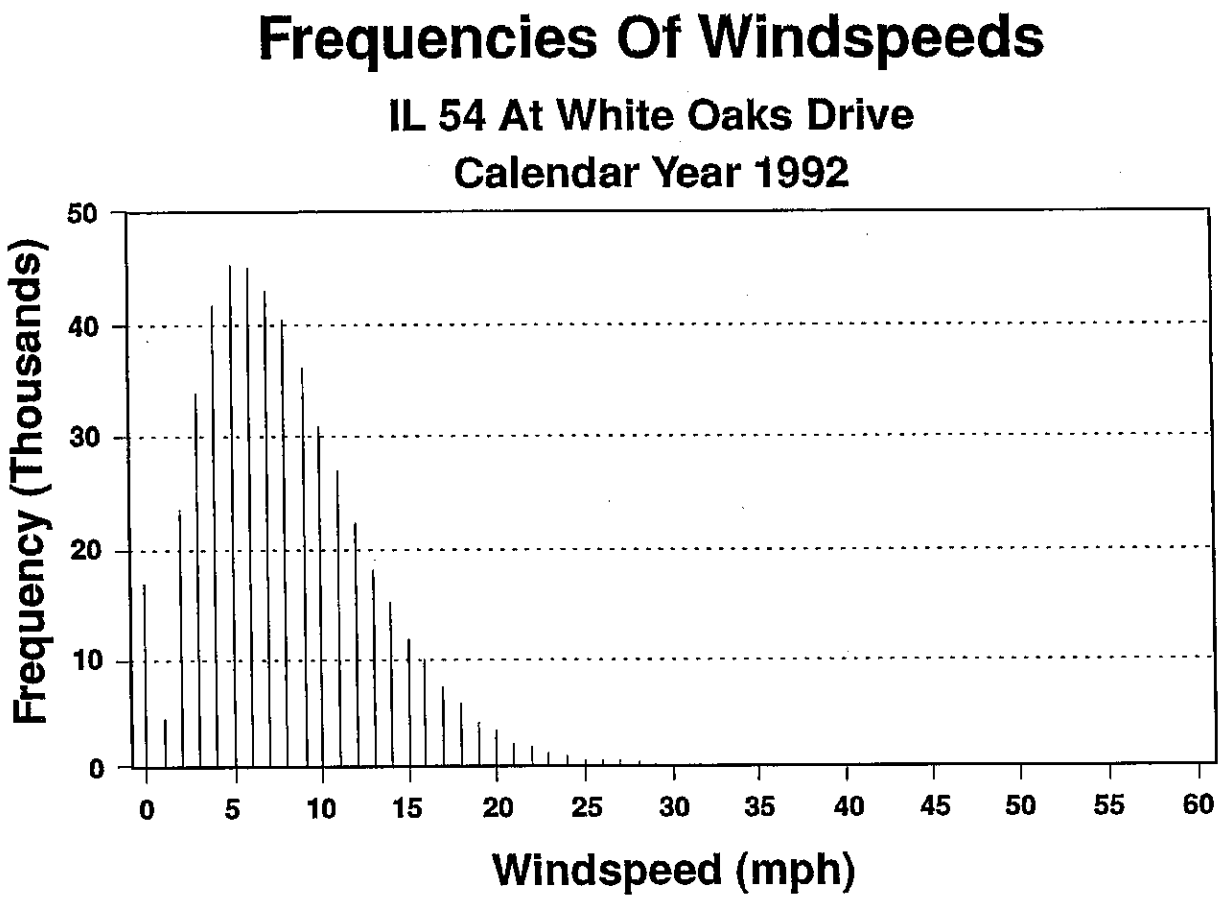

Note: See Table 3 for frequencies past 30 mph.

Figure 4. Wind speed versus frequency of occurrence histogram for signal stucture at Il-54 at White Oaks Drive in Springfield, Illinois for calendar year 1992.

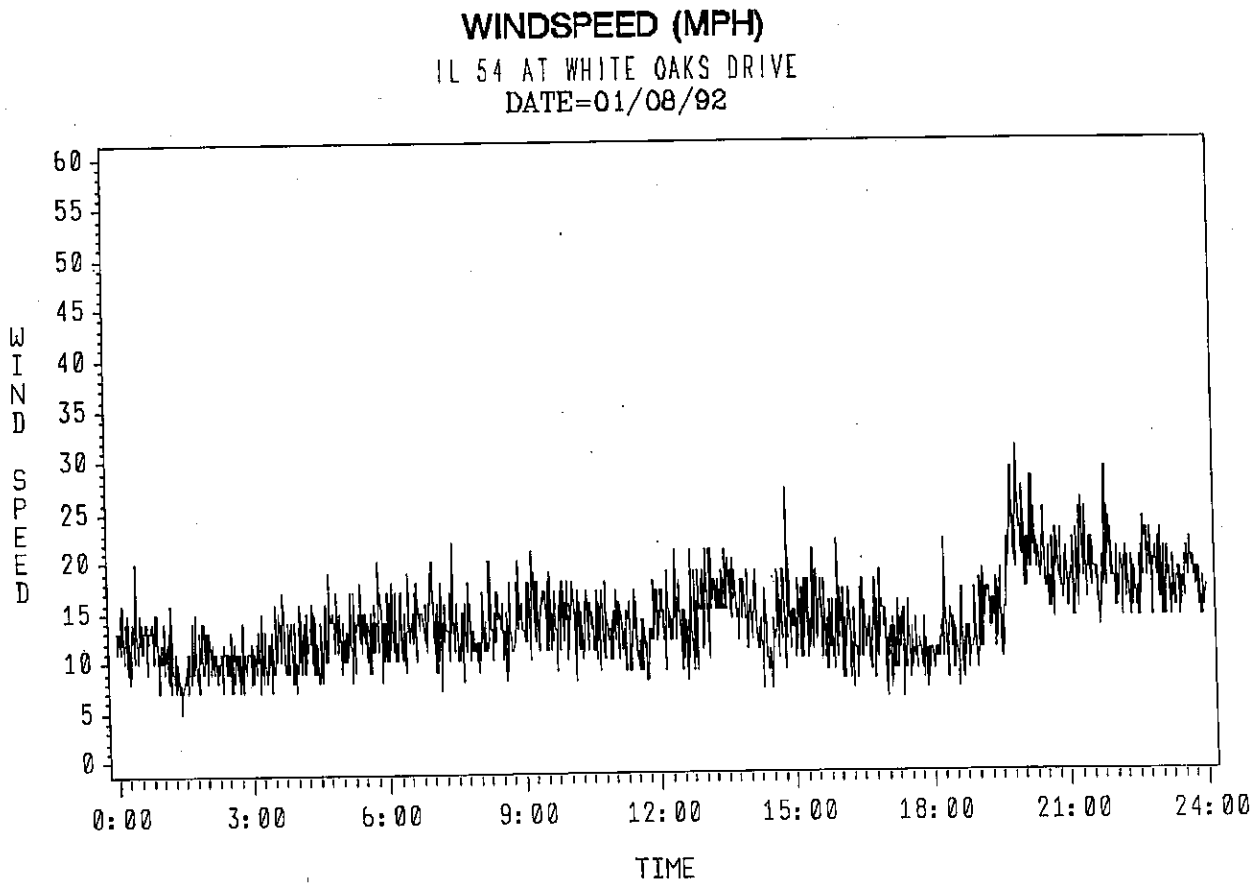

Figure 5. Wind speed data collected at Illinois 54 at White Oaks Drive in Springfield, Illinois on January 8, 1992. Data were collected at one-minute intervals.

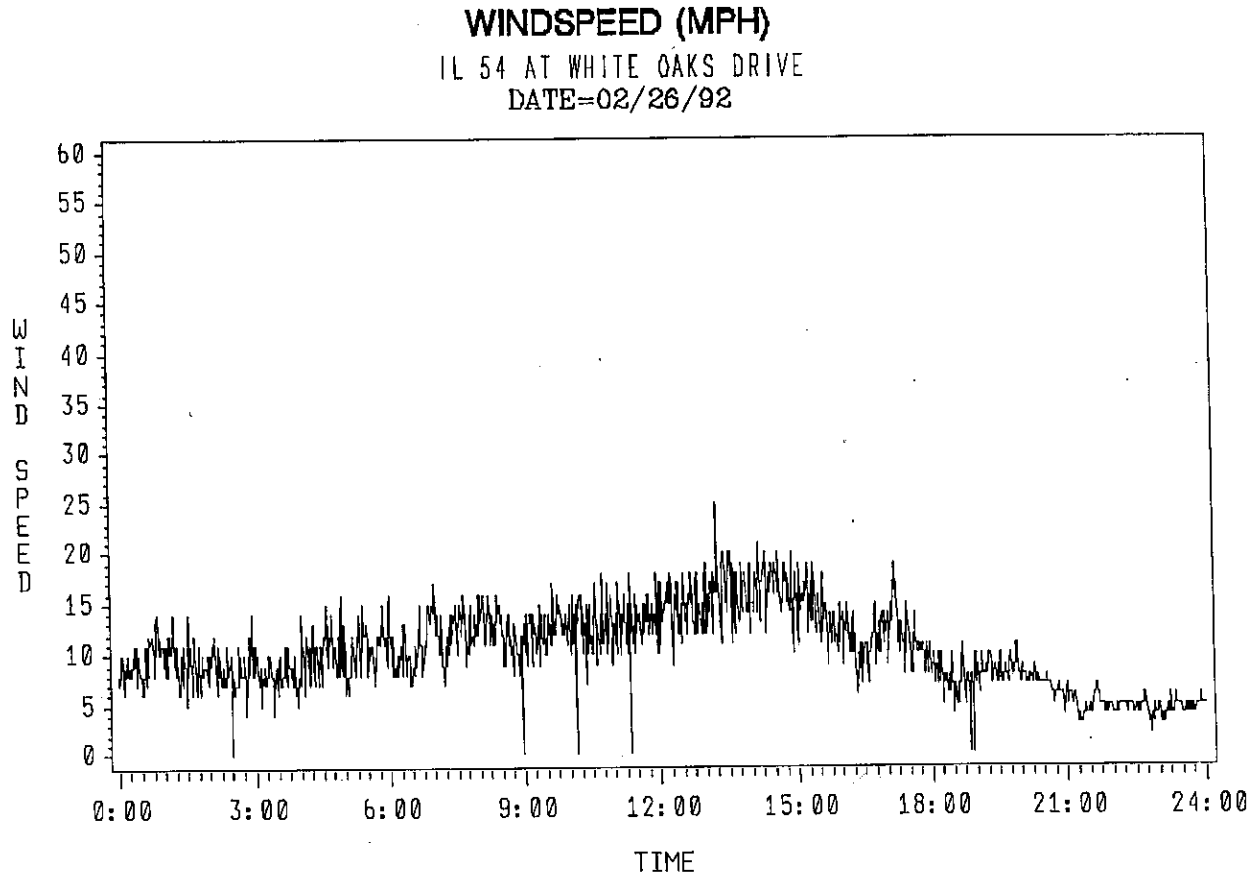

Figure 6. Wind speed data collected at Illinois 54 at White Oaks Drive in Springfield, Illinois on February 26, 1992. Data were collected at one-minute intervals.

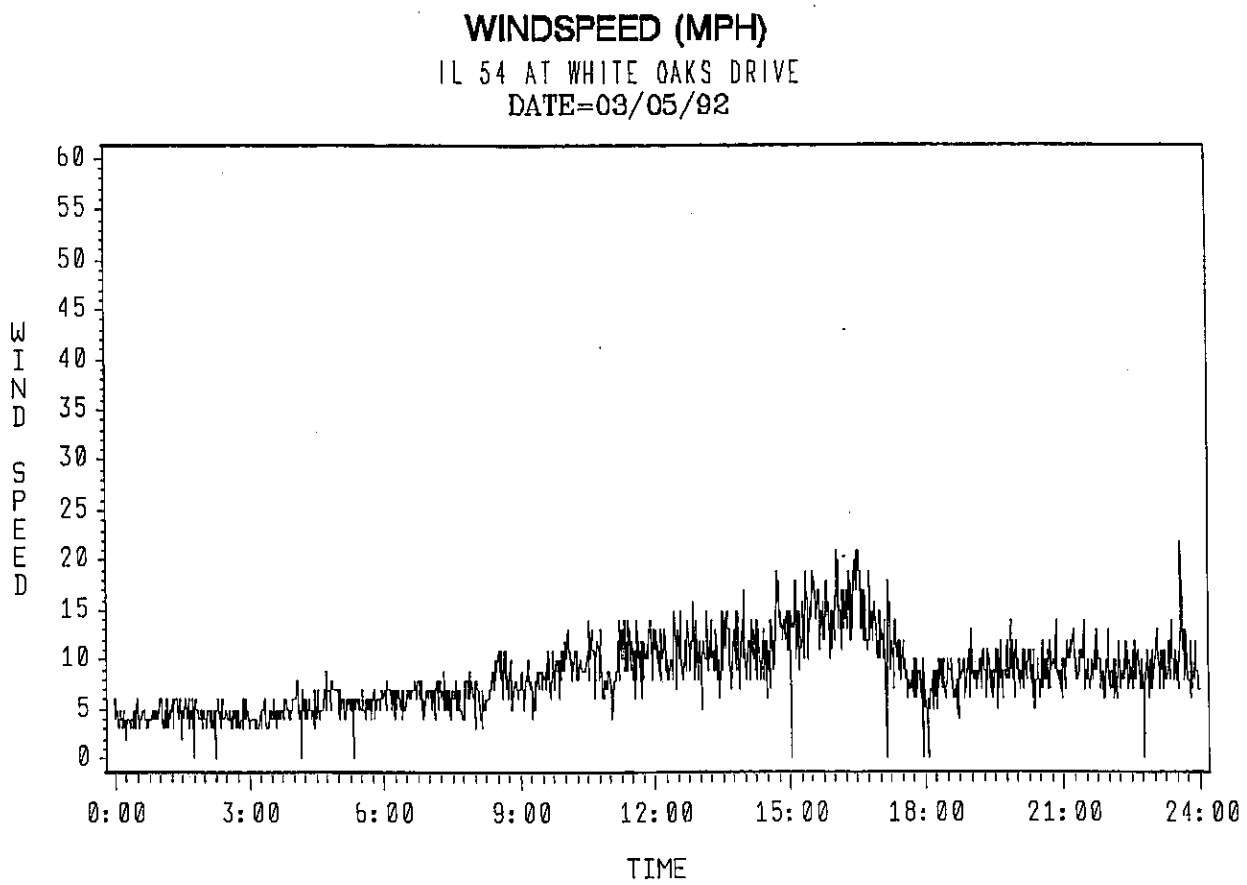

Figure 7. Wind speed data collected at Illinois 54 at White Oaks Drive in Springfield, Illinois on March 3, 1992. Data were collected at one-minute intervals.

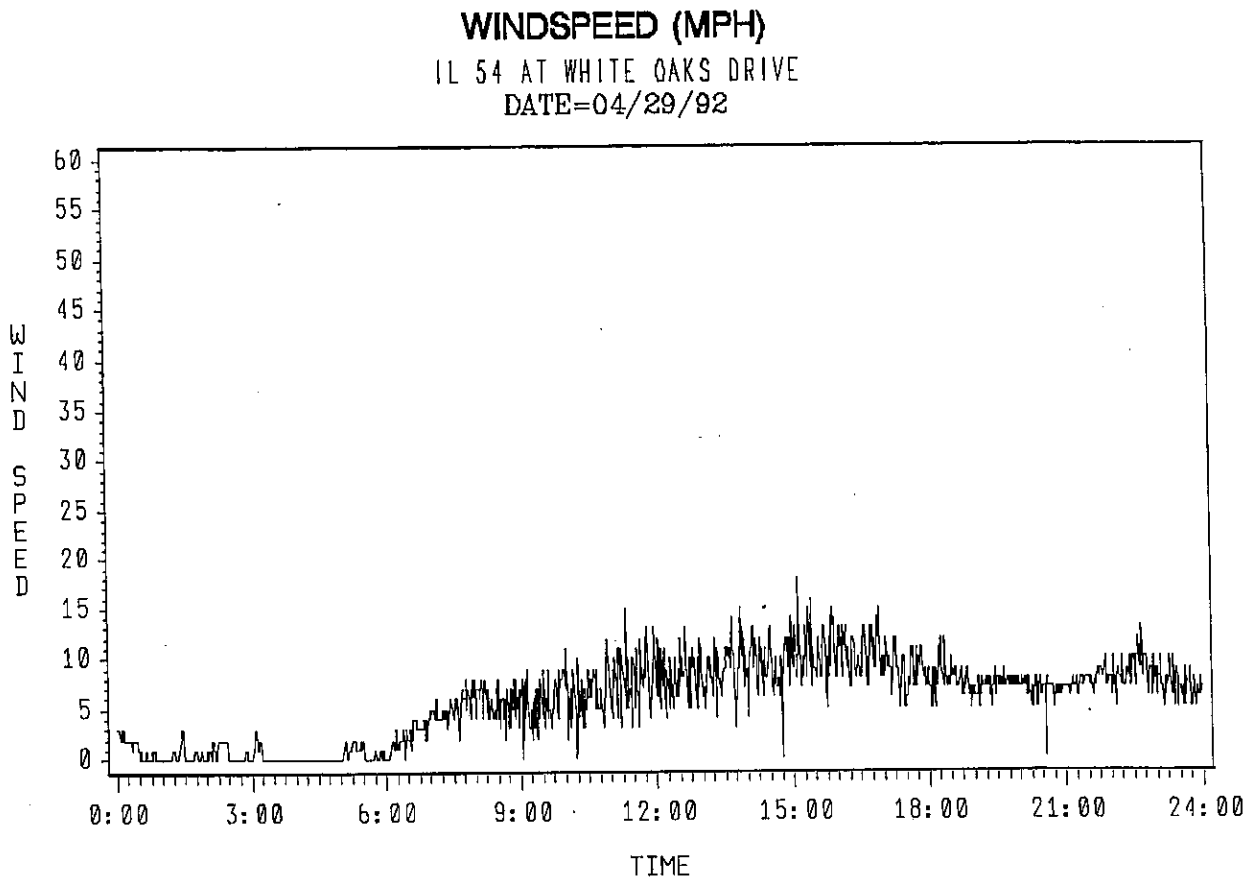

Figure 8. Wind speed data collected at Illinois 54 at White Oaks Drive in Springfield, Illinois on April 29, 1992. Data were collected at one-minute intervals.

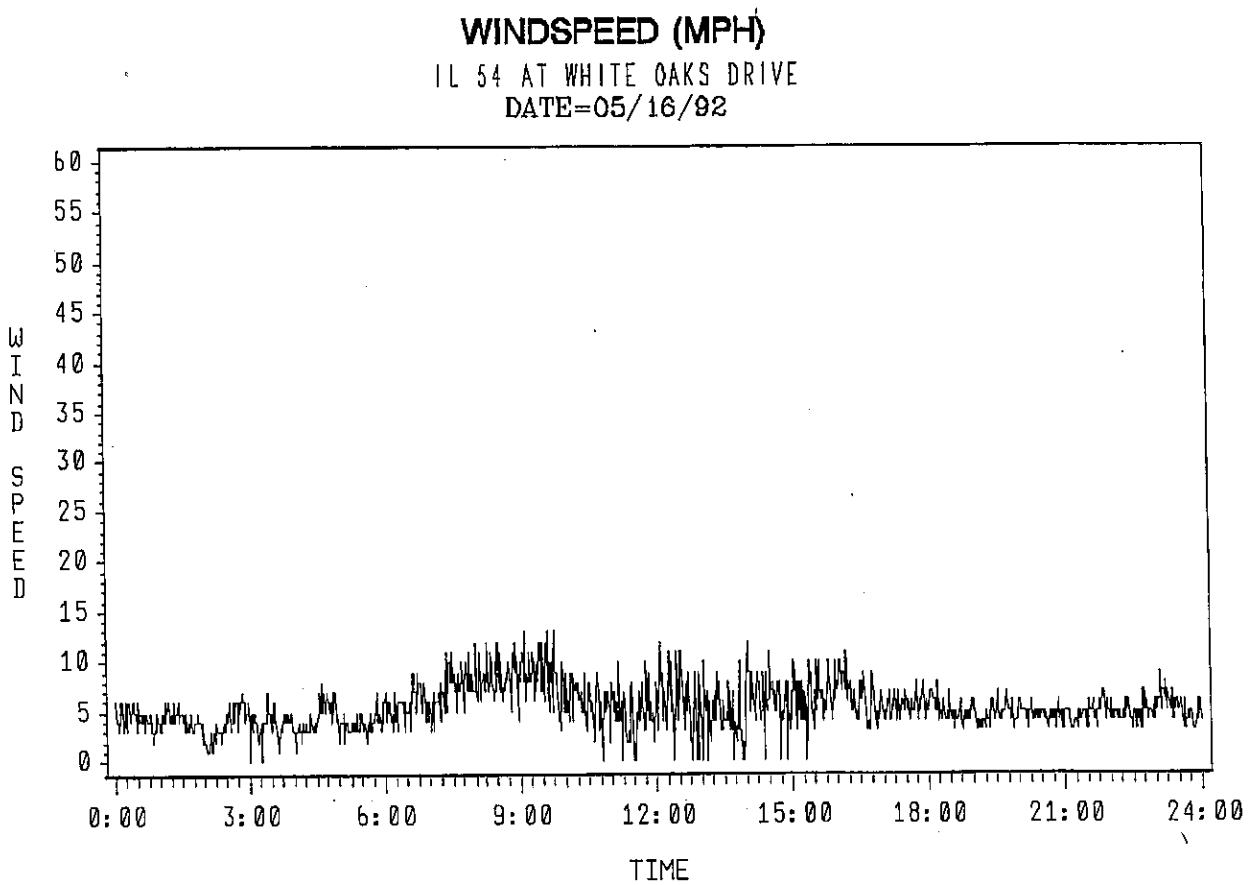

Figure 9. Wind speed data collected at Illinois 54 at White Oaks Drive in Springfield, Illinois on May 16, 1992. Data were collected at one-minute intervals.

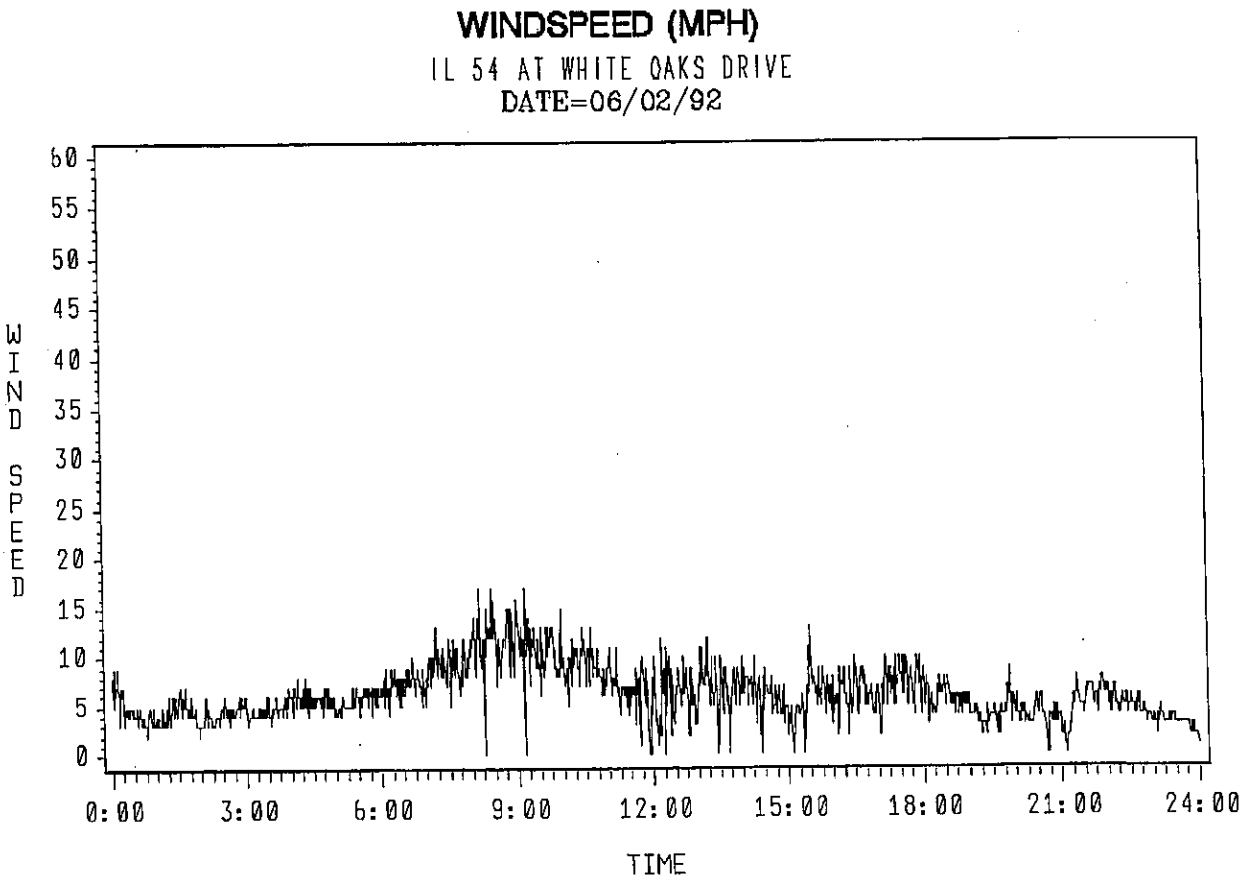

Figure 10. Wind speed data collected at Illinois 54 at White Oaks Drive in Springfield, Illinois on June 2, 1992. Data were collected at one-minute intervals.

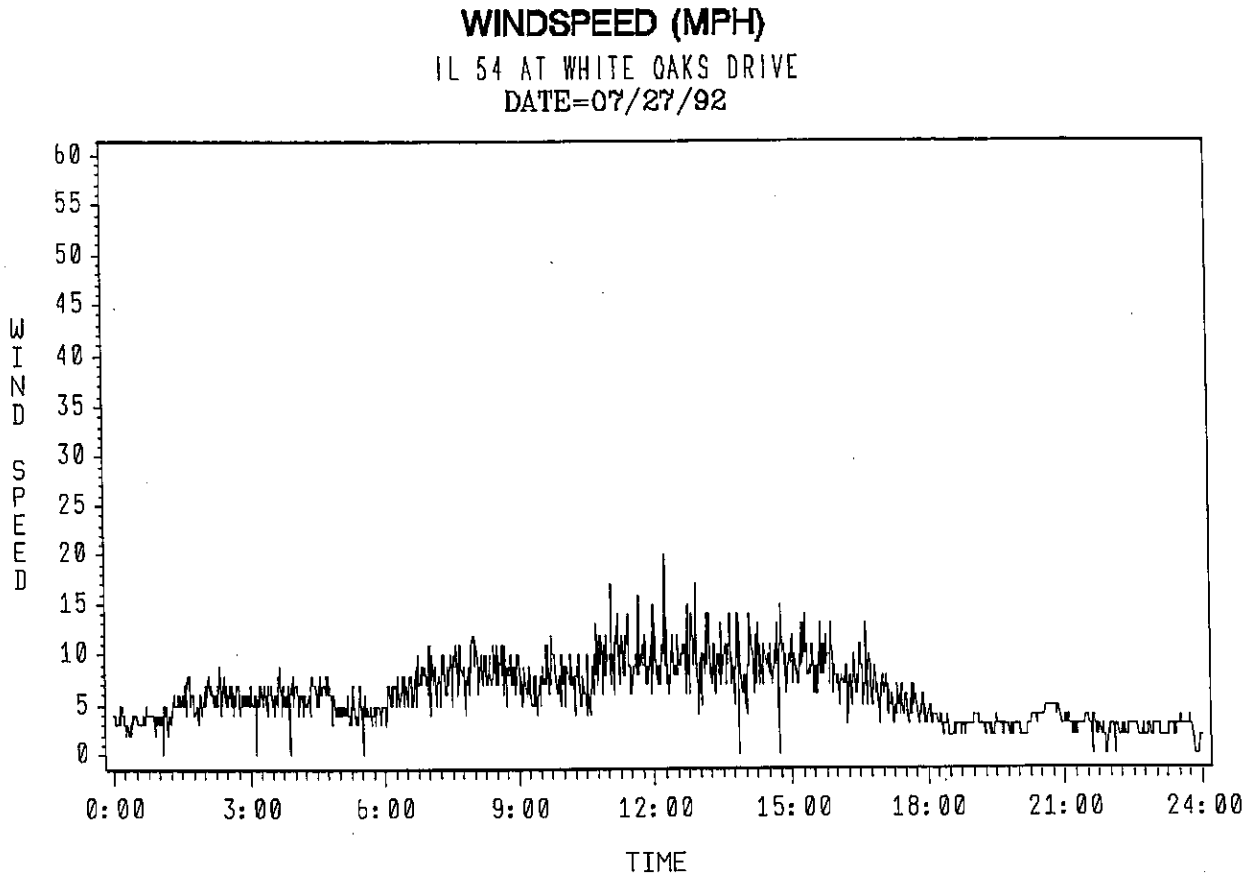

Figure 11. Wind speed data collected at Illinois 54 at White Oaks Drive in Springfield, Illinois on July 27, 1992. Data were collected at one-minute intervals.

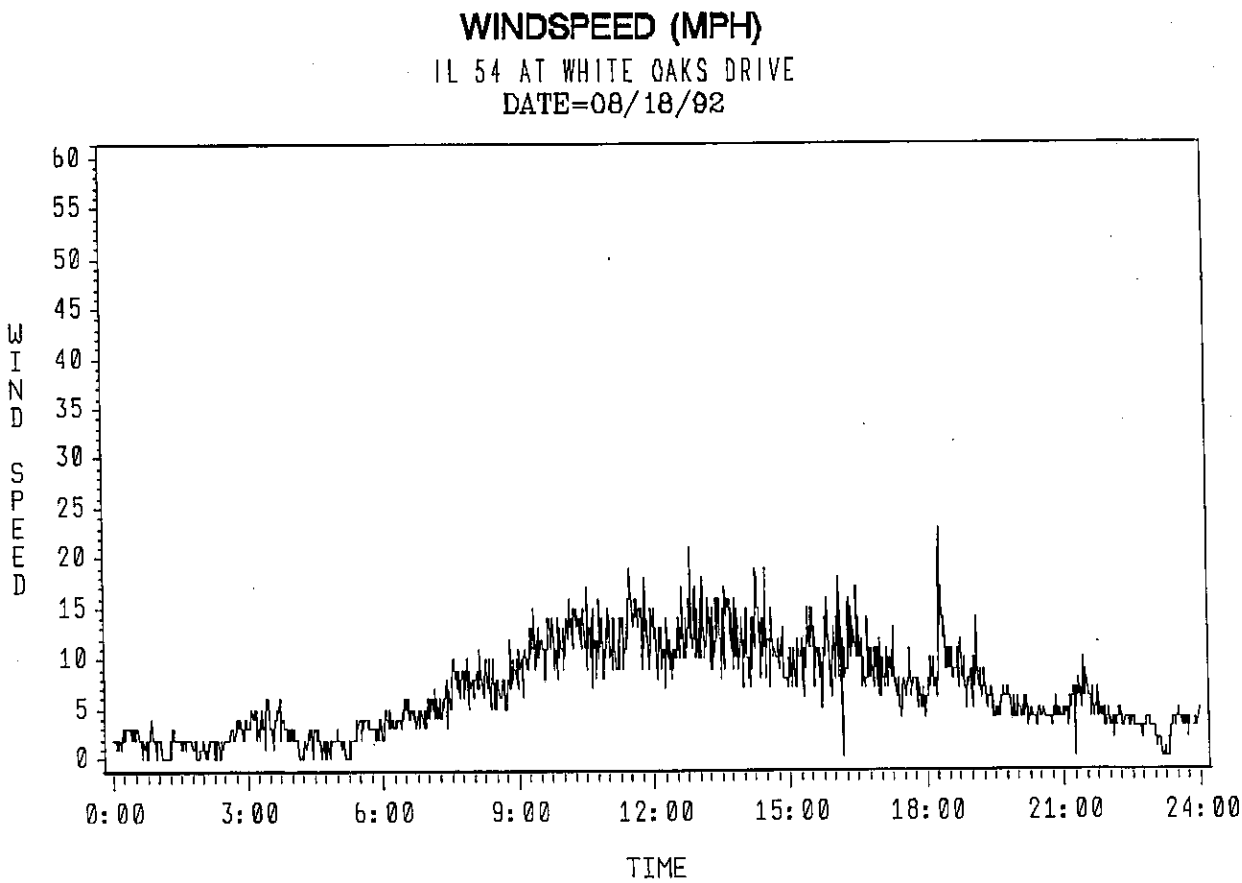

Figure 12. Wind speed data collected at Illinois 54 at White Oaks Drive in Springfield, Illinois on August 18, 1992. Data were collected at one-minute intervals.

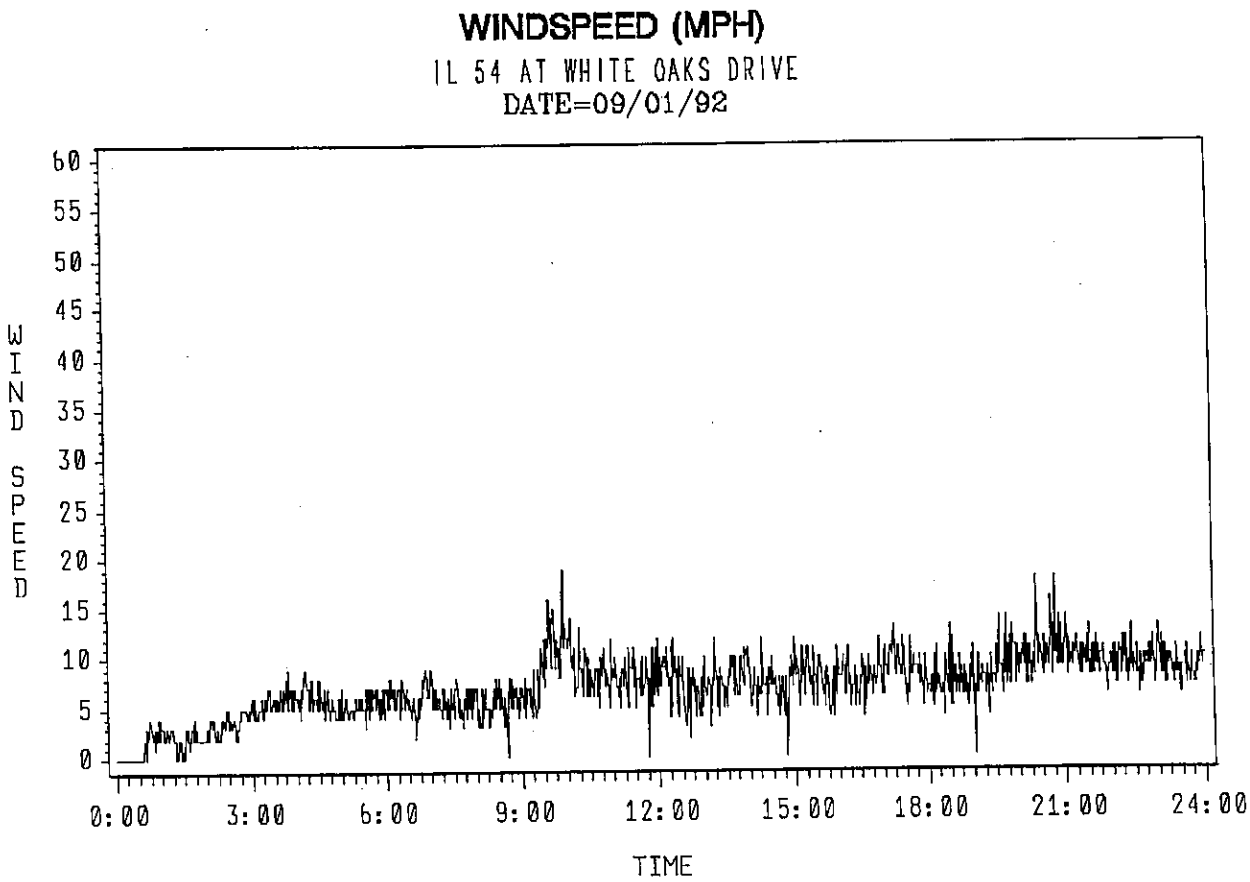

Figure 13. Wind speed data collected at Illinois 54 at White Oaks Drive in Springfield, Illinois on September 1, 1992. Data were collected at one-minute intervals.

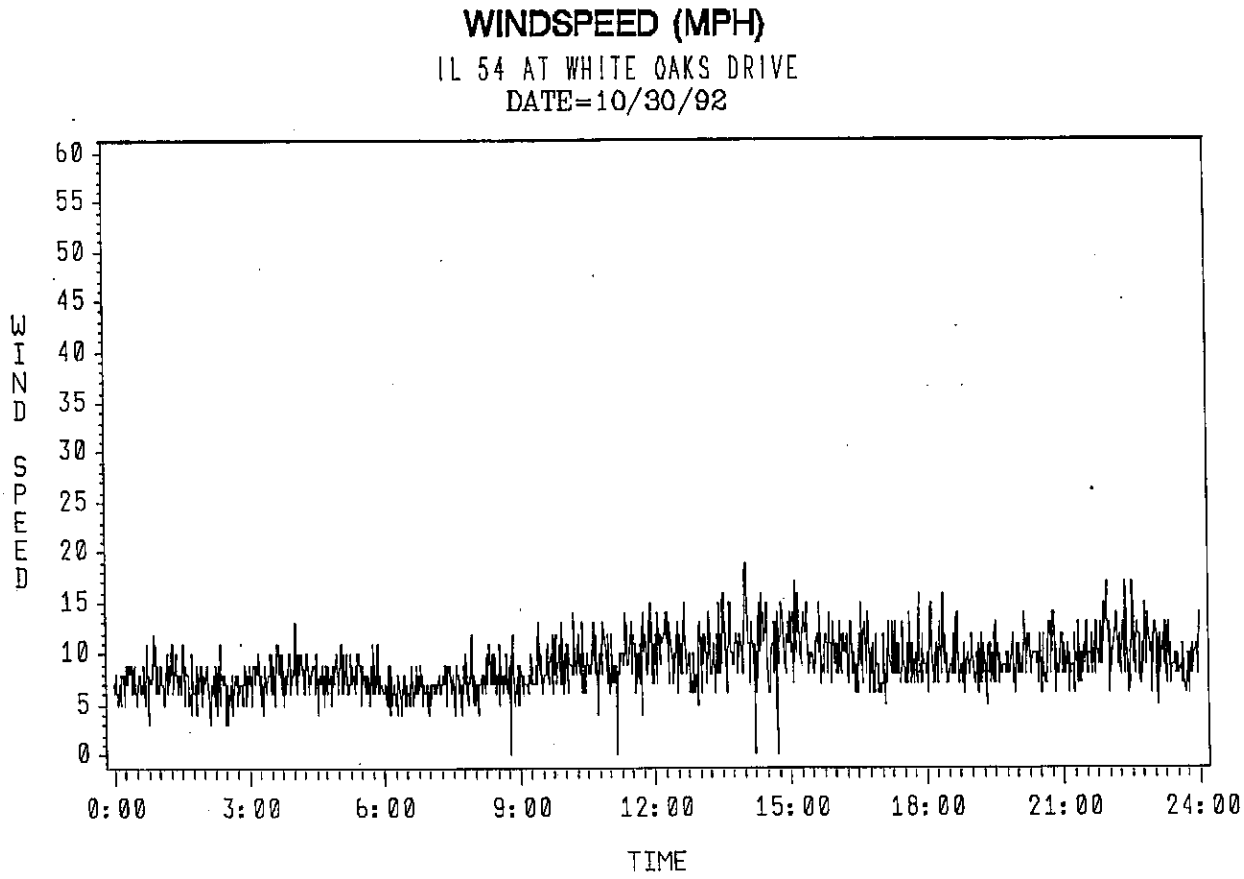

Figure 14. Wind speed data collected at Illinois 54 at White Oaks Drive in Springfield, Illinois on October 30, 1992. Data were collected at one-minute intervals.

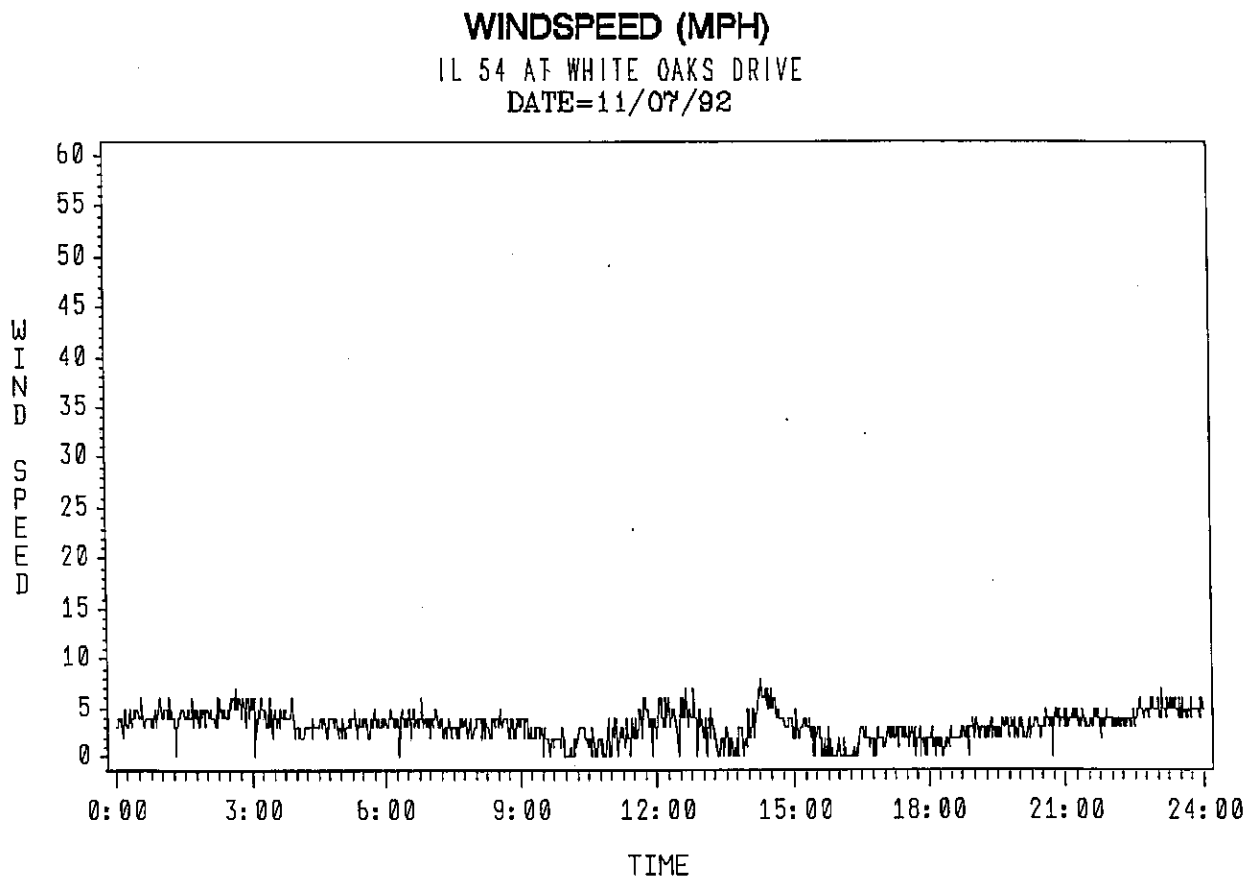

Figure 15. Wind speed data collected at Illinois 54 at White Oaks Drive in Springfield, Illinois on November 7, 1992. Data were collected at one-minute intervals.

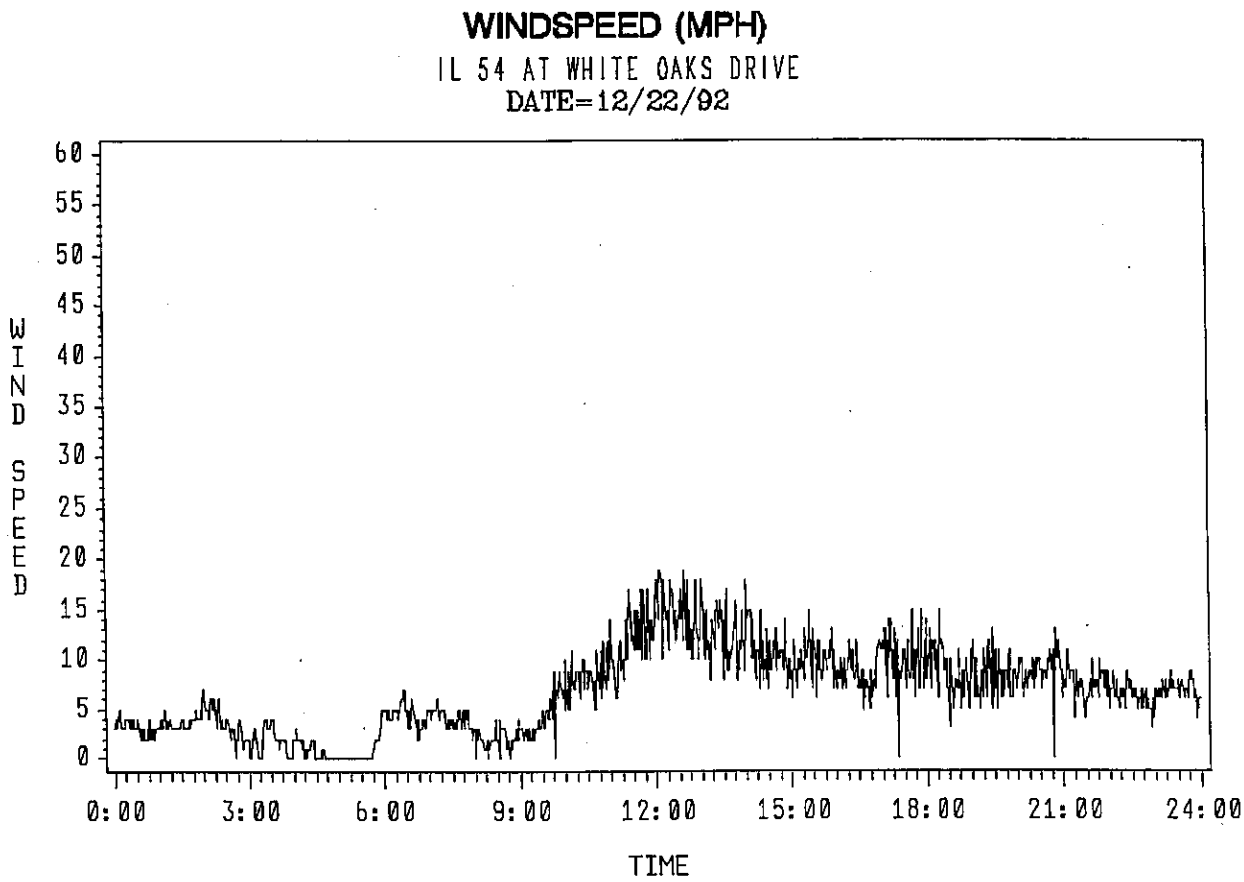

Figure 16. Wind speed data collected at Illinois 54 at White Oaks Drive in Springfield, Illinois on December 22, 1992. Data were collected at one-minute intervals.

4. STRAIN GAGE AND FREQUENCY DATA

This chapter discusses structural response data gathered during the course of this project. Data collected included strains due to ambient wind conditions, strain versus tip deflection, vortex shedding frequency for ambient wind conditions, dead load strains in anchor bolts and welded connections, and strains induced at a weld due to application of controlled wind speeds for a cantilevered traffic signal structure.

Stresses Due to Variable Speed Wind Loads (Ambient Winds)

A common steel traffic signal structure with a 44 foot (13.41 m) mastarm was installed at the Physical Research Laboratory in Springfield, Illinois in order to monitor applied stress range versus frequency of occurrence due to ambient winds. The structure and strain gage locations are shown in Figure 17. Strains at the exterior fillet weld connections were measured using weldable, electrical resistance strain gages (MicroMeasurements, Inc., Raleigh, NC, USA). Strains in the anchor bolts were measured using bolt gages (Type BTM-6C, TML, Ltd, Tokyo, Japan) which were installed after erection of the vertical pole. The data were collected and processed by a Rainflow cycle counting algorithm (ASTM E1049-85) incorporated in the SOMAT 2000 Data Acquisition System (SOMAT Corporation, Champaign, Illinois). The data were divided into 0.5 ksi (3.45 MPa) increments for ease of handling. The resulting stress range-frequency data for the fillet weld connection for a four-month period are shown in Table 4a.

There is a noticeable difference in the number of recorded stress cycles between the top strain gage (lift) and the side strain gage (drag). A total of 3,072,316 stress cycles were recorded for the side gage, while only 2,448,558 stress cycles were recorded for the top gage.

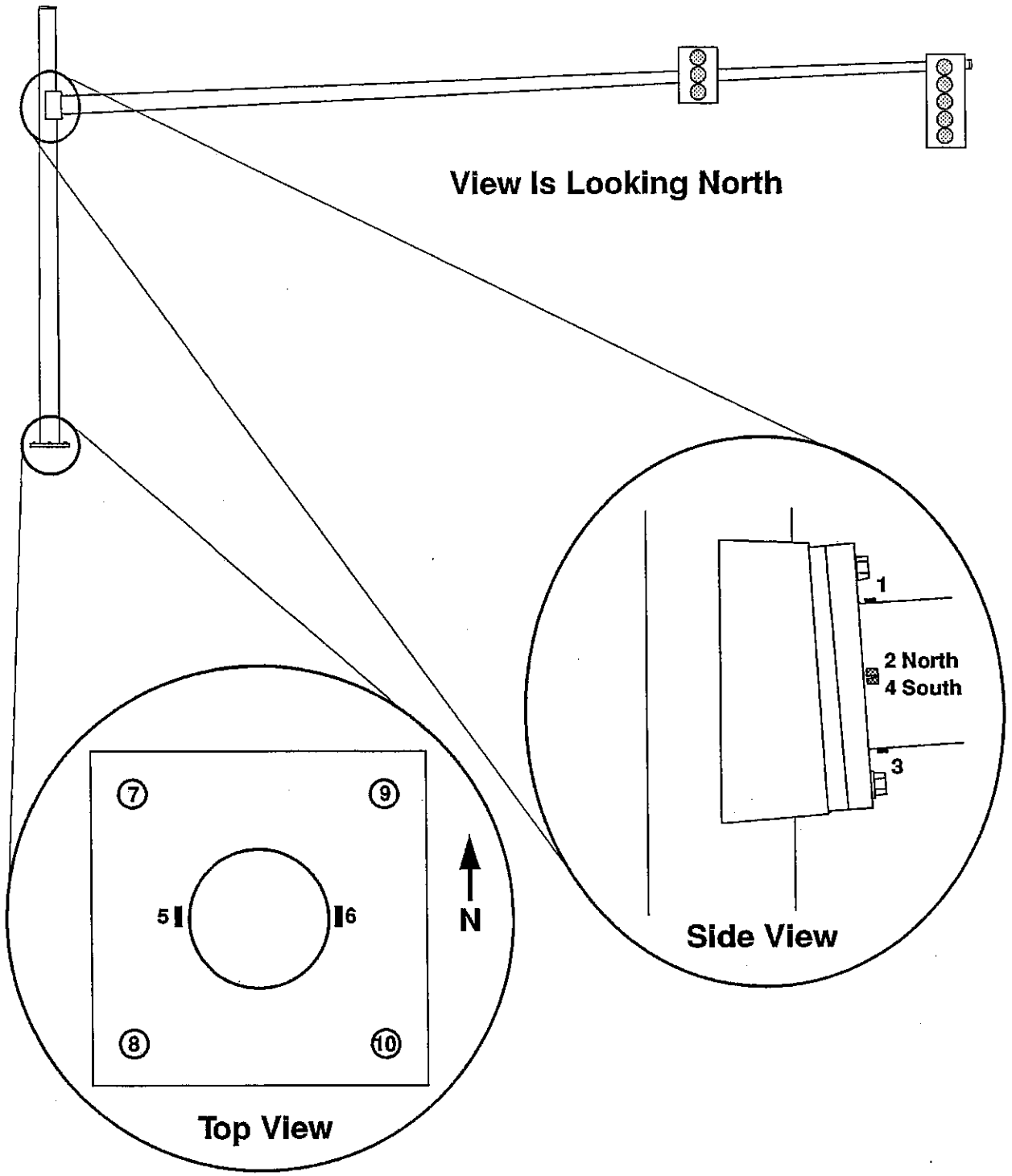

Figure 17. Instrumented traffic signal mastarm installed at Physical Research Laboratory in Springfield, Illinois. Strain gage locations are shown.

Note the high relative concentration of cycles at 4.5 ksi (31.03 MPa) and 9.0 ksi (62.06 Mpa) for the side gage, and at 9.0 ksi (62.06 MPa) for the top gage. This behavior is important, since it indicates that the detail is experiencing stress cycles at levels where the capacity for sustaining fatigue damage is more limited than at lower stress levels.

TABLE 4a

Stress Range-Frequency Data for Instrumented Fillet Weld Connection on Traffic Signal Mastarm*

Measured Stress Range (ksi)**	Frequency (Cycles) Top Gage (1)	Side Gage (2)
0.5	2,387,963	2,700,913
1.0	96,056	322,673
1.5	4,134	36,324
2.0	161	4,610
2.5	64	3,382
3.0	12	846
3.5	9	140
4.0	21	131
4.5	13	3,095
5.0	7	12
5.5	14	22
6.0	7	11
6.5	3	7
7.0	0	2
7.5	5	2
8.0	2	4
8.5	5	1
9.0	78	136
9.5	0	1
10.0	0	1
11.0	0	2
12.5	1	0
13.5	1	0
14.0	0	1

*Data were collected between February 1993 and June 1993.
**Multiply ksi values by 6.895 to obtain stress in MPa.

Stress range versus frequency data for the tension dead load anchor bolts is given in Table 4b.

TABLE 4b
Stress Range-Frequency Data for Instrumented Anchor Bolts for Cantilevered Traffic Signal Structure*

Measured Stress Range (ksi)**	Frequency (Cycles) Northwest Bolt (7)	Southwest Bolt (8)
0.5	3,536,599	4,686,394
1.0	201,288	52,748
1.5	1,254	1,274
2.0	292	288
2.5	280	376
3.0	137	315
3.5	47	162
4.0	59	272
4.5	67	67,424
5.0	86	58
5.5	84	135
6.0	92	134
6.5	266	112
7.0	37	50
7.5	505	83
8.0	898	89
8.5	769	38
9.0	1,495	2,200
9.5	5	68
10.0	0	37
10.5	3	56
11.0	3	55
11.5	0	13
12.0	1	46
12.5	2	23
13.0	1	12
13.5	1	34
14.0	8	68
14.5	0	14
15.0	0	30
15.5	2	44
16.0	1	14
16.5	1	25
17.0	0	20
17.5	0	15
18.0	0	17
18.5	6	13
19.0	17	278

*Data were collected between June 1993 and November 1993.
**To obtain stress in MPa, multiply ksi values by 6.895.

There are large discrepancies between the two sets of bolt data. Some of this discrepancy may be attributed to wind direction effects (prevailing southwesterly winds), which could influence the number of tension cycles experienced. The maximum stress ranges measured for the welds and anchor bolts are reasonable.

Dead Load Stresses Measured in Anchor Bolts and Welds

The structure was instrumented before assembly so that dead load stresses could be determined. Measured strains for both mastarm erection and traffic signal attachment are shown in Table 5.

TABLE 5

Measured Dead Load Strains on Traffic Signal Structure

Gage Location	Strain Due to Mastarm*	Strain Due to Traffic Signals*
1	338	404
2	195	180
3	-144	-253
4	68	37
5	106	118
6	-194	-250
7	16	21
8	102	123
9	-44	-64
10	-92	-136

*Units are 10^{-6} in/in. To calculate stress in psi, multiply strain values by 30×10^6. To calculate stress in MPa, multiply strain values by 207×10^3.

The strains recorded do not quite conform to the generally expected behavior. That is, Gages 1 and 3 are expected to show equal but opposite strains, as are Gages 5 and 6. Gages 2 and 4, located near the neutral

axis for vertical bending, should be showing more nearly zero strain. The anchor bolt strain gages would be expected to show comparable tensile strains in Gages 7 and 8 and comparable compressive strains in Gages 9 and 10. Some of the apparent discrepancies in these readings are attributed to experimental errors. However, most of the difference in expected behavior at the weld connection is attributed to the rapidly changing strain gradient near the welds. The areas that are expected to be in tension are in tension and the areas which are expected to be in compression are in compression; the normally expected behavior of a cantilever beam in pure bending is simply modified in close proximity to the fillet welds. Another factor affecting the experimental results is that the connection, although analyzed using cantilever assumptions, is really not rigidly fixed because of the deflection of the vertical pole caused by the weight of the mastarm. This elastic support condition has the effect of reducing the stress at the connection. The maximum strains for the welds and the anchor bolts are reasonable.

Strain Versus Tip Deflection for Tapered Cantilevered Mastarm

In order to note the sensitivity of certain details, strains were measured for a series of downward tip deflections. Strains in Gages 1, 5, and 8 were measured for downward tip deflections of 0.5 inch (12.7 mm) increments to a total deflection of 6.0 inches (157.4 mm). The deflection was accomplished using a steel cable attached to the mastarm tip, and a hand winch fastened to the back end of a 10,000 pound fork lift used as a dead weight. Deflections were measured to the nearest 1/32 inch (0.794 mm) using a fixed steel ruler and a reference mark on the cable. Strain versus tip deflection data are given in Table 6. The data show some variability between deflection increments.

TABLE 6

Measured Strain Versus Tip Deflection

Gage Number	Deflection (inches) 0	0.5	1.0	1.5	2.0	2.5	3.0	3.5	4.0	4.5	5.0	5.5	6.0
						Measured Strain*							
1	0	23	34	43	54	64	73	84	93	102	112	122	133
5	0	15	20	28	35	40	44	50	58	65	67	72	79
8	0	15	16	21	27	32	38	38	45	49	53	57	61

*Strains are given in units of microstrain (10^{-6} in/in). To convert strains to stress in psi, multiply strains by 30 x 10^6. To convert strains to stress in MPa, multiply strains by 207 x 10^3. To convert deflections to mm, multiply by 25.4.

Part of this variability is attributed to gusty wind conditions during the test. Significant transverse tip deflection was noted during data collection. Anchor bolt stresses would be affected in particular. Gage 1 (top of baseplate to mastarm weld connection) shows a sensitivity of 22 microstrain per inch deflection (0.866 microstrain per mm). Gage 5 (tension side of anchor bolt plate to vertical pole weld connection) shows a sensitivity of 13 microstrain per inch deflection. Gage 8 (southwest anchor bolt) shows a sensitivity of 10 microstrain per inch deflection (0.394 microstrain per mm). An analytical check of the strain expected in Gage 1 (due to a six-inch (152.4 mm) deflection) using a cantilevered cylinder of equivalent stiffness indicates that the cantilever assumption overestimated measured strains by a factor of 3.0. Thus, a static analysis using the cantilever assumption is conservative, and cannot accurately reflect the true state of stress due to wind loads. A finite element analysis using springs at the support points would improve the realism of an analytical model. However, as was seen in Chapter 2, there are many factors which affect the behavior of a sign or signal structure,

and a static analysis of a dynamic problem has inherent drawbacks and inaccuracies. Therefore, the use of static stress analysis methods for fatigue study of overhead sign and signal structures is not recommended.

Vibration Frequency and Damping for Tapered Cantilevered Mastarm

The frequency and amplitude of vertical vibration (due to vortex shedding) of the traffic signal at the Physical Research Laboratory was measured experimentally using an accelerometer and an oscillographic chart recorder. At the time of measurement, wind speeds recorded at this site ranged from 12 - 20 mph (19.31 - 37.19 kmph). Conditions were very gusty. It was of interest to measure the vortex shedding frequencies and to compare these frequencies to calculated natural frequencies. Natural frequencies were calculated for the mastarm by finite element analysis (ALGOR). Vibration frequencies for a windspeed range of 12 - 16 mph (19.31 - 26.75 kmph) varied between 1.8 and 2.2 Hz. Vibration frequencies for windspeeds between 15 and 20 mph (24.14 and 37.19 kmph) ranged between 3.5 and 5.3 Hz. Calculated natural frequencies for the tapered mastarm for the first three vertical modes were 1.06, 5.5, and 14.2 Hz respectively. Obviously, the mastarm was vibrating in synchronization with the first two natural modes at certain windspeeds.

The structural damping factor for the traffic signal mastarm was measured to be $\xi = 0.006$ using the chart recorder output and the following relation:

$$2\pi\xi = \ln(A_i/A_{i+1}) \qquad (12)$$

Where ξ = structural damping,
A_i = vibration amplitude,
A_{i+1} = next vibration amplitude.

As expected, the traffic signal structure is very lightly damped.

Controlled Wind Speed Test Data

Prior to installation and instrumentation at the Physical Research Laboratory, the traffic signal structure was shipped to Smith-Emery Company in Los Angeles, California to undergo controlled wind speed tests. The wind force was supplied by a blower which was set up to blow air on the outermost traffic signal. Unfortunately, the structure is too large to be tested with wind applied over the entire surface at any test facility short of a large scale wind tunnel. The wind load applied by this test was analogous to a point wind load at the outer traffic signal. Although this loading is not seen in practice, it was of interest to note the behavior of the structure to a constant wind speed. Figures 18 through 21 show photographs of the test setup and wind application. The instrumented section was the top fillet weld connection at the 12, 3, 6, and 9 o'clock positions. Strain data were collected over five minute intervals for wind speeds of 20, 40, 50, 60, 70, and 80 mph (32.19, 64.37, 80.47, 96.56, 112.65, and 128.74 km/hr). The wind speed for each test was set by a hand-held anemometer held in front of the traffic signal prior to data collection.

Collected strain data were converted to stresses. This stress data is presented graphically in Figures 22 through 45. The direction of wind load application was from west to east. The data are quite variable, and indicate that even steady winds will induce variable amplitude cyclic loading. Table 7 shows maximum, minimum, average, and range of stresses for each strain gage for each applied wind load.

The general trend of the data in Table 7 shows an expected increase in stress range with wind speed, although the increase is modest. It was noted in Chapter 2 that the drag coefficient for cylinders drops to 0.3 in

the transitional Reynolds number regime. A similar effect was noted for the experimental data for the west strain gage. The average strain data from the west strain gage were used to calculate the apparent C_D of the in-place traffic signal for each wind speed tested using equation (3). The results are shown in Table 8.

The average apparent C_D is 0.39. This finding is not in agreement with published data on drag of flat plates normal to the flow direction, where C_D is about 1.2 at Re = 10^5 for a rectangular shape with length to width ratio of 5:1.[20] Note, however, that Re = 10^5 is in the subcritical range, while the calculated values are for the transitional Reynolds number regime. Also, the traffic signal was mounted on a long, flexible mastarm which could have influenced the experimental response. Additional investigation of the in-situ estimation of drag coefficients for traffic signals and sign panels is needed to better characterize this behavior.

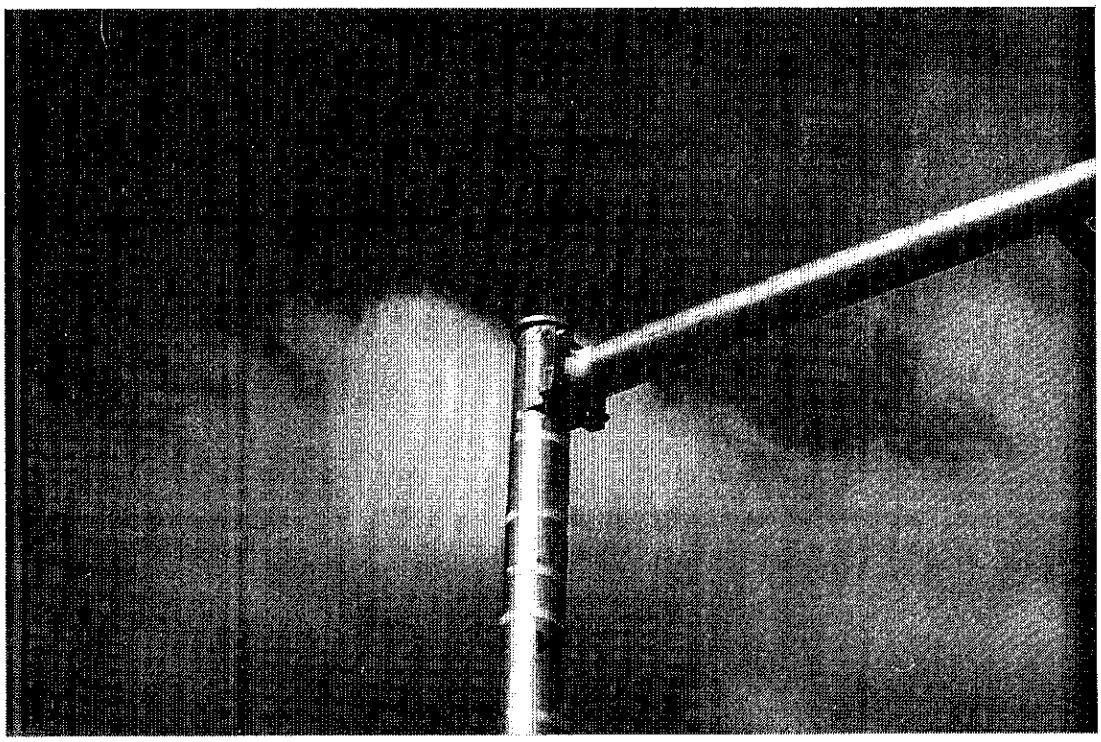

Figure 18. Instrumented section of traffic signal structure for controlled wind speed tests. Testing and instrumentation were conducted at Smith-Emery Company, Los Angeles, California. Strain gages were placed at 12, 3, 6, and 9 o'clock positions near the toe of the fillet weld.

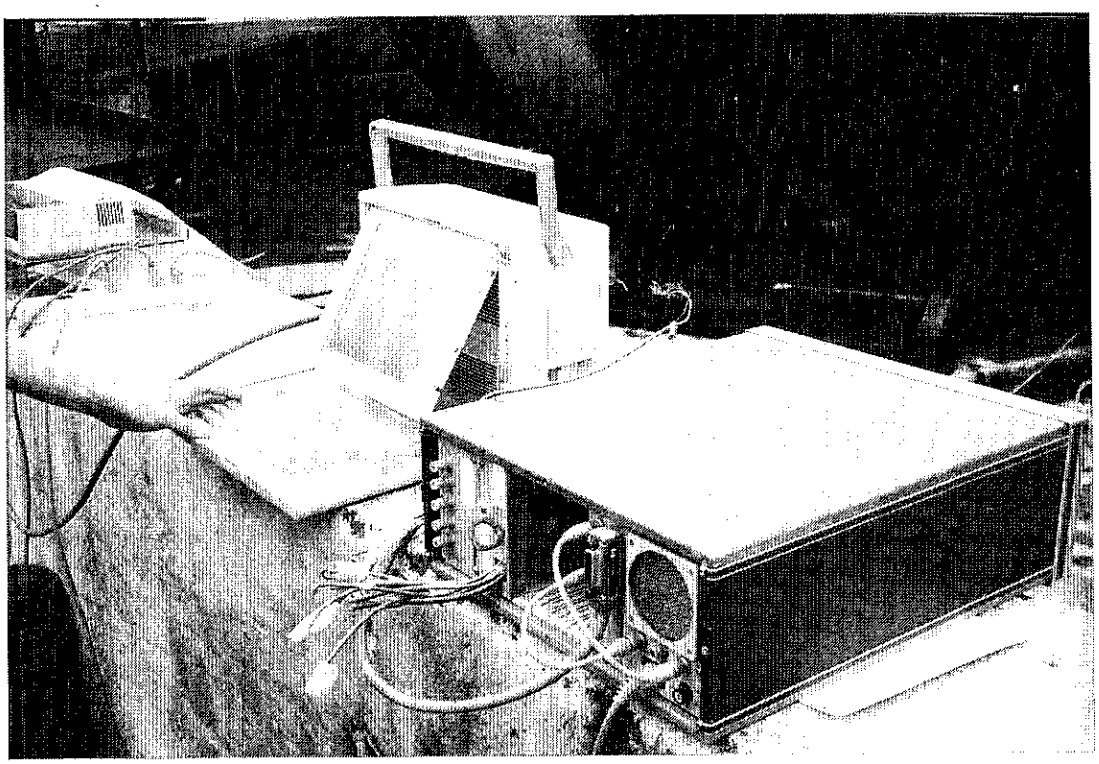

Figure 19. Data acquisition system used for controlled wind speed tests.

Figure 20. Equipment and setup used to apply wind loads. Technician is checking wind speed with a hand-held anemometer.

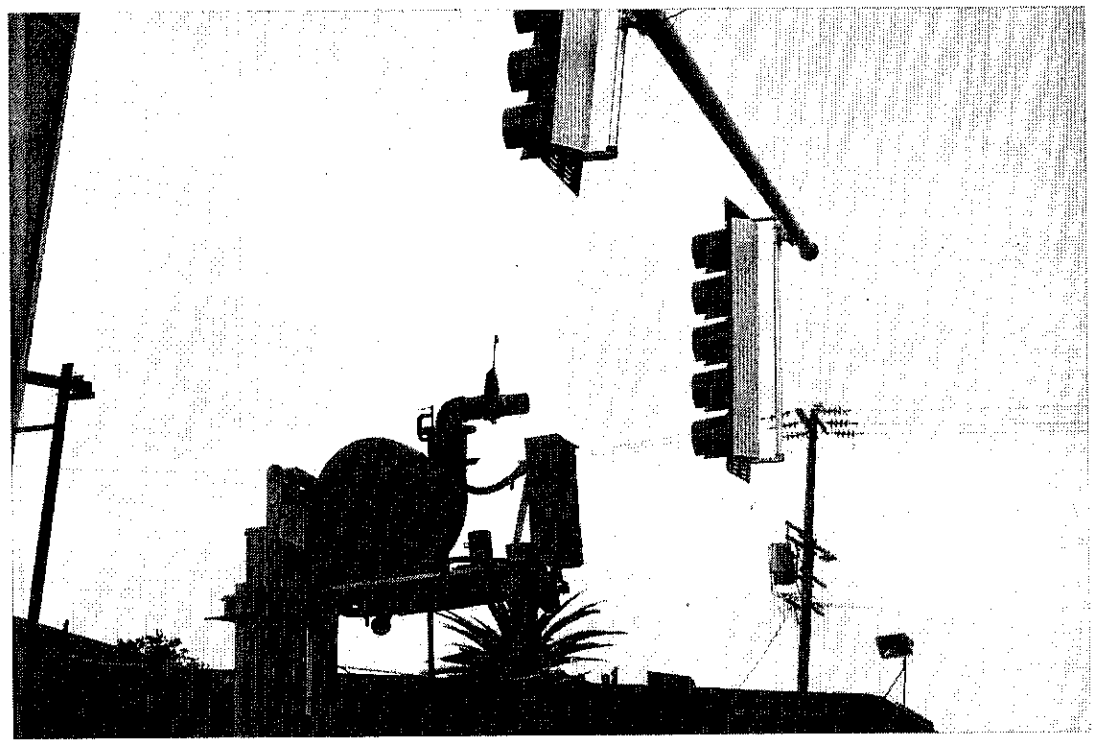

Figure 21. Eighty mile per hour (133.6 kmph)wind load being applied to traffic signal structure.

TABLE 7

Statistics For Controlled Wind Speed Test Data

	Maximum Stress (psi)*	Minimum Stress (psi)	Average Stress (psi)	Stress Range (psi)
Lift Stresses (Top Strain Gage) Wind Speed (mph)**				
20	-138.4	-2119.9	-1210.0	1981.5
40	868.5	-971.6	-6.3	1840.0
50	1544.5	-1003.6	304.5	2548.0
60	2252.3	-720.6	270.1	2972.9
70	2113.9	-434.2	705.8	2548.2
80	2393.9	-154.3	995.7	2548.2
Lift Stresses (Bottom Strain Gage) Wind Speed (mph)				
20	3.3	-2119.8	-1113.2	2123.1
40	869.2	-1819.8	-216.1	2689.0
50	1119.3	-1570.4	-17.6	2689.7
60	2110.2	-1287.3	-0.6	3397.5
70	1971.9	-1000.8	335.0	2972.8
80	2251.8	-1145.7	545.2	3397.5
Drag Stresses (West Strain Gage) Wind Speed (mph)				
20	3117.6	-4101.1	644.2	7218.7
40	3982.5	-2103.9	995.6	6086.4
50	4093.1	-2418.8	1474.4	6511.9
60	4801.2	-3268.1	1685.6	8069.4
70	4945.9	-2698.8	2814.3	7644.7
80	6783.9	-1994.2	2918.6	8778.1
Drag Stresses (East Strain Gage) Wind Speed (mph)				
20	994.3	-3251.8	-697.2	4246.1
40	1011.4	-2526.7	-733.7	3538.1
50	1543.5	-2136.9	-421.7	3680.4
60	1685	-1570.8	86.9	3255.9
70	839.1	-1425.8	-152.8	2264.8
80	1260.5	-1429.3	-0.3	2689.8

*To convert stress to MPa, multiply by 6.895×10^{-3}.
**To convert mph to km/hr, multiply by 1.67.

Note: Data is for wind applied to a single traffic signal only, not the entire structure.

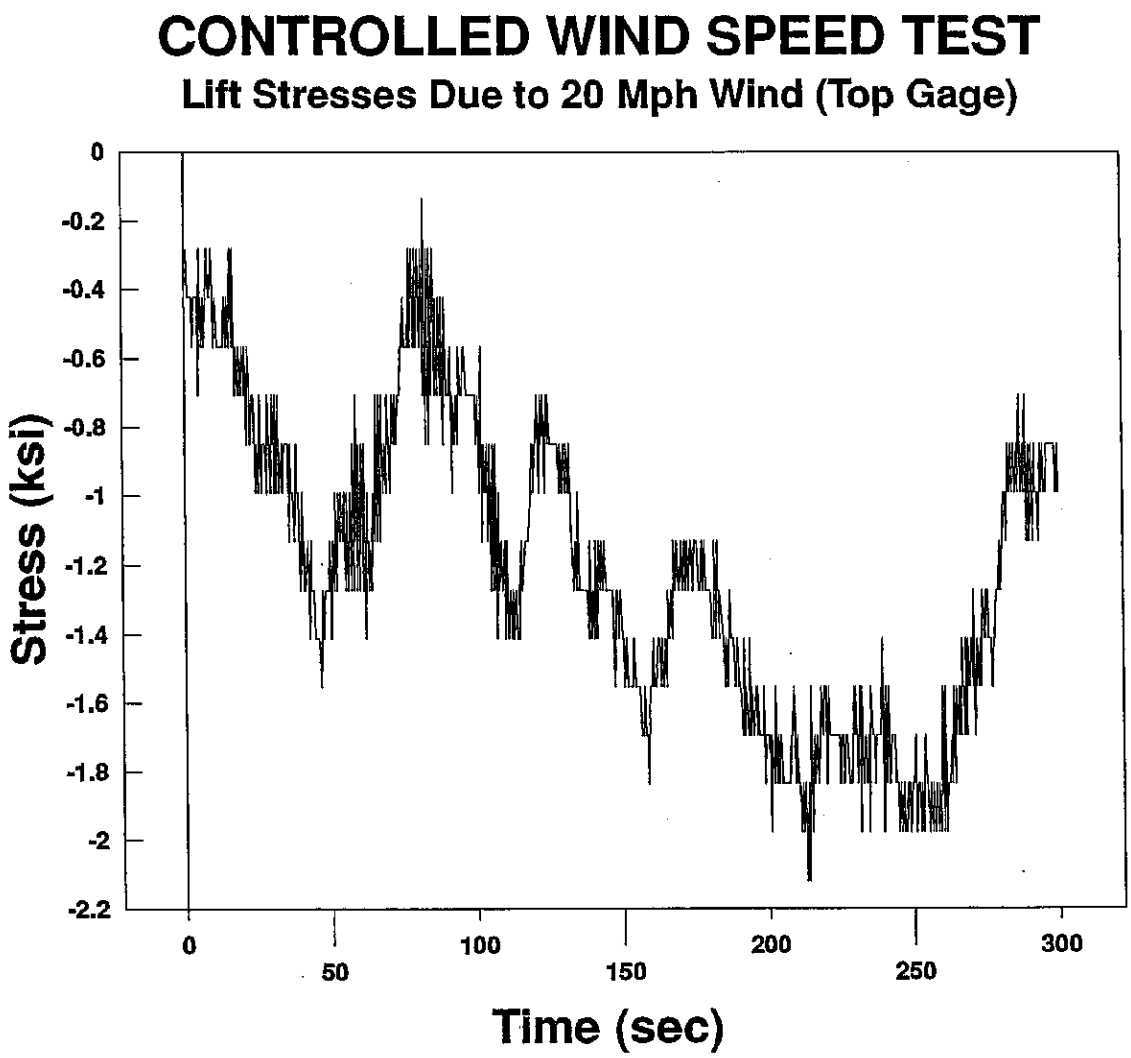

Figure 22. Lift stresses at top strain gage due to 20 mph (32.19 km/hr) controlled wind application.

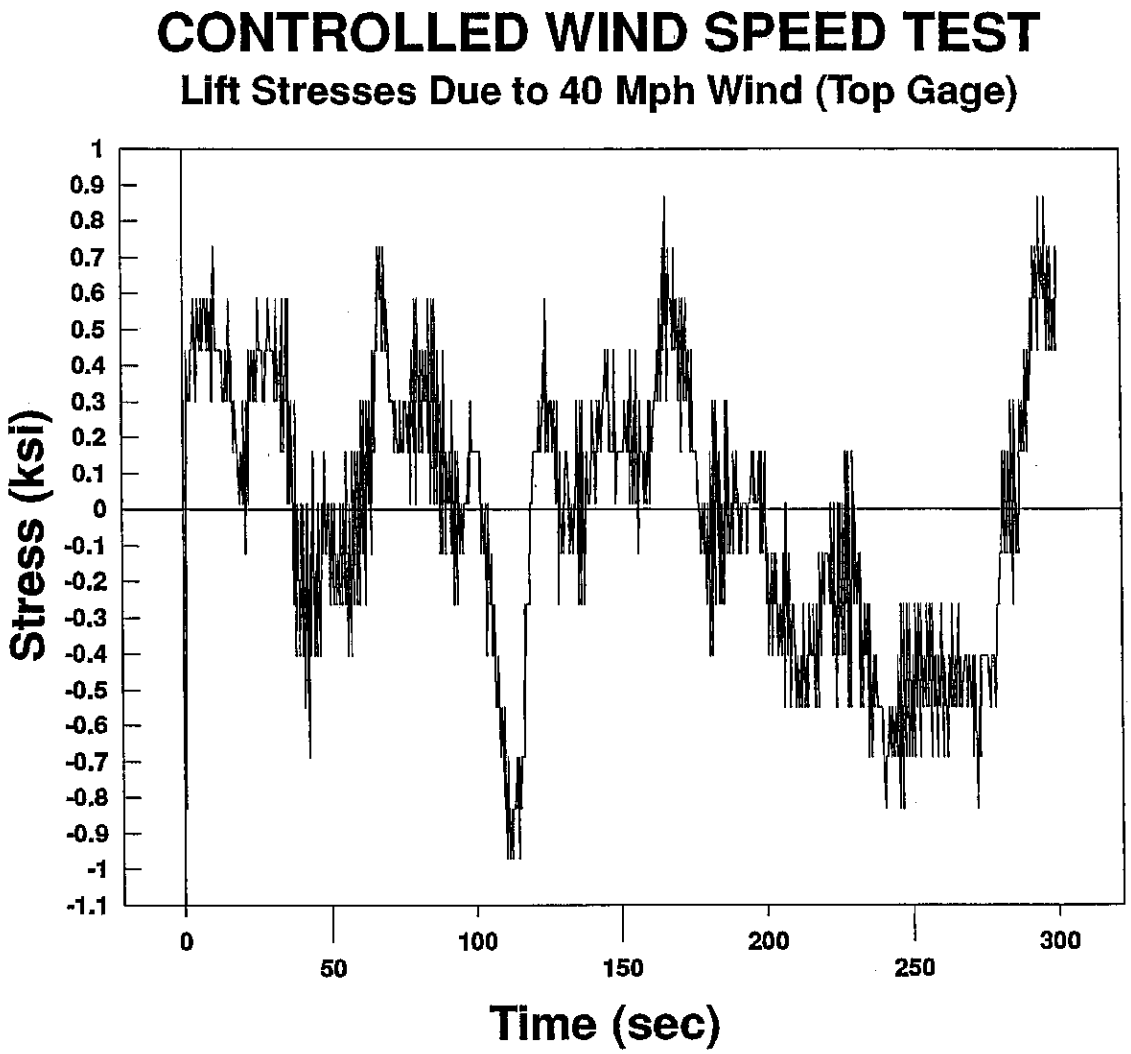

Figure 23. Lift stresses at top strain gage due to 40 mph (64.37 km/hr) controlled wind application.

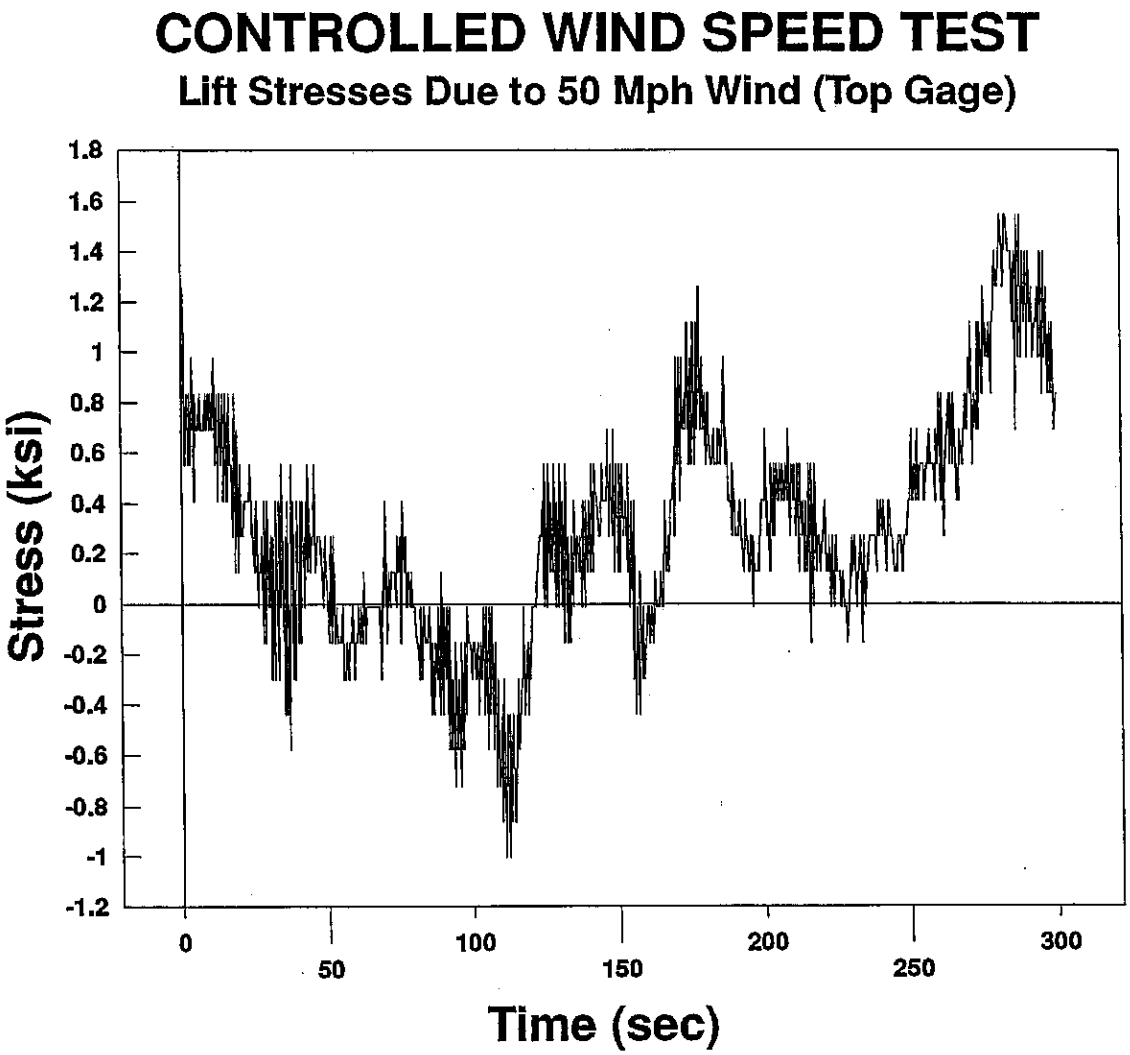

Figure 24. Lift stresses at top strain gage due to 50 mph (80.47 km/hr) controlled wind application.

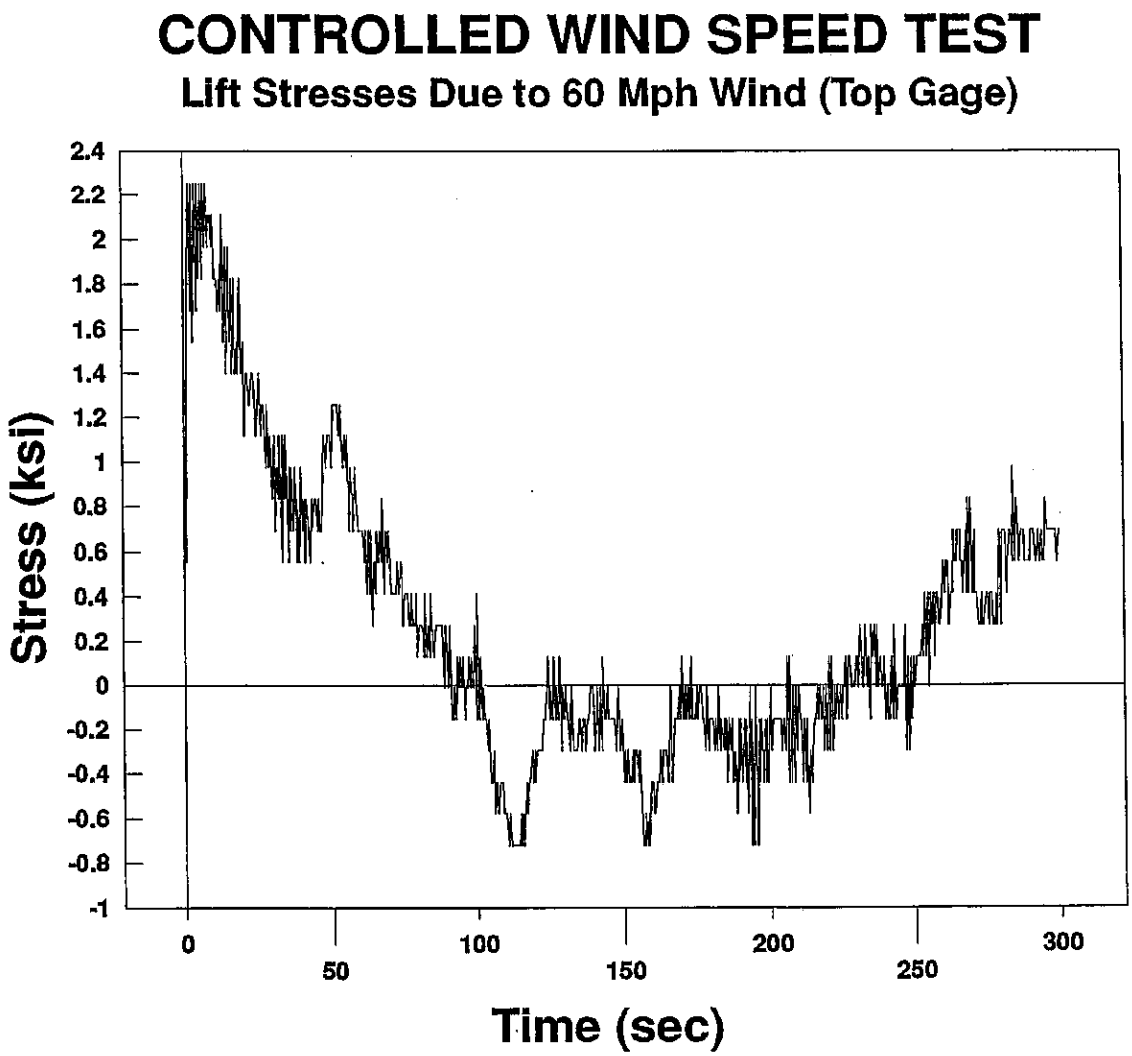

Figure 25. Lift stresses at top strain gage due to 60 mph (96.56 km/hr) controlled wind application.

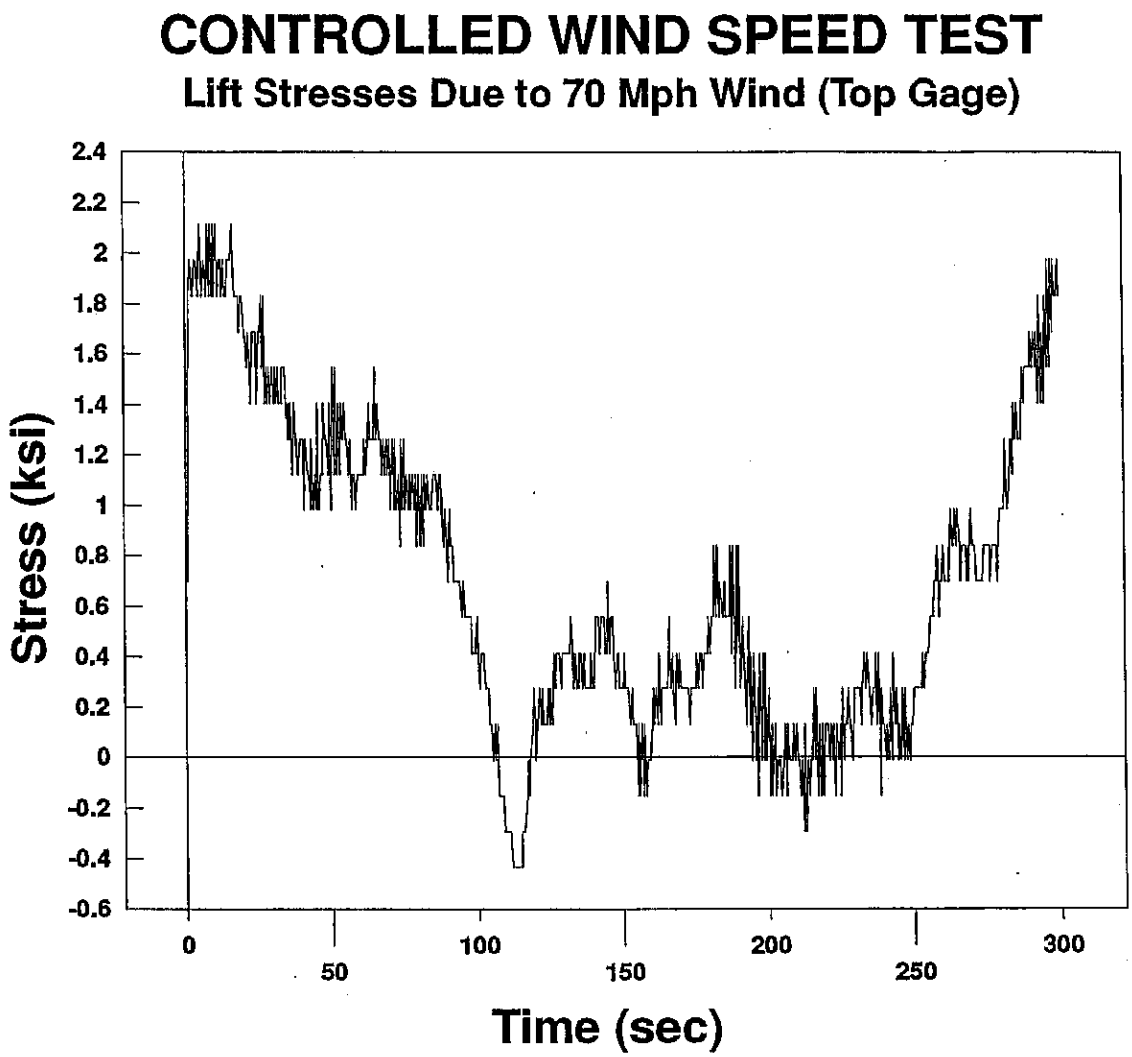

Figure 26. Lift stresses at top strain gage due to 70 mph (112.65 km/hr) controlled wind application.

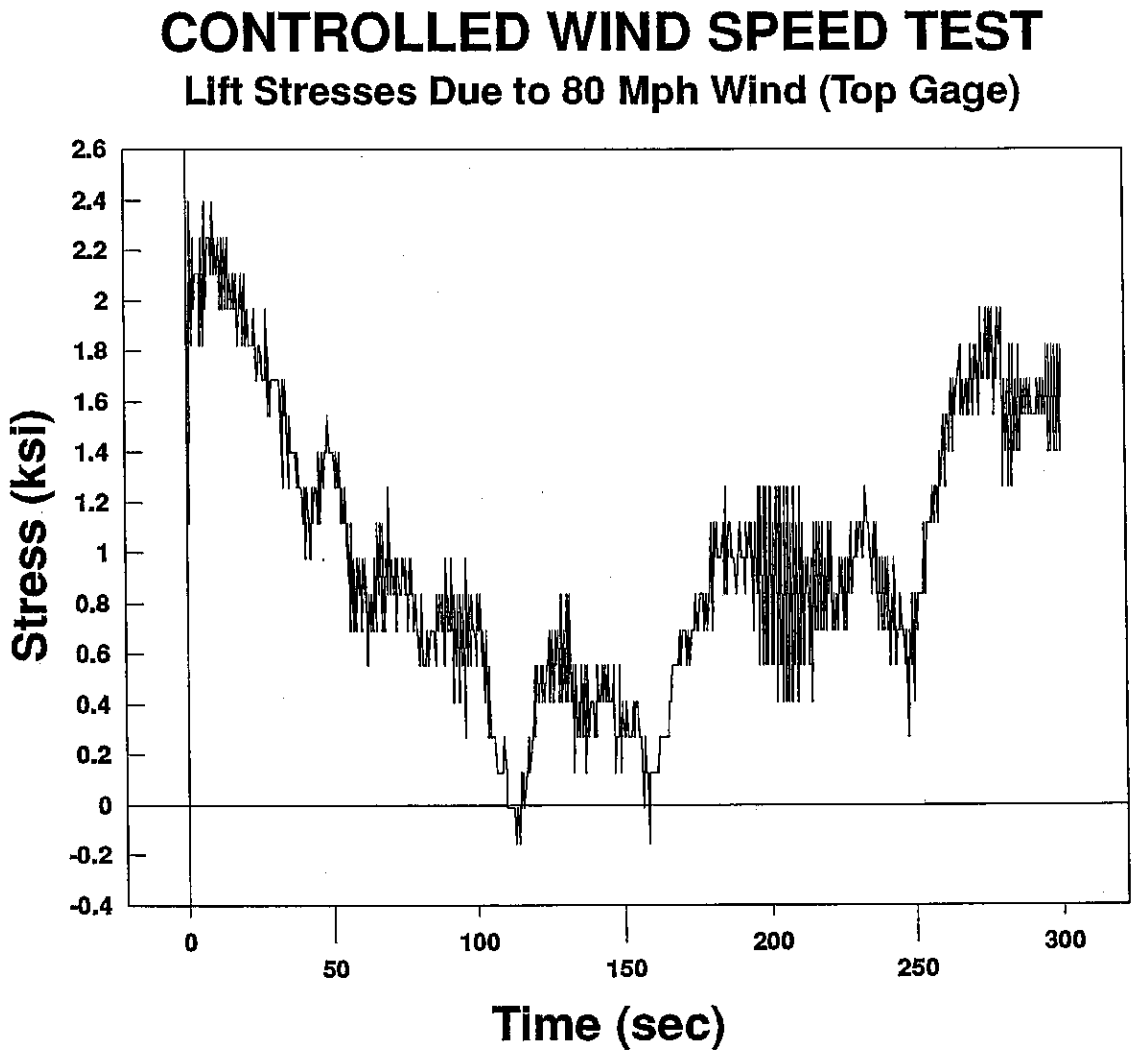

Figure 27. Lift stresses at top strain gage due to 80 mph (128.74 km/hr) controlled wind application.

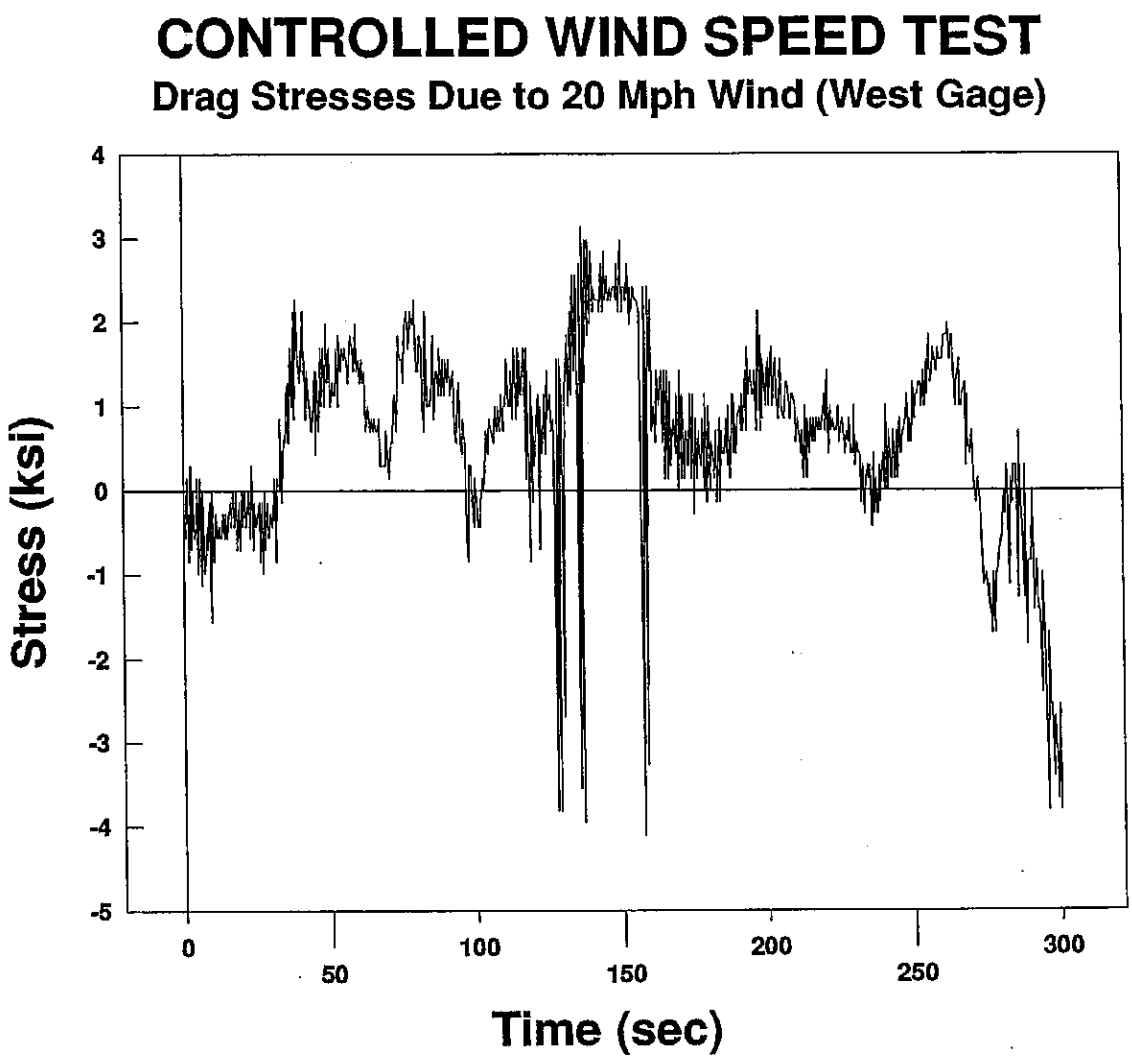

Figure 28. Drag stresses at west strain gage (facing wind) due to 20 mph (32.19 km/hr) controlled wind application.

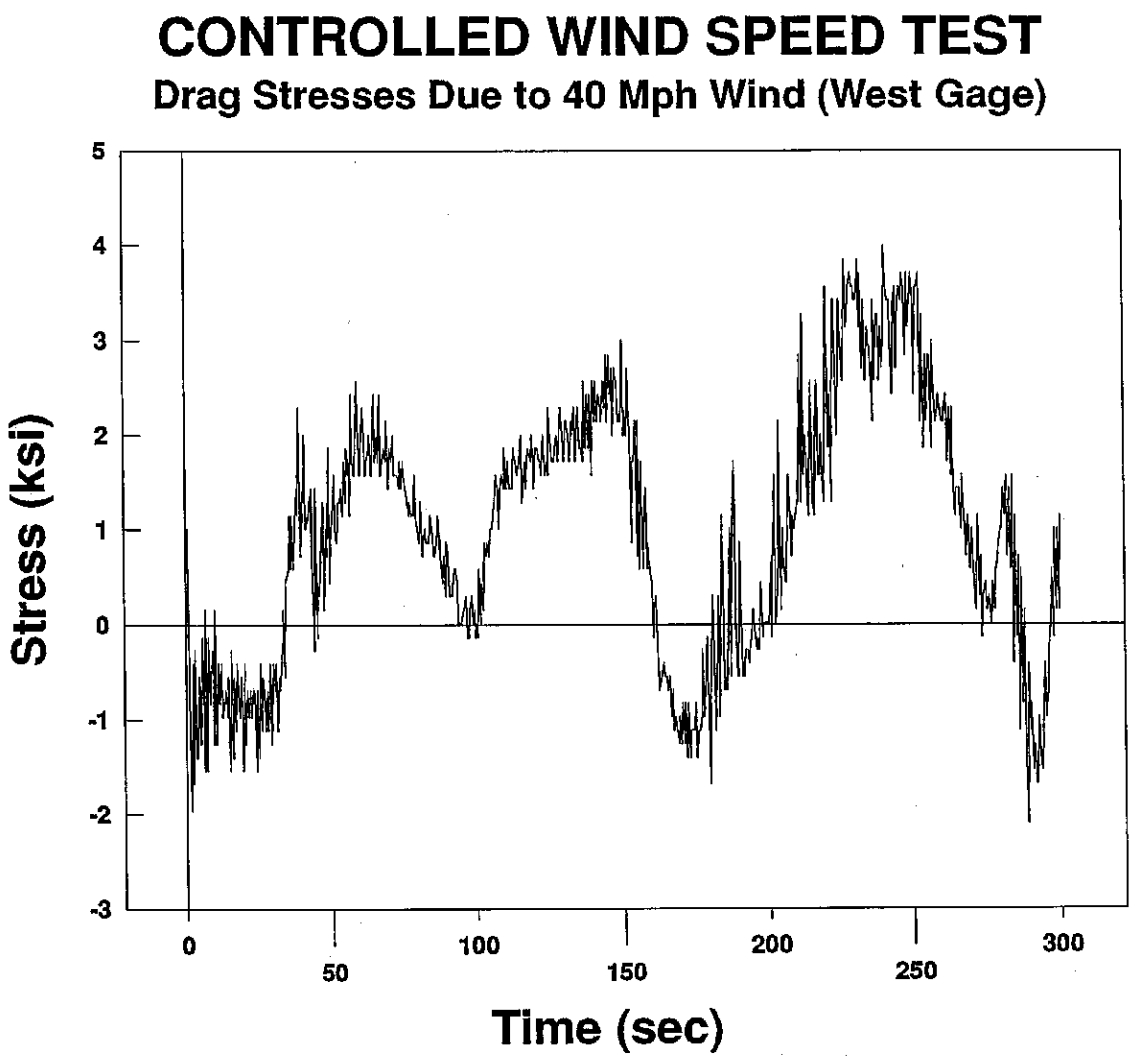

Figure 29. Drag stresses at west strain gage (facing wind) due to 40 mph (64.37 km/hr) controlled wind application.

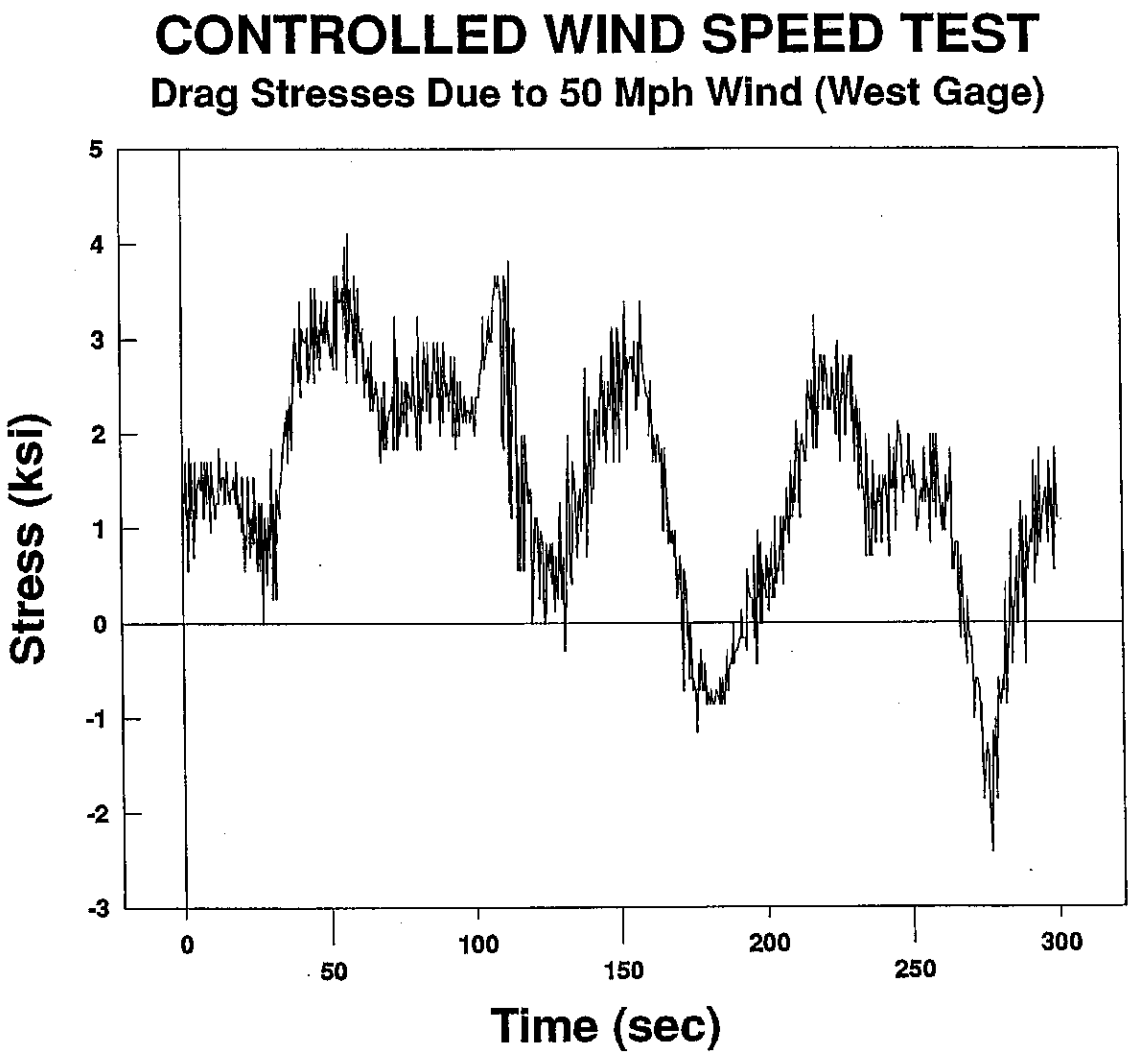

Figure 30. Drag stresses at west strain gage (facing wind) due to 50 mph (80.47 km/hr) controlled wind application.

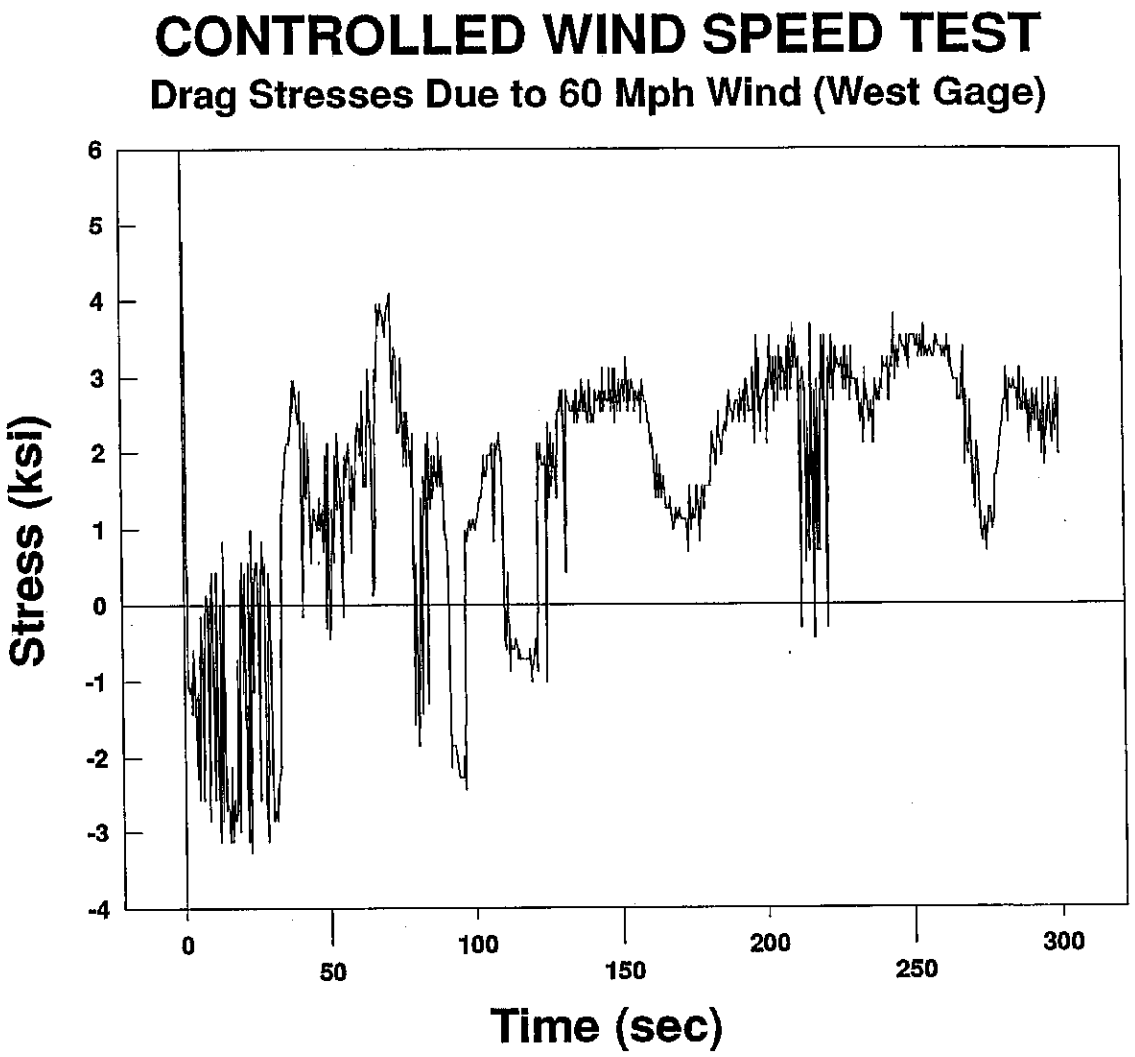

Figure 31. Drag stresses at west strain gage (facing wind) due to 60 mph (96.56 km/hr) controlled wind application.

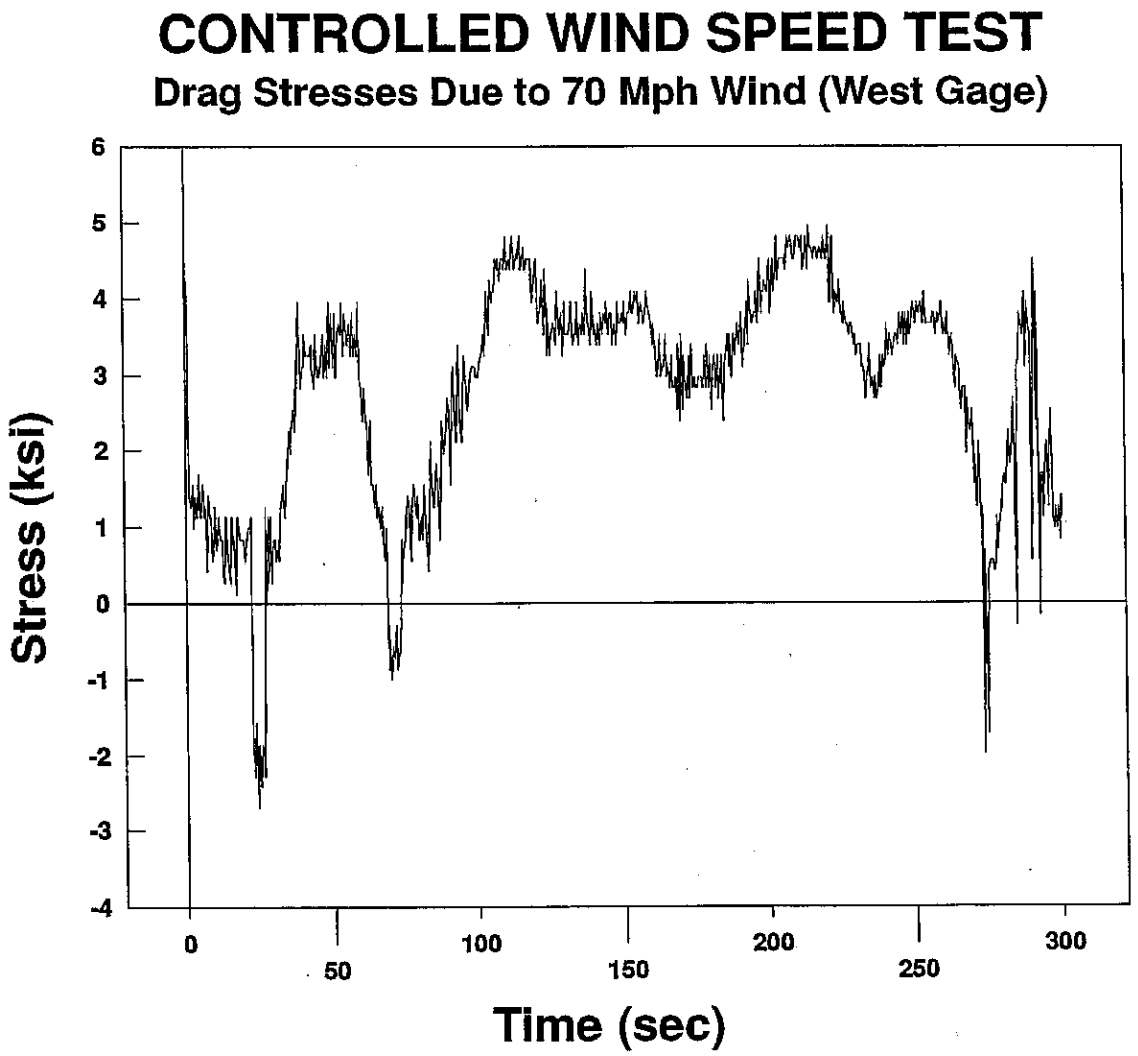

Figure 32. Drag stresses at west strain gage (facing wind) due to 70 mph (112.65 km/hr) controlled wind application.

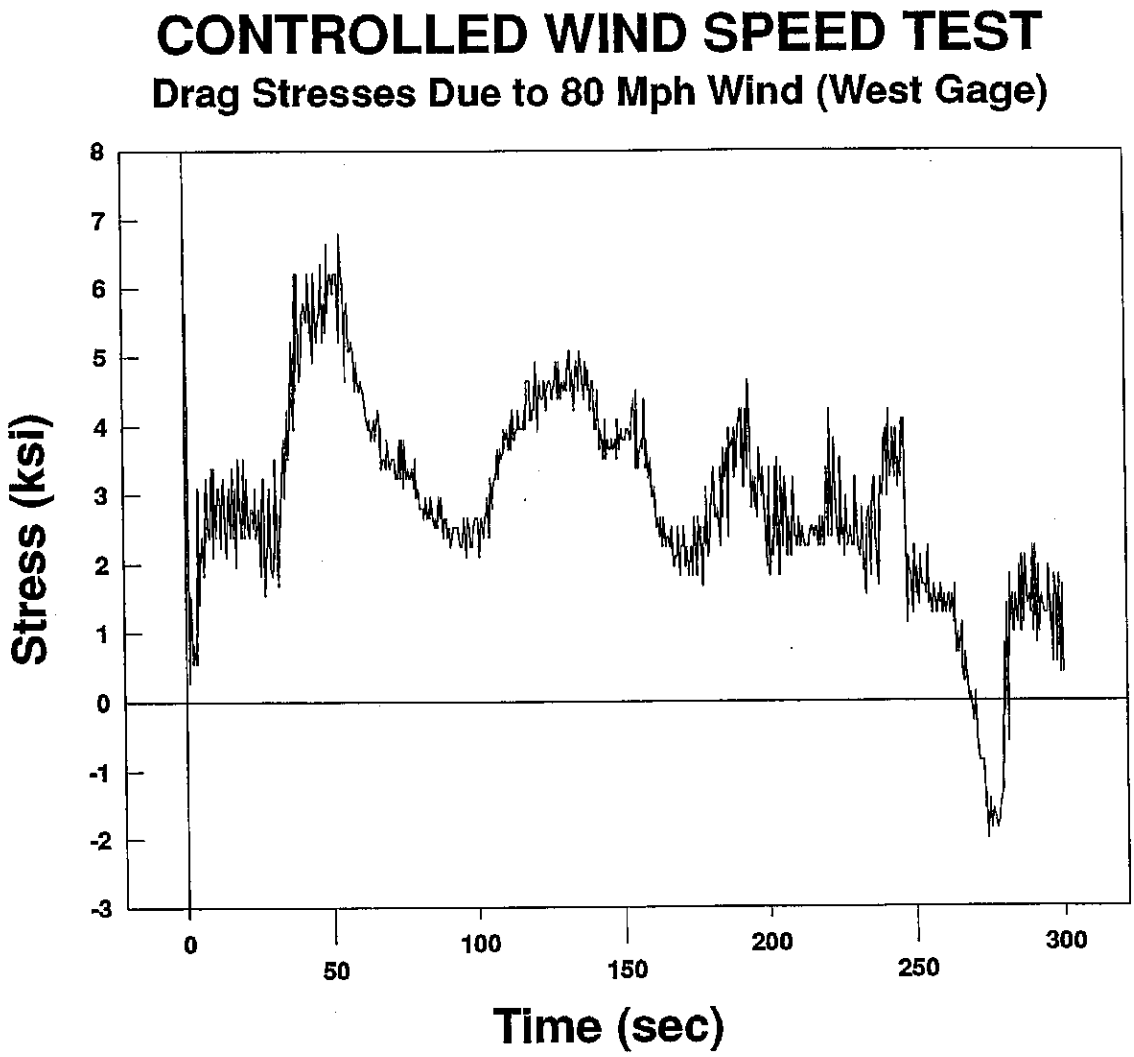

Figure 33. Drag stresses at west strain gage (facing wind) due to 80 mph (128.74 km/hr) controlled wind application.

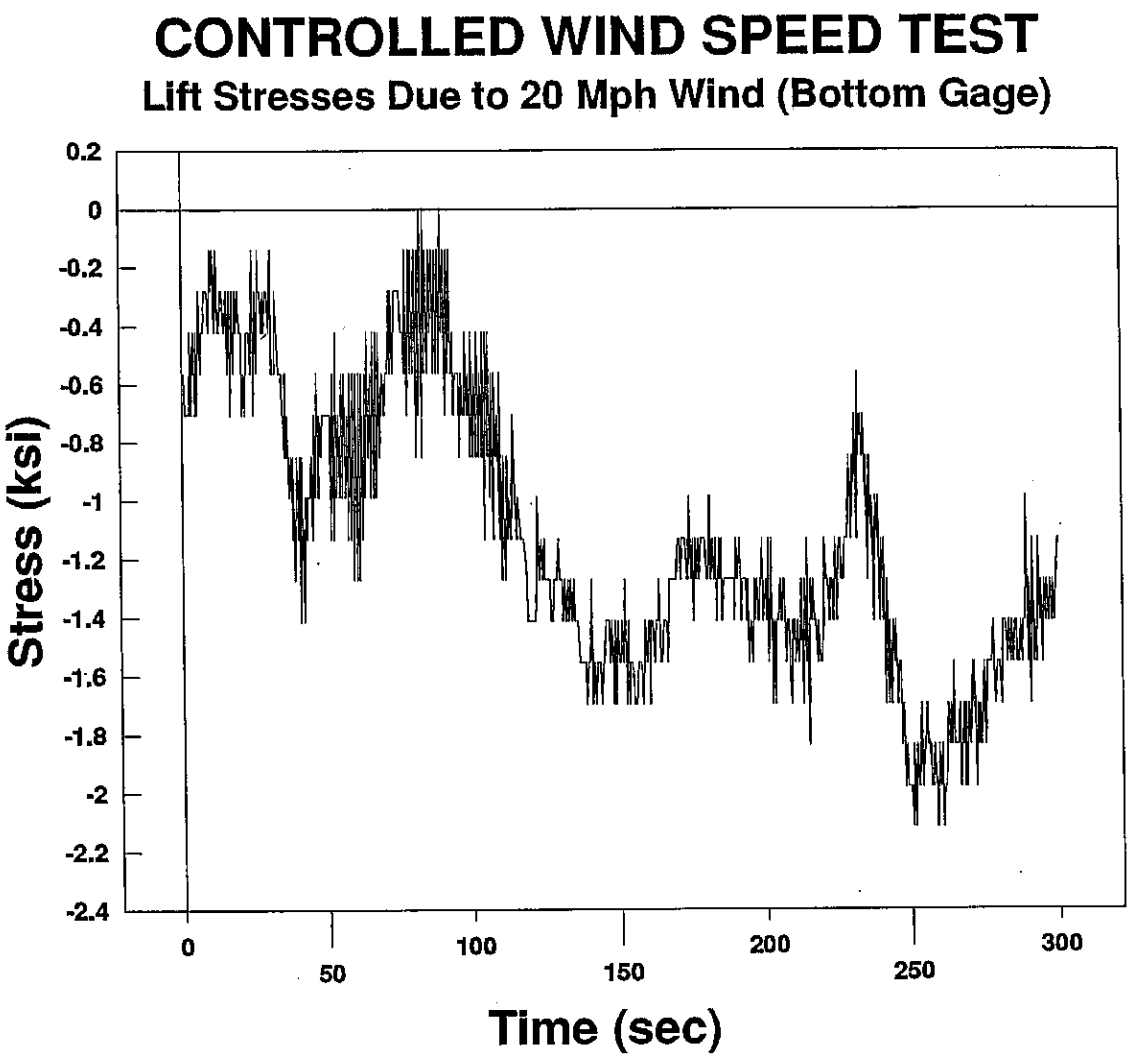

Figure 34. Lift stresses at bottom strain gage due to 20 mph (32.19 km/hr) controlled wind application.

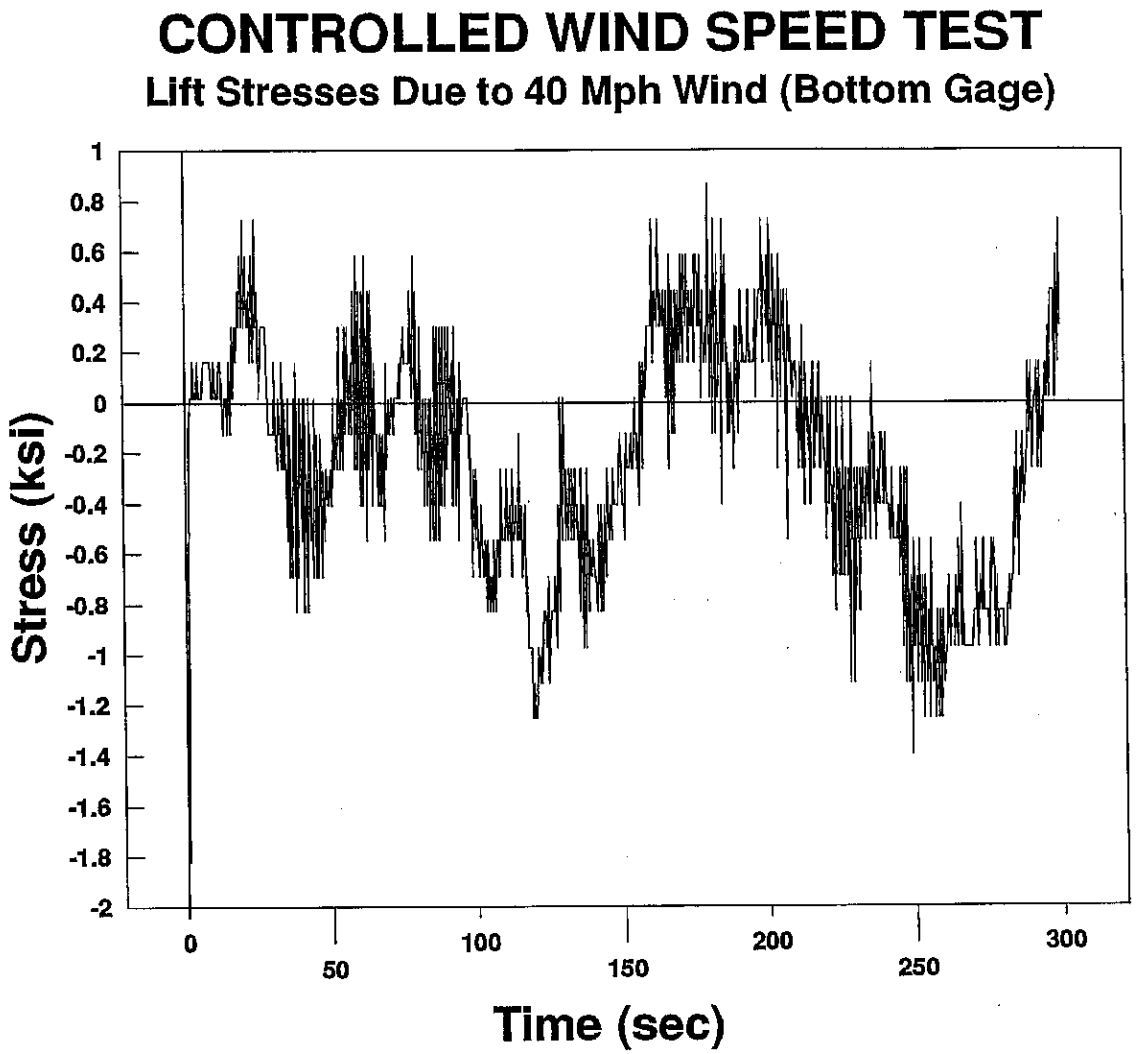

Figure 35. Lift stresses at bottom strain gage due to 40 mph (64.37 km/hr) controlled wind application.

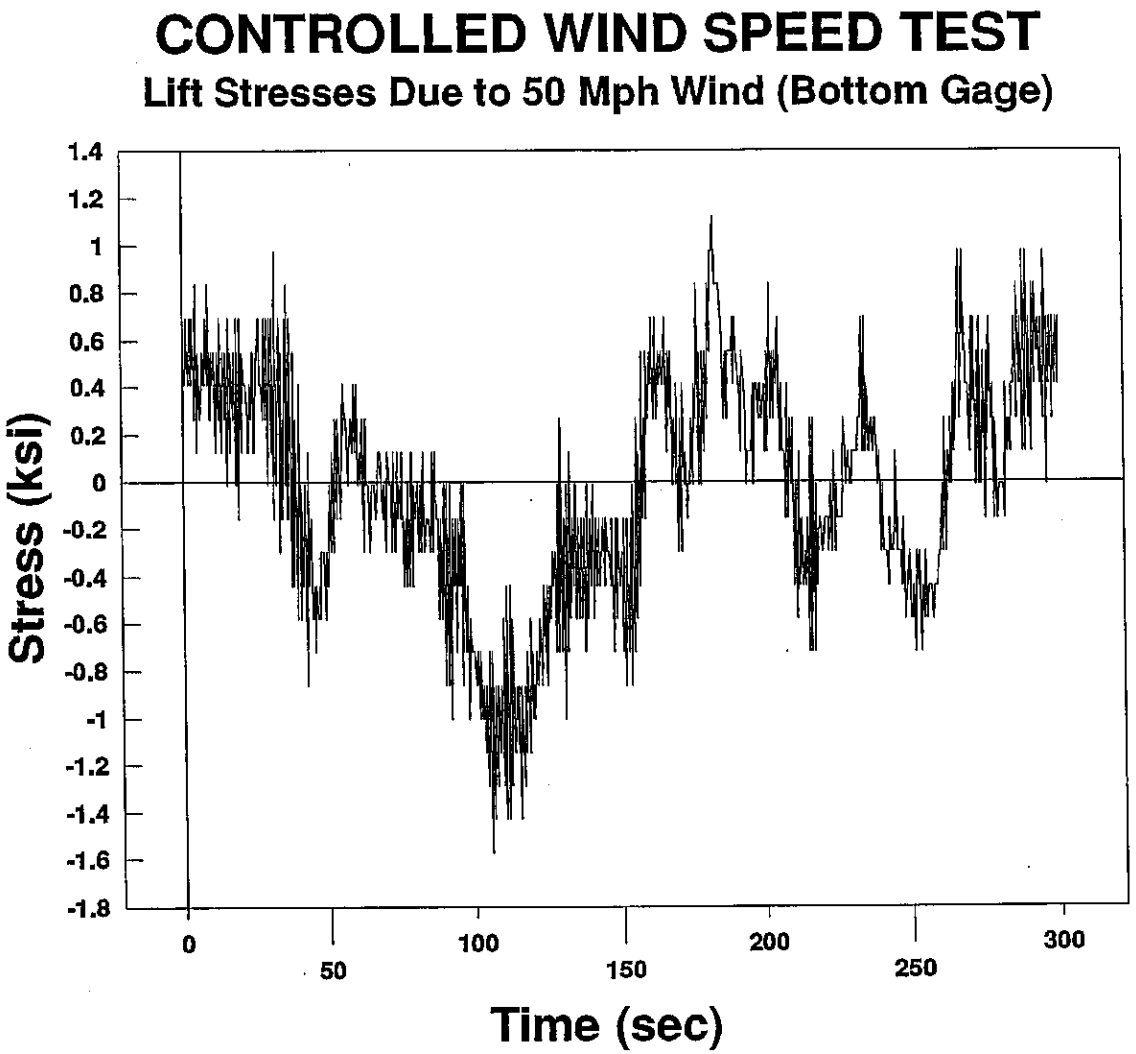

Figure 36. Lift stresses at bottom strain gage due to 50 mph (80.47 km/hr) controlled wind application.

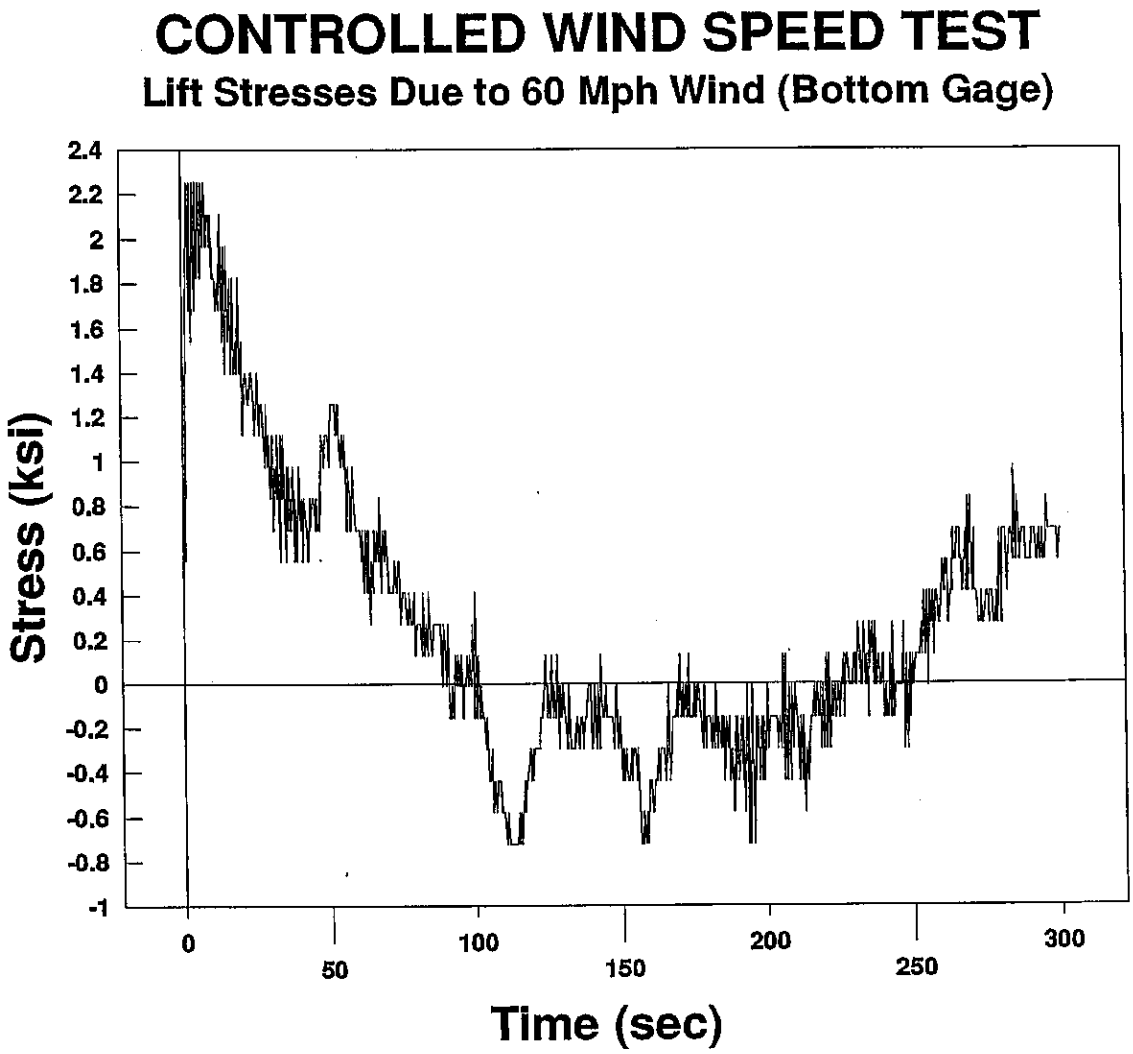

Figure 37. Lift stresses at bottom strain gage due to 60 mph (96.56 km/hr) controlled wind application.

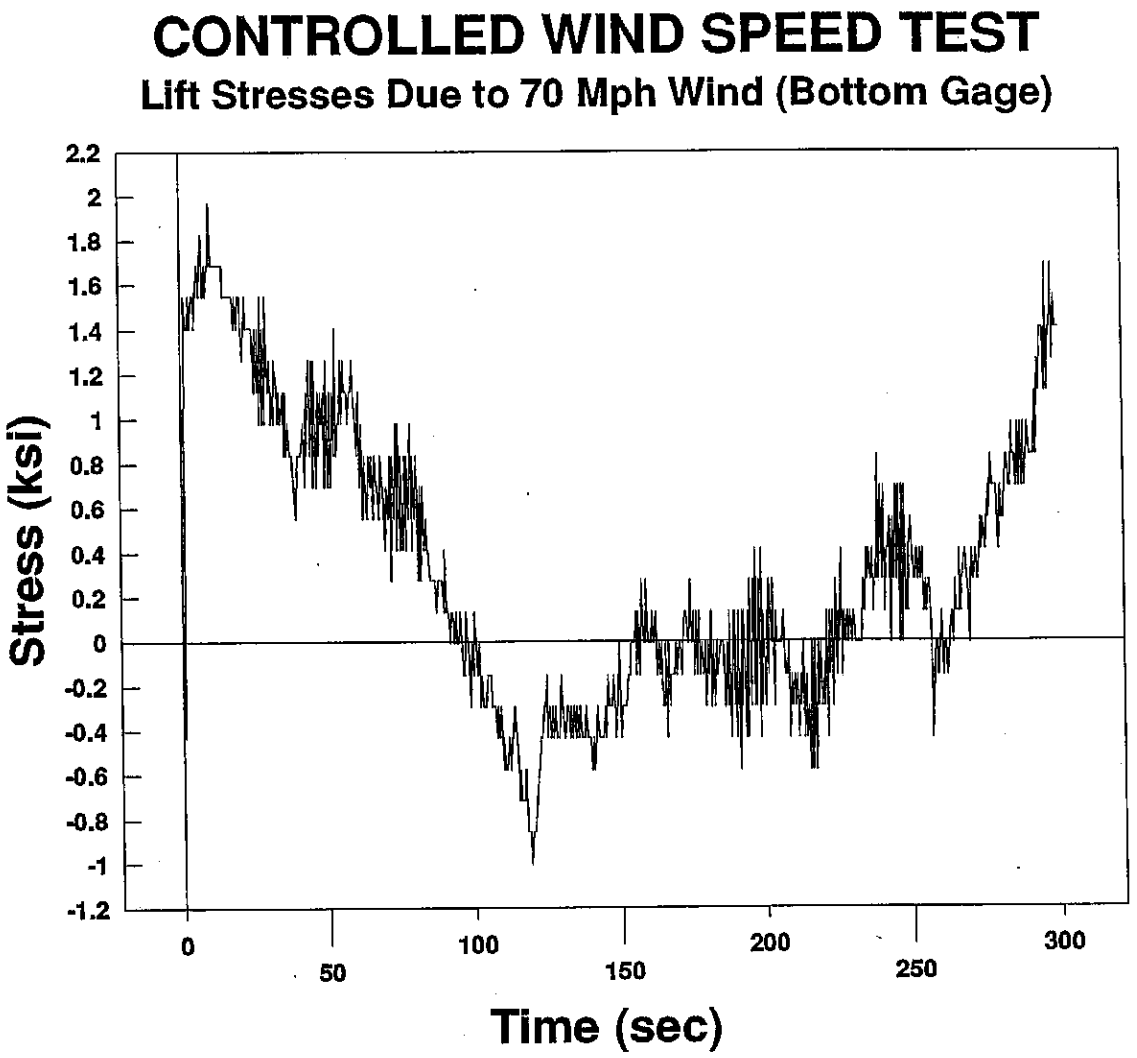

Figure 38. Lift stresses at bottom strain gage due to 70 mph (112.65 km/hr) controlled wind application.

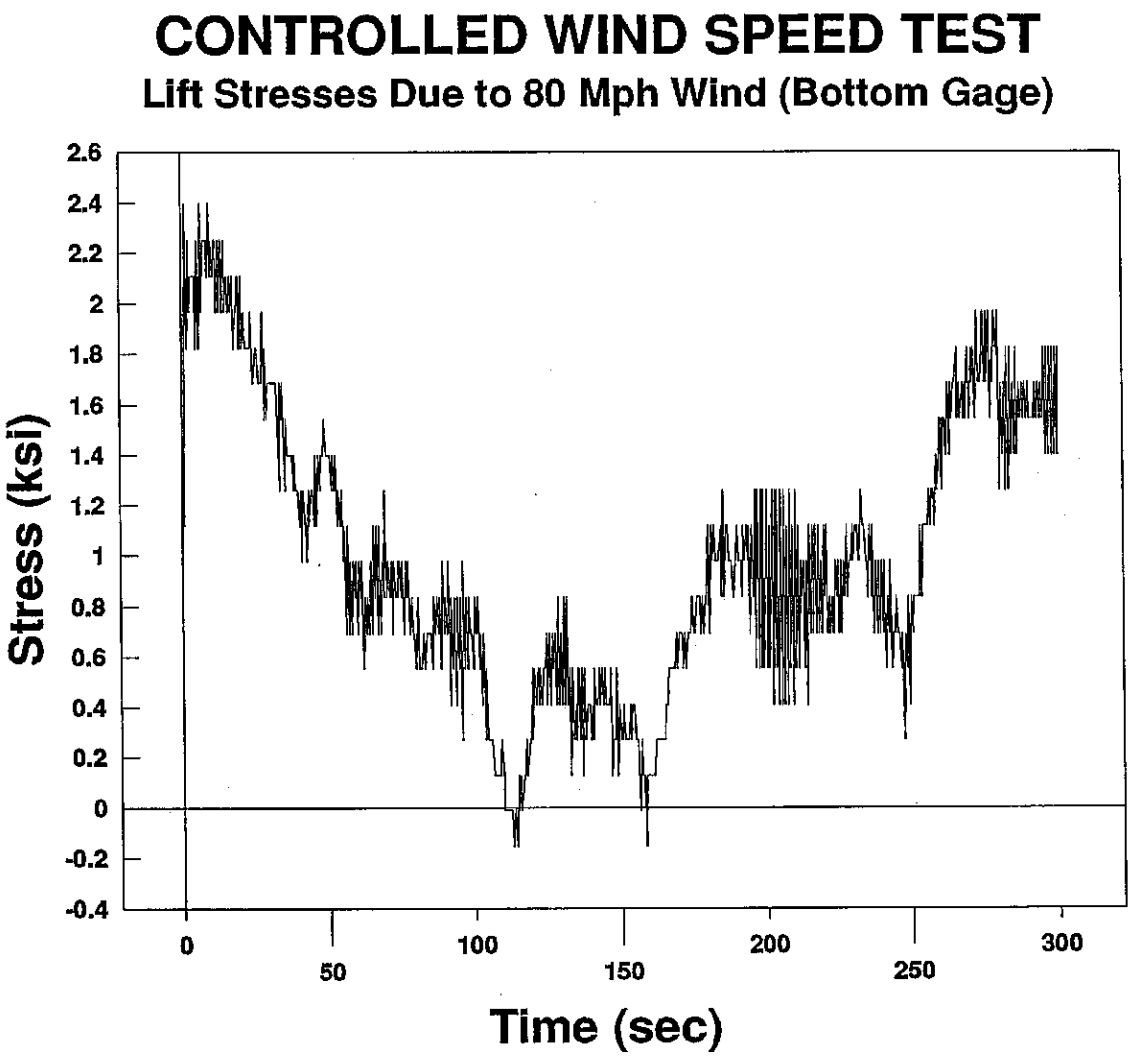

Figure 39. Lift stresses at bottom strain gage due to 80 mph (128.74 km/hr) controlled wind application.

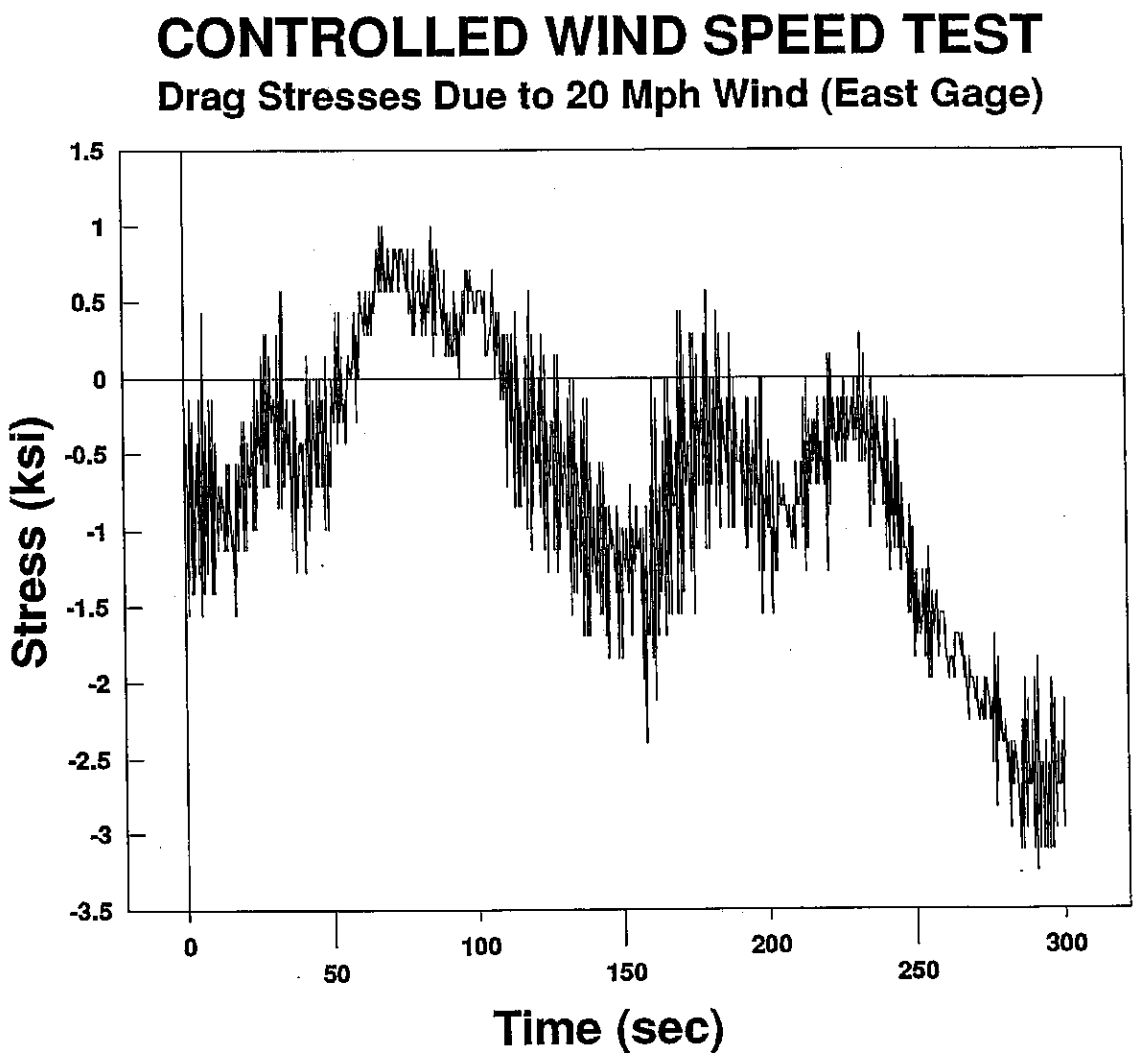

Figure 40. Drag stresses at east strain gage due to 20 mph (32.19 km/hr) controlled wind application.

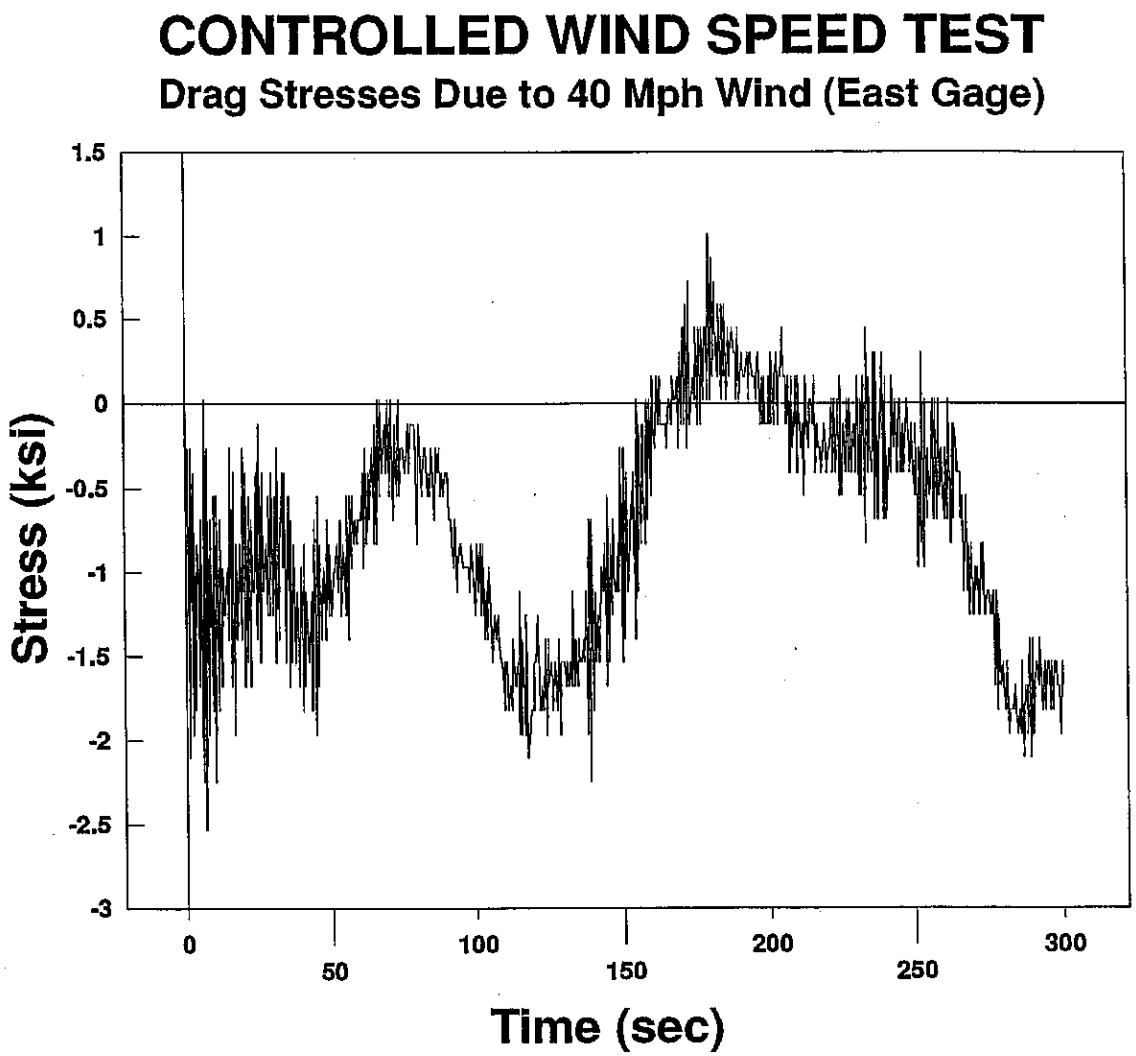

Figure 41. Drag stresses at east strain gage due to 40 mph (64.37 km/hr) controlled wind application.

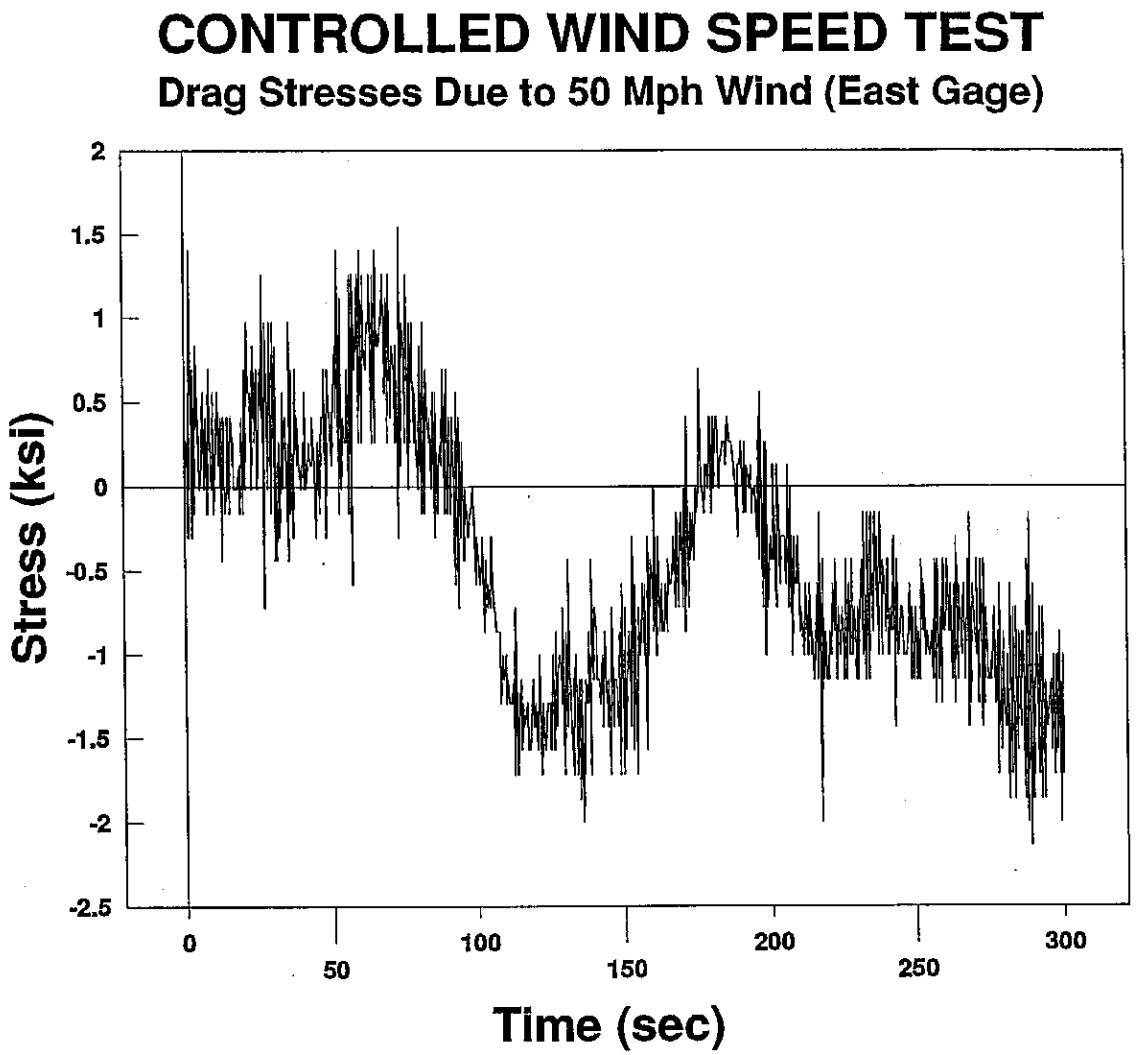

Figure 42. Drag stresses at east strain gage due to 50 mph (80.47 km/hr) controlled wind application.

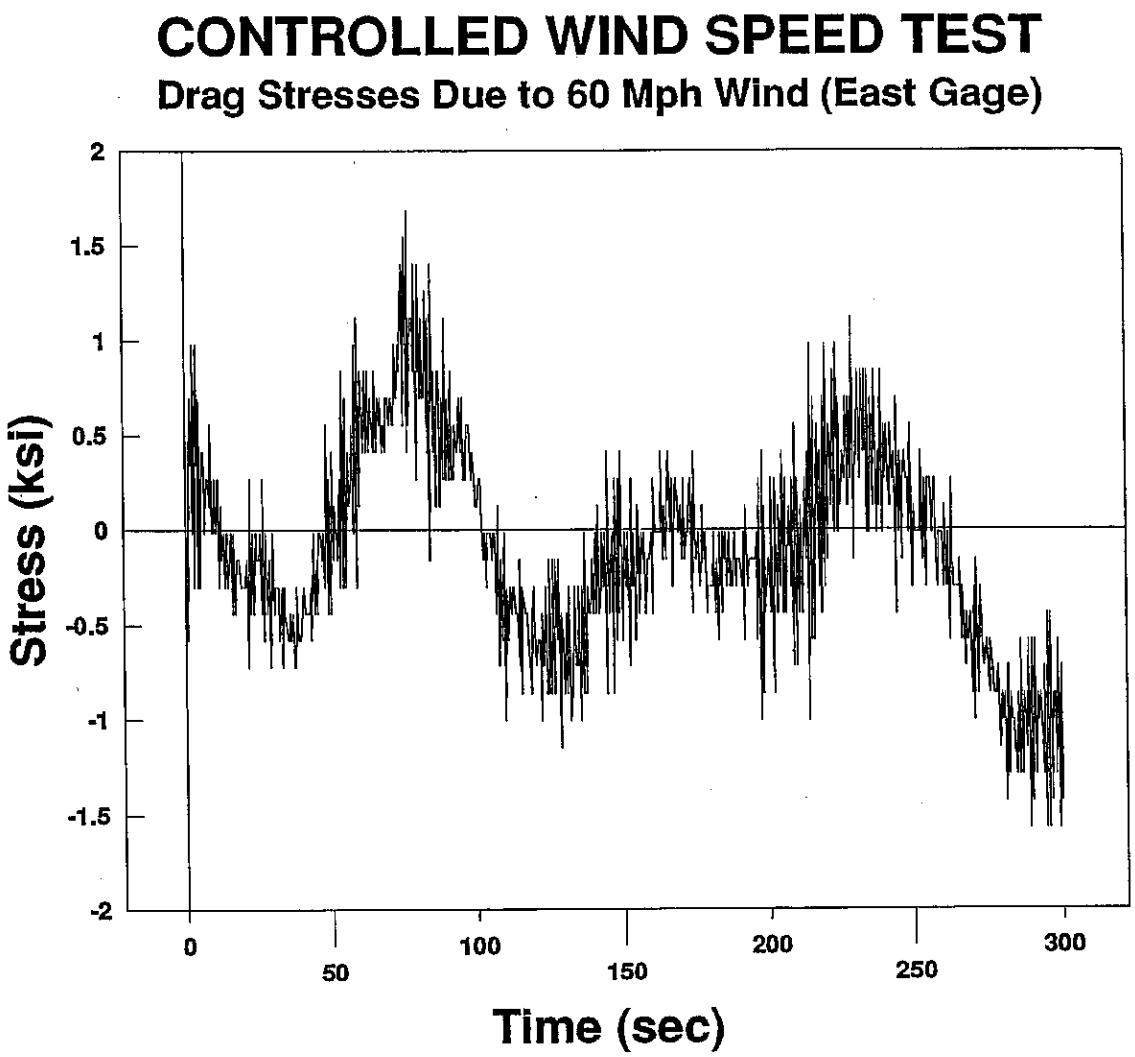

Figure 43. Drag stresses at east strain gage due to 60 mph (96.56 km/hr) controlled wind application.

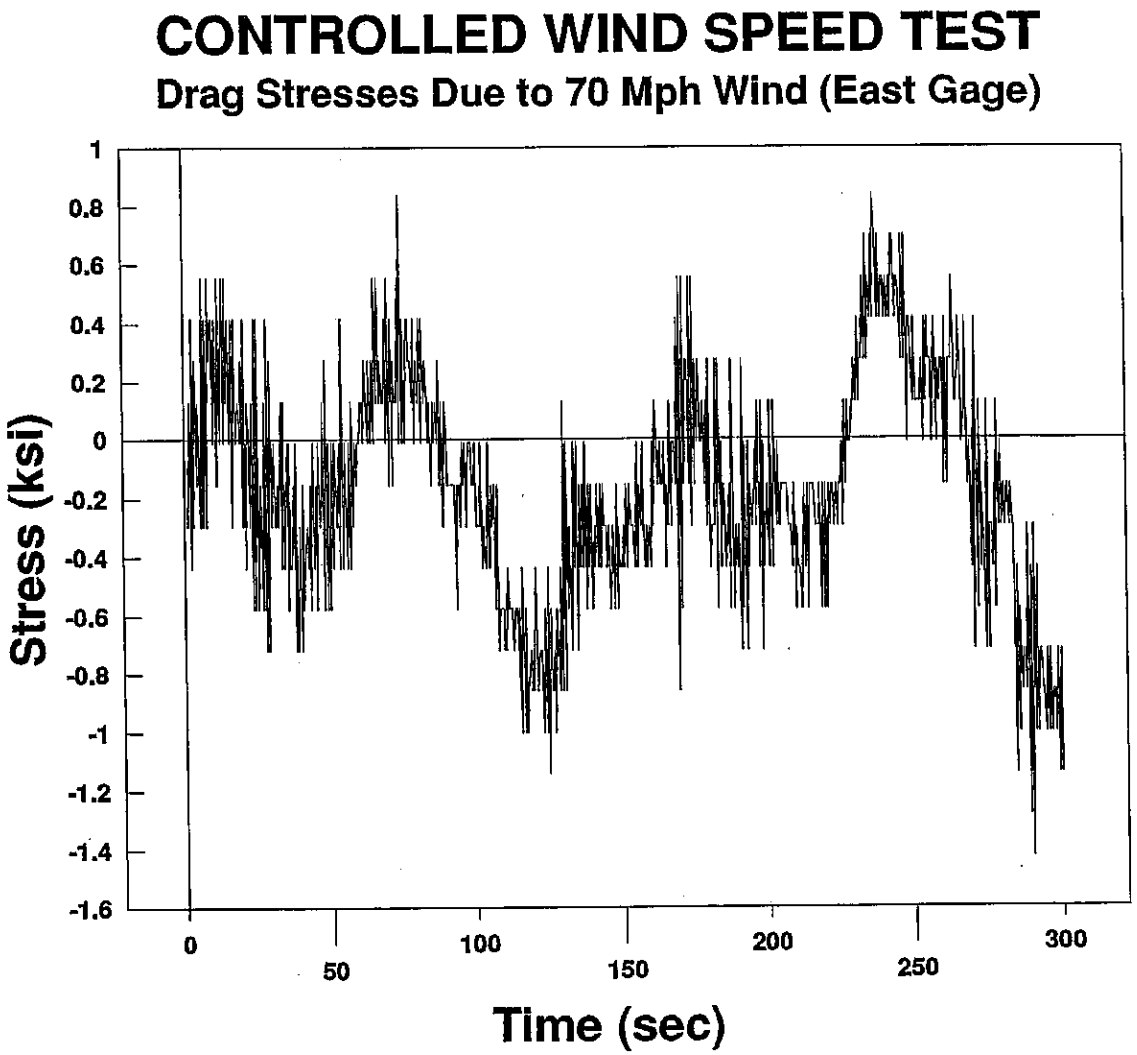

Figure 44. Drag stresses at east strain gage due to 70 mph (112.65 km/hr) controlled wind application.

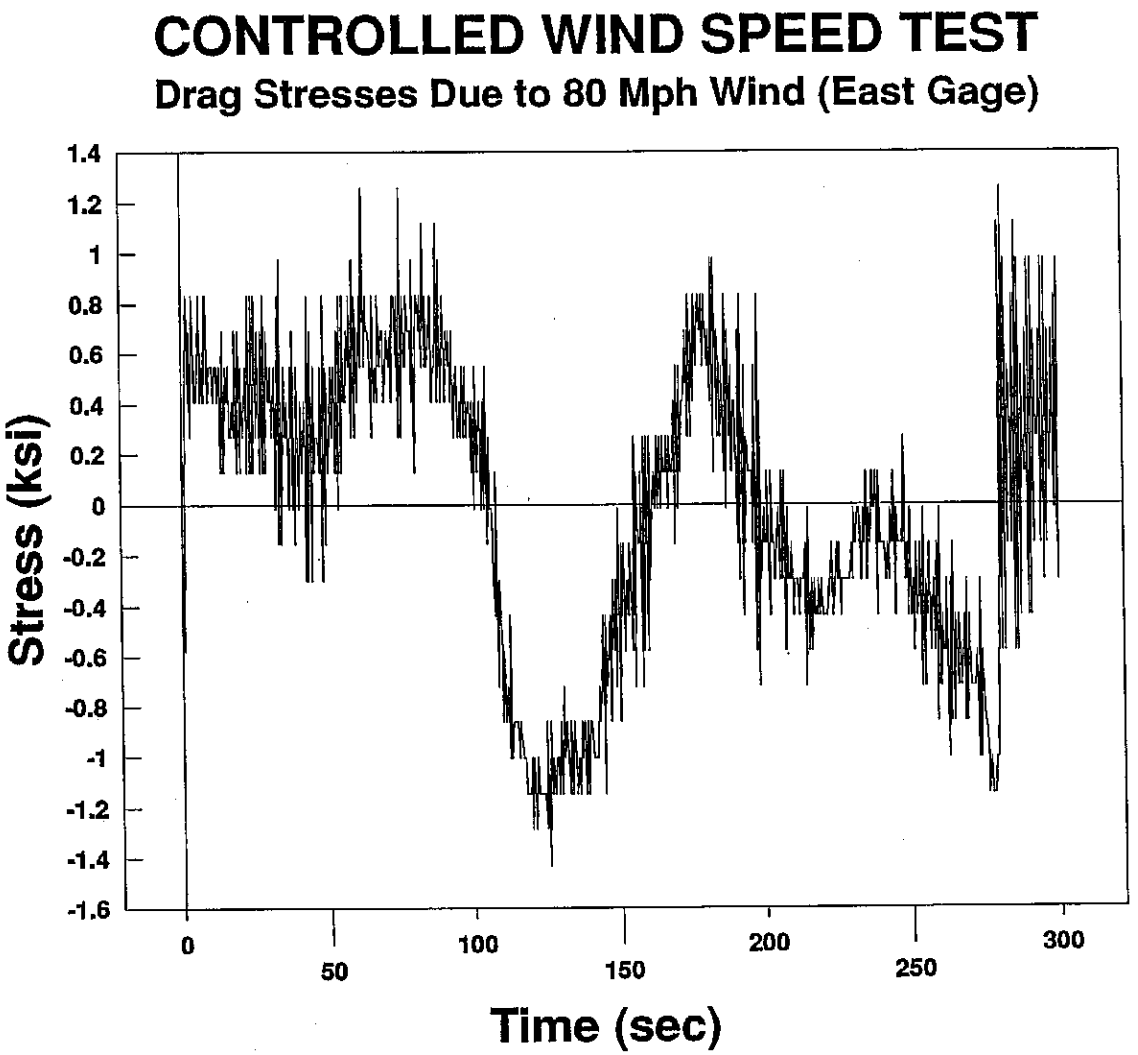

Figure 45. Drag stresses at east strain gage due to 80 mph (128.74 km/hr) controlled wind application.

TABLE 8

Apparent Drag Coefficient for In-Place Traffic Signal
Using Average Strain Data

Wind Speed (mph)*	Reynolds Number	Apparent Drag Coefficient (C_D)
20	9.3×10^5	0.86
40	1.8×10^6	0.33
50	2.3×10^6	0.32
60	2.8×10^6	0.25
70	3.2×10^6	0.31
80	3.7×10^6	0.24

*To convert to km/hr, multiply by 1.67.

Closure

This chapter presented data collected during the course of this research project for a common traffic signal structure. The structure was installed at the Physical Research Laboratory in Springfield, Illinois. Strain gages were mounted at weld details and inside anchor bolts. Data collection included stress range-frequency histograms for weld details at the mastarm-baseplate connection and the tension dead load anchor bolts; strains due to installation of the mastarm and traffic signals; strains as a function of vertical tip deflection; vibration frequency and amplitude due to wind loads; and weld strains as a function of controlled-velocity wind loads applied at the mastarm tip traffic signal.

The collected data showed some variability and uncertainty associated with experimental error, difficult experimental conditions, and differences between design assumptions and actual response. However, the strains measured were reasonable. Observation of the data indicates that welds and anchor bolts experience large numbers of stress cycles. The analysis of a tapered mastarm using a cantilevered tube of equivalent

stiffness produces conservative stress results. Experimental results revealed that the structure vibrated in synchronization with the first and second natural transverse modes during wind speeds of 12 - 20 mph (19.31 - 37. 19 kmph). The structural damping factor was measured to be 0.006, indicating light damping. The application of controlled winds to the structure showed that even constant wind speeds produce highly variable strain data. The reduction of the apparent drag coefficient of an in-place traffic signal as a function of Reynolds number was noted.

The nature of wind speed variability and the variable response of a wind-loaded structure indicate that the use of simple static analytical methods for fatigue analysis are subject to much uncertainty. Chapter 5 presents a discussion of fatigue and outlines a fatigue analysis method which utilizes experimental data.

5. DETERMINATION OF FATIGUE DAMAGE TO COMPONENTS

This chapter discusses calculation of fatigue damage. The histogram-linear damage method[21] is used to estimate fatigue damage and expected fatigue life.

Overview of Fatigue

Fatigue is a cumulative damage process caused by the repeated application of loads which results in cracking or rupture of components. The danger which fatigue presents is that failures can occur at applied stress levels much lower than the tensile strength of a given material. Fatigue may be divided into two domains in which failure is probably produced by different physical mechanisms. One domain, known as low-cycle fatigue, is characterized by the application of significant plastic strains during each load cycle. Low-cycle fatigue is associated with lives of less than about 10^4 cycles. The other domain is known as high-cycle fatigue. In this domain, cyclic strains are confined mostly to the elastic range and result in lives in excess of about 10^4 cycles.

The fatigue life of a component may also be considered in two phases. The portion of life which occurs before the appearance of a visible crack is known as the crack initiation life. The remaining life from crack initiation to unstable crack growth is known as the propagation life.

For practical purposes, especially for nonredundant components and the types of steels generally used for sign and signal structures, the crack propagation life of weld details is assumed to be a small fraction of the total life. This means that the appearance of a crack indicates that the effective fatigue life is used up. This report concentrates on high-cycle fatigue, with failure assumed to mean crack initiation.

There are many factors which can affect the fatigue life of a component. These factors include 1) material composition, 2) grain size and grain direction, 3) heat treatment, 4) welding, 5) geometrical discontinuities, 6) surface conditions, 7) size effects, 8) residual surface stresses, 9) corrosion, 10) fretting, and 11) mean stress effects. A discussion of most of these factors is beyond the scope of this report; however, geometrical discontinuities are discussed in a subsequent section. Mean stress effects are discussed in Chapter 7.

The various fatigue damage theories in use assume that the application of any cyclic stress amplitude will result in fatigue damage. The seriousness of the fatigue damage is related to the number of applied cycles at that stress amplitude and also to the total number of cycles needed to produce failure of an undamaged specimen at that stress amplitude. Fatigue damage is assumed to be permanent. Application of several different stress amplitudes results in the accumulation of total damage which is equal to the sum of the damage increments caused by each applied stress level. Failure is assumed when the total damage reaches a critical value. Many different fatigue damage theories exist. The first cumulative damage theory proposed was attributed to Palmgren[22] and Miner,[23] and is still in wide use. This report focuses on use of the Palmgren-Miner linear damage rule in combination with stress range-frequency histograms to quantify fatigue damage.

Quantification of Fatigue Damage

The Palmgren-Miner fatigue damage equation assumes a linear relationship between number of applied stress cycles and number of stress cycles to failure at each stress range. The ratio of applied to available cycles at each stress range quantifies the damage. The total damage is the sum of the damage fractions at each stress range. Failure is assumed

to occur when the total damage reaches unity. The relationship is shown below in equation form:

$$\sum_{i=1}^{N_t} \frac{n_{sri}}{N_{sri}} = 1 \qquad (13)$$

where n_{sri} = number of applied stress cycles at the ith stress range, ksi or MPa,

N_{sri} = number of available stress cycles at the ith stress range, ksi or MPa,

N_t = total number of stress ranges applied to component.

In order to determine the amount of fatigue damage suffered by a fatigue-prone detail, a stress range-frequency histogram must be available for the ambient stresses applied to that detail. In addition, the number of available cycles to failure at each stress level must be known. The American Welding Society (AWS) publishes conservative stress range versus frequency (S-N) curves for various categories of welded tubular connections.[24] This data may also be expressed as a family of N-S equations, where the number of cycles, N, is the dependent variable instead of stress range. The equation has the form:

$$N = C(S_r)^m \qquad (14)$$

where N = number of available stress cycles at stress range S_r,
C = fatigue strength coefficient,
m = fatigue strength exponent,
S_r = stress range, ksi.

Table 9 summarizes fatigue strength coefficients and exponents for various welded tubular steel details using the conservative data of AWS. Stress range must be in ksi.

Applied stress ranges and frequencies may be calculated analytically or measured experimentally. The total number of available cycles to failure at each stress range is calculated by equation (14), and the total damage is calculated by the Palmgrem-Miner linear damage equation (13).

TABLE 9

Fatigue Strength Coefficients and Exponents
for Various Welded Tubular Steel Details, AWS Data

Detail Description (Category)	Fatigue Coefficient, C	Fatigue Exponent, m
Plain, unwelded pipe (A)	8.299×10^{16}	-7.388
Pipe with longitudinal seam; butt splices, complete joint penetration groove welds, ground flush and inspected by RT or UT; members with continuously welded longitudinal stiffeners. (B)	4.906×10^{12}	-5.062
Butt splices, complete joint penetration groove welds, as welded (C_1); unreinforced cone-cylinder intersection (X_1); Intersecting members at simple T-, Y-, and K-connections; any connection whose adequacy is determined by accurate scale model tests or by theoretical analysis, with profile improved by a capping layer, or grinding (X_2).	1.499×10^{11}	-4.280
Members with transverse (ring) stiffeners (C_2); Intersecting members at simple T-, Y-, and K-connectors; any connection whose adequacy is determined by accurate scale model testing or by theoretical analysis (X_2).	2.329×10^{10}	-3.844
Members with miscellaneous attachments such as clips, brackets, etc., cruciform and T-joints with complete joint penetration welds (except at tubular connections) (D).	3.098×10^{9}	-3.400

TABLE 9 (Continued)

Detail Description (Category)	Fatigue Coefficient, C	Fatigue Exponent, m
Balanced cruciform and T-joints with partial joint penetration groove welds or fillet welds (except at tubular connections); members where doubler wrap, coverplates, longitudinal stiffeners, gusset plates, etc., terminate (except at tubular connections) (E).	$1.270X10^{9}$	-3.254
End weld of coverplate or doubler wrap; welds on gusset plates, stiffeners, etc., cruciform and T-joints, loaded in tension or bending, having filled on partial joint penetration-groove welds (except at tubular connections) (F).	$2.168X10^{13}$	-7.050
Connections designed as simple T-, Y-, or k-connections with complete joint penetration groove welds meeting prequalification requirements of AWS D1.1 - 84 Figure 10.13.1A (DT).	$9.148X10^{9}$	-4.691
Simple T-, Y-, and K-connections with partial joint penetration groove welds or fillet welds; complex tubular connections in which the punching shear capacity of the main member cannot carry the entire load and load transfer is accomplished by overlap, gusset plates, ring stiffeners, etc. (ET).	$1.003X10^{8}$	-3.393
Simple T-, Y-, or k-connections loaded in tension or bending, having fillet or partial joint penetrating groover welds (shear stress in welds) (FT).	$2.303X10^{11}$ (stress range less than 5.5 ksi [37.9 MPa])	-7.246
	$1.468X10^{9}$ (stress range greater than 5.5 ksi [37.9MPa])	-4.306

TABLE 9 (Continued)

Detail Description (Category)	Fatigue Coefficient, C	Fatigue Exponent, m
Simple T-, Y-, and k-connections in which the gamma ratio of main member does not exceed 24 (K_2).	$2.701X10^7$	-4.281
Same as above with profile improved per AWS D1.1-84 10.7.5 (K_1).	$6.276X10^7$	-4.397

*For more complete descriptions of these detail categories, see AWS D1.1-84 Table 10.7.3.

If the stress range-frequency histogram is calculated or measured for a year-long period, the expected fatigue life of the detail is simply calculated by:

$$L = \frac{1}{D} \qquad (15)$$

Where L = expected fatigue life of detail, years, and
D = total damage caused by stress range-frequency histogram.

One should be aware of the possible variation of wind speeds at a specific site from year to year. If a five-year histogram were constructed from local weather station data, the fatigue life estimation equation would return life (L) as the expected number of five-year loading blocks.

Anchor Bolts

Anchor bolts may also be analyzed for fatigue using the same basic N-S equation. Fatigue strength coefficients and exponents vary with material and type of fatigue test (i.e. notched or unnotched). Steels commonly used in anchor bolts have similar tensile and physical properties

to SAE 1020, 1035, and 1045 steels. Table 10 presents fatigue strength coefficients and exponents for various steels.

TABLE 10

Fatigue Strength Coefficients and Exponents for Some Steels

Description	Fatigue Coefficient, C	Fatigue Exponent, m
SAE 1020 HR Plate*	6.66×10^{19}	-8.33
SAE 1020, Circular Notch**	5.38×10^{19}	-9.76
SAE 1035, Circular Notch**	1.36×10^{21}	-10.26
SAE 1045, Kommers Notch** ($K_t = 5$)	5.22×10^{23}	-12.07

*Calculated from SAE Handbook J1099 (typical data).
**Grover, H., Gordon, S., Jackson, L., "Fatigue of Metals and Structures," Department of the Navy, 1960 (mean data).

Fracture Mechanics Methods

Methods of fatigue analysis which utilize fracture mechanics concepts are also available.[25] Hahin[26] accurately recreated a traffic signal mastarm failure using only wind speed and fracture mechanics data. The method used the Barsom equation for ferritic-pearlitic steels:[27]

$$\frac{da}{dn} = 3.6X10^{-10}(\Delta K_I)^3 \qquad (16)$$

Where $\Delta K_I = C_I \Delta\sigma\sqrt{\pi a}$,
σ = wind-induced stress,
a = instantaneous crack length,
C_I = 1.0 for initiating crack,
= 1.1 for through-thickness center crack,
da/dn = change in crack length in inches per stress cycle n.

The incremental crack growth induced by fluctuating wind speeds in excess of 10 mph (16.09 km/hr) was calculated using official wind speed data obtained from a local airport and an estimate of the fundamental

frequency. The incremental increase, da, was added to the existing crack length, a, and this new crack length was used in the equation above. A daily record of the crack length progression was constructed, and fatigue transition-to-overload was predicted with less than 12% error compared to the actual failure history.

The context of this application was a failure analysis. As such, the initial and final transition-to-overload (critical) crack lengths were known. The accuracy of fracture mechanics methods depends strongly on knowledge of initial defect size, and has a weaker dependence on critical crack size. The initial defect used in Hahin's analysis was a 2.54-inch (64.5 mm) long, 0.057-inch (1.45 mm) deep fingernail crack which was probably popped-in during erection of the structure. The structure failed catastrophically after five months of service. This rapid failure reinforces the assumption that most of the fatigue life of a weldment is taken up by the crack initiation process.

Stress Concentration Effects

The simple formulas used for stress calculations in design are based on constant or slowly varying member cross sections. When these conditions are not met, such as in the presence of shoulders, grooves, holes, threads, and other sharp discontinuities, the simple stress distributions are modified so that localized high stresses occur. The localization of high stresses is known as a stress concentration, and is measured by the stress concentration factor, defined as:

$$K_t = \sigma_{max}/\sigma_{nom} \qquad (17)$$

Where σ_{max} = maximum stress at region of interest, and
σ_{nom} = nominal stress in region of interest.

The subscript 't' indicates that the stress concentration factor is obtained from theoretical analysis, usually based on assumptions common in theory of elasticity (Hooke's law, homogeneity, etc.). Stress concentration factors are also obtained experimentally by means such as photoelasticity and precision strain gages. When experimental work is sufficiently precise, excellent agreement is obtained with well-established mathematical results.

The impact of stress concentrations on fatigue analysis is that nominal section stresses are magnified at sharp section changes by a factor that can range from 1.10 to about 10 in extreme cases. Because the histogram linear damage method uses stresses to calculate the number of available cycles, an underestimation of actual stress at the detail of interest will result in a higher number of available cycles. This results in a lower damage fraction for a given number of applied cycles and, consequently, a longer expected fatigue life.

The most common sites of stress concentration in overhead sign and signal supports are at welds and anchor bolts. Stress concentration factors for fillet welds may be estimated by treating the connection as a stepped round shaft in tension or bending with a certain fillet radius and by using appropriate published stress concentration curves. Anchor bolts may be considered as grooved shafts in tension. Several reference books, such as Peterson,[28] are available to quantify stress concentration factors for various geometries. Figures 46 and 47 show graphs of stress concentrations for the details mentioned above.

Current design specifications only address the issue of stress concentrations in the corners of poly-sided tubes. The influence of

stress concentrations in weld design is restricted to reference in notes 2, 3, and 4 of Table 10.7.3 in AWS D1.1-84 - Structural Welding Code, Steel, 1984. The stress concentration effect is predicted by theory and proven by experiment, and should be explicitly included in both static and fatigue analysis.

Closure

The discussion in this chapter shows how to quantify fatigue damage to a structural detail. The histogram-linear damage method is very straightforward to use and results in a rational fatigue damage analysis. There are no statistical parameters to evaluate, as in other fatigue analysis methods, so no accuracy is lost. The method is based on the Palmgren-Miner linear fatigue damage theory, with stress ranges and number of applied stress cycles supplied by a stress-range frequency histogram, and the number of available stress cycles calculated from published stress range-cycles to failure data. Individual damage fractions at each stress range are summed to quantify the total damage. If the histogram data represents one year of loading, the inverse of the total fatigue damage is the expected fatigue life of the detail in years. If the histogram data represents a multi-year load history, the inverse of the total fatigue damage is the expected fatigue life of the detail in terms of the multi-year blocks used. The remaining fatigue life is the expected life minus the number of years in service.

Stress concentration effects were discussed because of their influence on localization of fatigue damage and on fatigue life. Proper use of stress concentration factors in both static and fatigue design will result in an increased accuracy of the design, and also in increased fatigue life of the structure.

The following chapter uses the fatigue damage methods discussed here in a sample calculation.

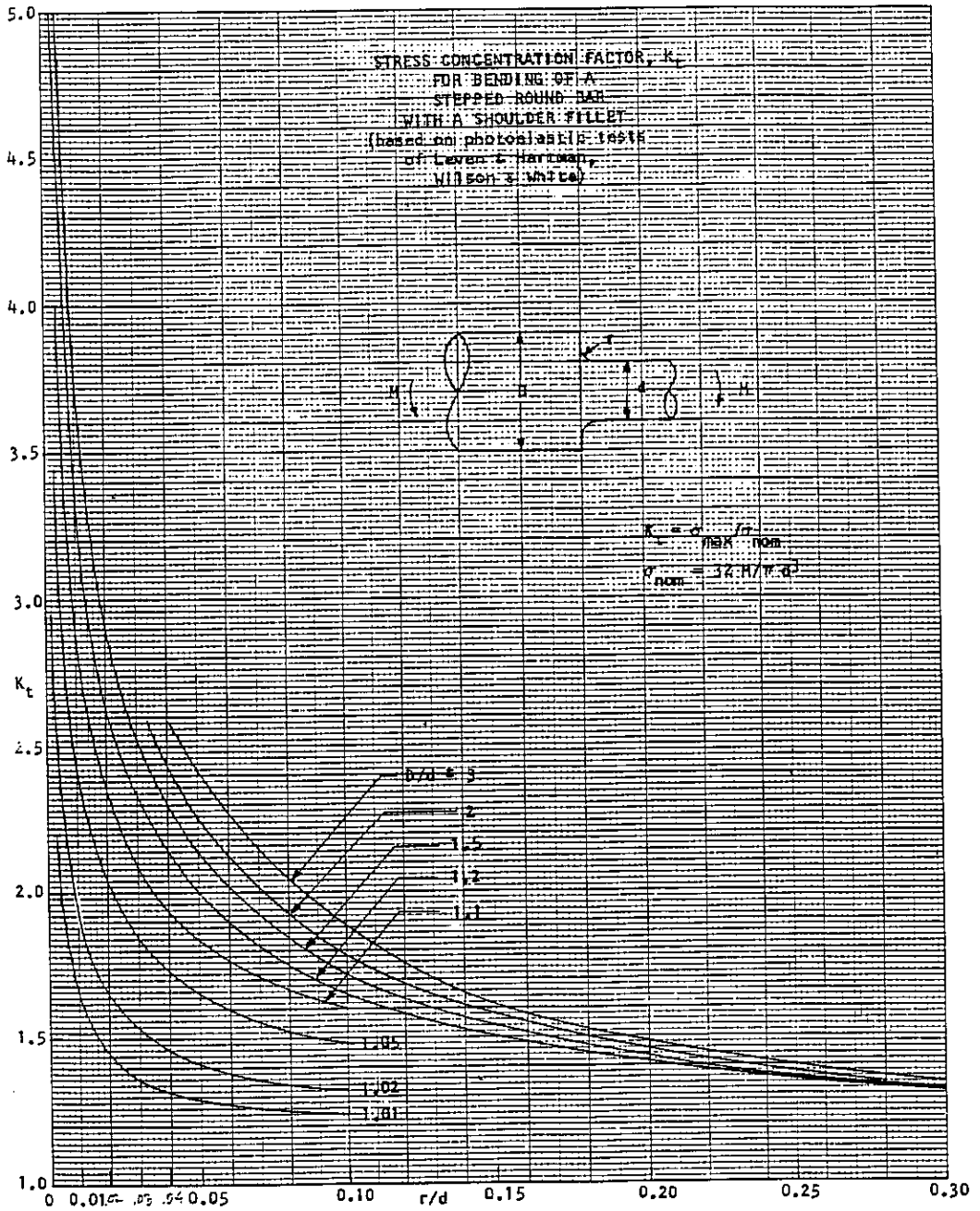

Figure 46. Stress concentration factor, K_t, for a stepped, round bar with a shoulder fillet in bending, from Peterson[28] (Stress Concentration Factors, R. E. Peterson, Wiley, New York, 1974. Reprinted by permission of John Wiley & Sons, Inc.)

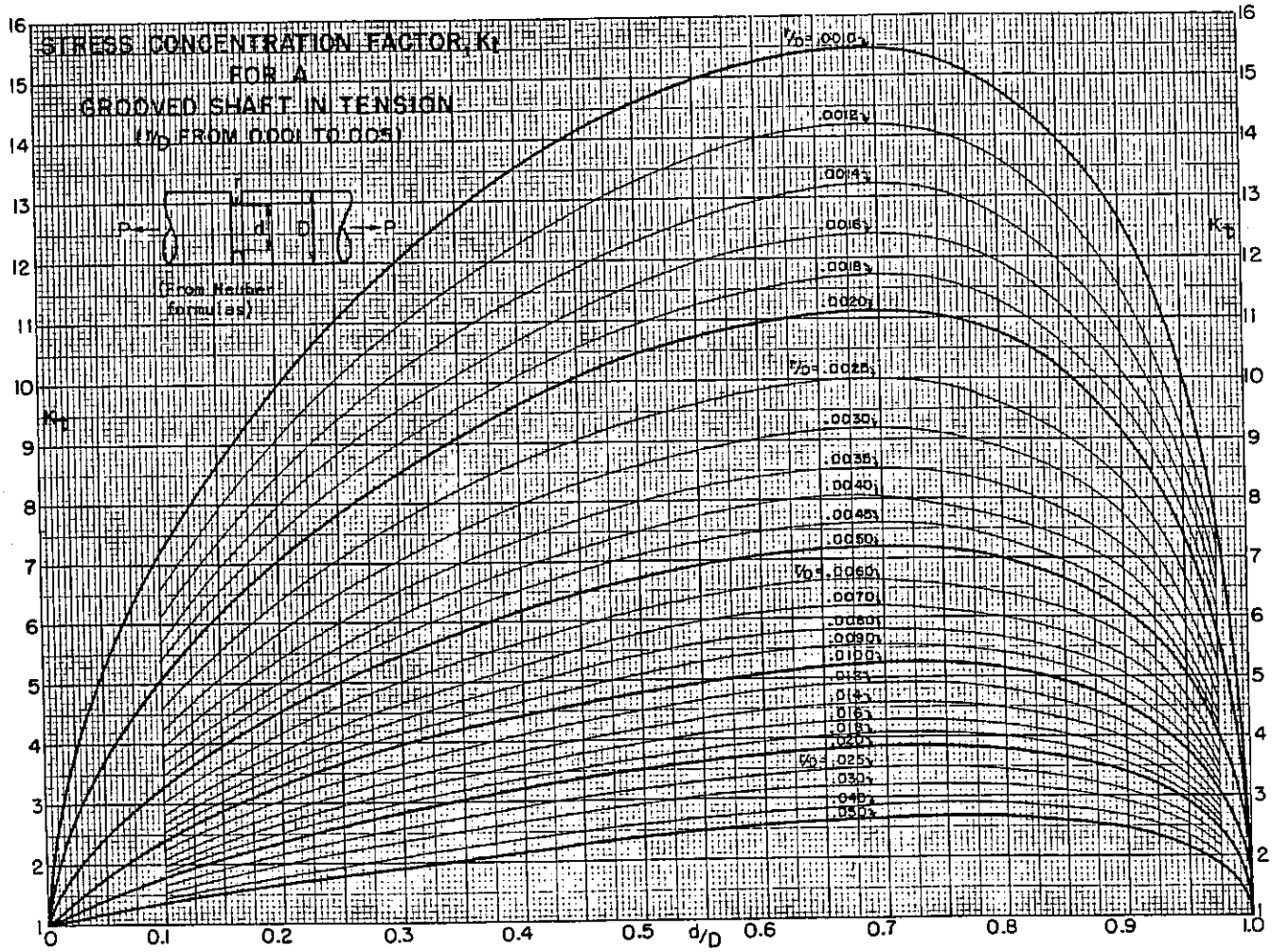

Figure 47. Stress concentration factor, K_t, for a grooved shaft in tension, from Peterson[28] (Stress Concentration Factors, R. E. Peterson, Wiley, New York, 1974. Reprinted by permission of John Wiley & Sons, Inc.)

6. SAMPLE FATIGUE DAMAGE ANALYSES USING BOTH STRAIN GAGE AND ANALYTICAL METHODS

The purpose of this chapter is to use the methods outlined in Chapters 2 and 5 to estimate the expected fatigue life of a particular example overhead traffic signal structure. This chapter is provided as an example to the reader, and should be considered as such.

The structure to be analyzed is a 44 foot long (13.41 m) traffic signal mastarm, the minimum (tip) diameter is four inches (101.6 mm), the maximum (at the weld) diameter is ten inches (254 mm). The detail to be analyzed is the fillet weld connecting the mastarm to the attachment plate. The fillet weld is assumed to be AWS category ET. This structure was shown in Figure 17. The strain gage histogram linear damage method is used first.

Analysis Using Strain Gage Histogram Data

The stress range-frequency data for Gage Two (Table 4a) are used to estimate the expected fatigue life of the weld detail. Since data were collected for four months, a reasonable estimated stress range-frequency histogram for a one year period is made by multiplying the number of cycles by three (3). The equation relating stress range to available number of cycles for a category ET weld detail is $N=1.003X10^{8}(S_r)^{-3.393}$. Calculations and results are given in Table 11.

TABLE 11
Expected Fatigue Damage Calculation for Traffic Signal Mastarm Using Strain Gage Data

Measured Stress Range (ksi)*	Applied Cycles for 1 year (n_{sri})**	Available cycles (N_{sri})	Damage Fraction (n_{sri}/N_{sri})
0.5	$8.103X10^{6}$	$1.054X10^{9}$	0.0077
1.0	$9.680X10^{5}$	$1.003X10^{8}$	0.0097
1.5	$1.090X10^{5}$	$2.534X10^{7}$	0.0043

TABLE 11 (Continued)

Measured Stress Range (ksi)*	Applied Cycles for 1 year (n_{sri})**	Available Cycles (N_{sri})	Damage Fraction (n_{sri}/N_{sri})
0.5	$8.103X10^6$	$1.054X10^9$	0.0077
2.5	$1.015X10^4$	$4.478X10^6$	0.0023
3.0	2538	$2.412X10^6$	0.0011
3.5	420	$1.430X10^6$	0.0003
4.0	393	$9.089X10^5$	0.0004
4.5	9285	$6.095X10^5$	0.0152
5.0	36	$4.263X10^5$	0.0001
5.5	66	$3.085X10^5$	0.0002
6.0	33	$2.296X10^5$	0.0001
6.5	21	$1.750X10^5$	0.0001
7.0	6	$1.361X10^5$	$4X10^{-5}$
7.5	6	$1.077X10^5$	$5X10^{-5}$
8.0	12	$8.652X10^4$	0.0001
8.5	3	$7.043X10^4$	$4X10^{-5}$
9.0	408	$5.802X10^4$	0.0007
9.5	3	$4.829X10^4$	$6X10^{-5}$
10.0	3	$4.058X10^4$	$7X10^{-5}$
11.0	6	$2.937X10^4$	0.0002
14.0	3	$1.296X10^4$	0.0002
		Total Damage (D) =	0.05066

*To convert to MPa, multiply by 6.895.
**Data from Table 4a, Gage 2, multiplied by 3 to approximate one year period.

The expected fatigue life of the detail is calculated by equation (15): L=1/D=1/0.05066=19.74 years. This correlates with many actual fatigue failures of light poles and highmast structures using weathering steel. It is interesting to note that 30% of the fatigue damage is caused by cycling at the 4.5 ksi (31.03 MPa) stress range. The procedures outlined above in Table 11 allow a direct, rapid quantification of fatigue damage for a given weld detail. Because actual measured stress ranges and frequencies were used in the calculations, the analysis is also as accurate as possible given the statistical nature of fatigue data. An estimate of the remaining fatigue life of the detail is obtained by subtracting the number of years of service from the expected life. This

estimate assumes that wind speeds do not vary markedly from year to year. The validity of such an assumption should be proved or disproved before the remaining fatigue life can be calculated with confidence.

Analysis Using Calculated Stress Histogram Data

The availability of a wind speed versus frequency histogram (Table 3) suggests a method by which expected fatigue life may be roughly estimated using the wind speed histogram, force calculation methods presented in Chapter 2, and the histogram-linear damage calculation methods shown in Chapter 5. The goal is to develop a stress range-frequency histogram using the analytical methods. A cylinder of equivalent stiffness is used. An equivalent cylinder is defined by the following relationships:[29]

$$D_e = \frac{D_{max} + D_{min}}{2} \qquad (18)$$

$$L_e = L\sqrt{\frac{2D_{min}}{D_{max} + D_{min}}}$$

Where D_e = equivalent diameter,
D_{max} = maximum diameter,
D_{min} = minimum diameter,
L_e = equivalent length,
L = original length.

The method proceeds as follows:

1. Calculate the vortex shedding frequency for each wind speed in the histogram using equation (2). This is the vibration frequency of the stucture at each wind speed.

2. Calculate drag forces for each wind speed using the flow chart presented in Figure 2.

3. Using the drag forces, calculate the applied stresses at the detail(s) of interest. Total force F equals F_D x L_e for each windspeed. Applied moment M equals F x $L_e/2$ at the weld. Nominal bending stress at the weld, σ_{nom} equals Mc/I. Maximum bending stress σ equals K_t x σ_{nom}.

4. Assume the counts in the histogram to be one-second intervals of constant wind speed application; then the histogram frequency represents the total number of seconds of application of a particular wind speed. Multiply the number of seconds by the vortex shedding frequency to estimate the total number of applied cycles at each wind speed for a year.

5. Use the results from steps 3 and 4 to construct a new histogram for each detail of interest. The result is a stress versus cycles-per-year histogram.

6. Use the histogram developed above in conjunction with the methods outlined in Chapter 5 to calculate the expected fatigue life of the detail(s) of interest.

Estimates of several parameters are needed in order to estimate the expected fatigue life analytically. These estimates are given in Table 12.

The first step in the analysis is to determine the wind speeds at which synchronization is expected. The results of this calculation are shown in Table 13. The criteria used for synchronization are $0.6 \leqq f_n/f_s \leqq 1.4$ and reduced damping (δ_r)<64.

Use the reduced damping (δ_r) from equation (8), the mode factors (γ) for each transverse vibration mode from Table 2, and the Strouhal Number (S) to calculate A_y/D for each mode using equation (10). Amplified drag coefficients are then calculated from equation (4).

One is now ready to calculate drag stresses due to each wind speed experienced. Results are shown in Table 14.

TABLE 12

Parameters Used For Analytical Fatigue Life Estimation

Equivalent pole diameter (D_e) = 0.583 ft. (0.178 m)
Equivalent pole length (L_e) = 33.25 ft. (10.13 m)
Wall thickness (t) = 0.20 in. (5.08 mm)
Elastic Modulus (E) = $30X10^6$ psi (207 GPa)
Moment of Inertia at Weld ($I=\pi R^3t$) = 24.7 $in.^4$ ($5.93X10^{-5}$ mm^4)
Fluid density (ρ) = 0.002378 $slug/ft^3$ ($9.85X10^{-4}$ kg/m^3)
Kinematic Viscosity (ν) = $1.564X10^{-4}$ $ft^2/sec.$ ($1.681X10^{-3}m^2/sec.$)
Structural Damping (ξ) = 0.006
Mass per unit length (m) = 0.449 slug/ft (21.49 kg/m)
Stress concentration factor (K_t) = 2.2
First transverse mode fundamental frequency (f_{n1}) = 1.705 Hz
Second transverse mode fundamental frequency (f_{n2}) = 10.66 Hz
Third transverse mode fundamental frequency (f_{n3}) = 29.87 Hz
Dimensionless mode factor (Y_1) = 1.305
Dimensionless mode factor (Y_2) = 1.499
Dimensionless mode factor (Y_3) = 1.537
Strouhal number (S) = 0.2
Reduced Damping (δ_r) = 34.9

TABLE 13
Wind Speeds at Which Synchronization is Expected

Wind Speed (mph)*	Reynolds Number**	Vortex Shedding Frequency (Hz)	f_{n1}/f_s***	f_{n2}/f_s***	f_{n3}/f_s***
1	$5.5X10^3$	0.5			
2	$1.1X10^4$	1.0			
3	$1.6X10^4$	1.5	1.14		
4	$2.2X10^4$	2.0	0.85		
5	$2.7X10^4$	2.5	0.68		
6	$3.3X10^4$	3.0			
7	$3.8X10^4$	3.5			
8	$4.4X10^4$	4.0			
9	$4.9X10^4$	4.5			
10	$5.5X10^4$	5.0			
11	$6.0X10^4$	5.5			
12	$6.6X10^4$	6.0			
13	$7.1X10^4$	6.5			
14	$7.7X10^4$	7.0			
15	$8.2X10^4$	7.5			
16	$8.7X10^4$	8.0		1.33	
17	$9.3X10^4$	8.5		1.25	

TABLE 13 (Continued)

Wind Speed (mph)*	Reynolds Number**	Vortex Shedding Frequency (Hz)	f_{n1}/f_s***	f_{n2}/fs***	f_{n3}/f_s***
18	$9.8X10^4$	9.0		1.18	
19	$1.04X10^5$	9.5		1.12	
20	$1.09X10^5$	10.0		1.07	
21	$1.15X10^5$	10.5		1.02	
22	$1.20X10^5$	11.0		0.97	
23	$1.26X10^5$	11.5		0.93	
24	$1.31X10^5$	12.0		0.89	
25	$1.37X10^5$	12.5		0.85	
26	$1.42X10^5$	13.0		0.82	
27	$1.48X10^5$	13.5		0.79	
28	$1.53X10^5$	14.0		0.76	
29	$1.59X10^5$	14.5		0.74	
30	$1.64X10^5$	15.0		0.71	
31	$1.70X10^5$	15.5		0.69	
32	$1.75X10^5$	16.0		0.67	
33	$1.80X10^5$	16.5		0.65	
34	$1.86X10^5$	17.0		0.63	
35	$1.91X10^5$	17.5		0.61	
36	$1.97X10^5$	18.0			
37	$2.02X10^5$	18.5			
38	$2.08X10^5$	19.0			
39	$2.13X10^5$	19.5			
40	$2.19X10^5$	20.0			
41	$2.24X10^5$	20.5			
42	$2.30X10^5$	21.0			
43	$2.35X10^5$	21.5			1.39
44	$2.41X10^5$	22.0			1.36
45	$2.46X10^5$	22.5			1.33
46	$2.52X10^5$	23.0			1.30
48	$2.62X10^5$	23.5			1.27
60	$3.28X10^5$	24.0			1.24

*To convert to km/hr, multiply by 1.67.
**Reynolds number is for the equivalent cylinder.
***Only those frequency ratios contained in the lock-in band are shown.

TABLE 14
Calculated Drag Stresses on Mastarm for Each Measured Wind Speed

Wind Speed (mph)*	Drag Coefficient (C'_D)	Total Force (lbs)**	Stress (ksi)***
1	1.12	0.06	0.003
2	1.12	0.22	0.014
3	1.21	0.54	0.034
4	1.21	0.96	0.060
5	1.21	1.51	0.094
6	1.12	2.00	0.125
7	1.12	2.72	0.170
8	1.12	3.56	0.221
9	1.12	4.50	0.280
10	1.12	5.56	0.346
11	1.12	6.72	0.419
12	1.12	8.00	0.498
13	1.12	9.39	0.585
14	1.12	10.89	0.678
15	1.12	12.51	0.778
16	1.23	15.58	0.970
17	1.23	17.59	1.094
18	1.23	19.72	1.227
19	1.23	21.97	1.367
20	1.23	24.35	1.515
21	1.23	26.84	1.670
22	1.23	29.46	1.833
23	1.23	32.12	2.003
24	1.23	35.06	2.181
25	1.23	38.04	2.367
26	1.23	41.14	2.560
27	1.23	44.37	2.761
28	1.23	47.72	2.969
29	1.23	51.19	3.185
30	1.23	54.78	3.408
31	1.23	58.49	3.639
32	1.23	62.32	3.878
33	1.23	66.28	4.124
34	1.23	70.36	4.378
35	1.23	74.56	4.639
36	1.12	78.88	4.908
37	1.12	83.32	5.185

TABLE 14 (Continued)

Wind Speed (mph)*	Drag Coefficient (C_D)	Total Force (lbs)*	Stress (ksi)***
38	1.12	87.89	5.469
39	1.12	92.57	5.760
40	1.12	97.38	6.059
41	1.12	102.31	6.366
42	1.12	107.36	6.681
43	1.23	112.54	7.002
44	1.23	117.83	7.332
45	1.23	123.25	7.669
46	1.23	128.79	8.014
48	1.23	140.23	8.726
60	1.23	219.11	13.634

*To convert to km/hr, multiply by 1.67.
**To convert pounds (lbs) to Newtons (N), multiply by 4.45.
***Stress values include estimated $K_t = 2.2$. To convert to MPa, multiply by 6.895.

The stresses due to each wind speed have now been calculated. Steps 1 through 3 of the analytical method outlined above are complete. Step 4 is concerned with relating the shedding frequency for each wind speed to the collected wind speed data. Results from Steps 4 through 6 are shown in Table 15.

TABLE 15
Expected Fatigue Damage Estimation Using Measured Wind Speed Data

Wind Speed (mph)*	Stress at Wind Speed (ksi)**	Stress Cycles Experienced (n_{sri})	Available Stress Cycles (N_{sri})	Damage Fraction (n_{sri}/N_{sri})
1	0.003	2358	$2.25X10^{16}$	$1.1X10^{-13}$
2	0.014	$2.35X10^{4}$	$2.03X10^{14}$	$1.2X10^{-10}$
3	0.034	$5.09X10^{4}$	$9.93X10^{12}$	$5.1X10^{-9}$
4	0.060	$8.38X10^{4}$	$1.41X10^{12}$	$6.0X10^{-8}$
5	0.094	$1.14X10^{5}$	$3.10X10^{11}$	$3.7X10^{-7}$
6	0.125	$1.40X10^{5}$	$1.19X10^{11}$	$1.2X10^{-6}$
7	0.170	$1.52X10^{5}$	$4.18X10^{10}$	$3.7X10^{-6}$
8	0.221	$1.62X10^{5}$	$1.68X10^{10}$	$9.7X10^{-6}$
9	0.280	$1.62X10^{5}$	$7.54X10^{9}$	$2.2X10^{-5}$
10	0.346	$1.54X10^{5}$	$3.67X10^{9}$	$4.2X10^{-5}$
11	0.419	$1.48X10^{5}$	$1.93X10^{9}$	$7.7X10^{-5}$
12	0.498	$1.34X10^{5}$	$1.07X10^{9}$	$1.3X10^{-4}$
13	0.585	$1.19X10^{5}$	$6.22X10^{8}$	$1.9X10^{-4}$
14	0.678	$1.06X10^{5}$	$3.77X10^{8}$	$2.8X10^{-4}$
15	0.778	$9.14X10^{4}$	$2.35X10^{8}$	$3.9X10^{-4}$
16	0.970	$7.87X10^{4}$	$1.11X10^{8}$	$7.1X10^{-4}$
17	1.094	$6.48X10^{4}$	$7.38X10^{7}$	$8.8X10^{-4}$
18	1.227	$5.39X10^{4}$	$5.01X10^{7}$	$1.1X10^{-3}$
19	1.367	$4.42X10^{4}$	$3.47X10^{7}$	$1.3X10^{-3}$

TABLE 15 (Continued)

Wind Speed (mph)*	Stress at Wind Speed (ksi)**	Stress Cycles Experienced (n_{sri})	Available Stress Cycles (N_{sri})	Damage Fraction (n_{sri}/N_{sri})
20	1.515	$3.39X10^4$	$2.45X10^7$	$1.4X10^{-3}$
21	1.670	$2.70X10^4$	$1.76X10^7$	$1.5X10^{-3}$
22	1.833	$2.12X10^4$	$1.28X10^7$	$1.7X10^{-3}$
23	2.003	$1.60X10^4$	$9.49X10^6$	$1.7X10^{-3}$
24	2.181	$1.29X10^4$	$7.11X10^6$	$1.8X10^{-3}$
25	2.367	9600	$5.39X10^6$	$1.8X10^{-3}$
26	2.560	7891	$4.13X10^6$	$1.9X10^{-3}$
27	2.761	5981	$3.20X10^6$	$1.9X10^{-3}$
28	2.969	4984	$2.50X10^6$	$2.0X10^{-3}$
29	3.185	4017	$1.97X10^6$	$2.0X10^{-3}$
30	3.408	2670	$1.56X10^6$	$1.7X10^{-3}$
31	3.639	1984	$1.25X10^6$	$1.6X10^{-3}$
32	3.878	1584	$1.01X10^6$	$1.6X10^{-3}$
33	4.124	1353	$8.19X10^5$	$1.7X10^{-3}$
34	4.378	1105	$6.69X10^5$	$1.7X10^{-3}$
35	4.639	788	$5.50X10^5$	$1.4X10^{-3}$
36	4.908	396	$4.54X10^5$	$8.7X10^{-4}$
37	5.185	278	$3.77X10^5$	$7.4X10^{-4}$
38	5.469	247	$3.15X10^5$	$7.9X10^{-4}$
39	5.760	156	$2.64X10^5$	$5.9X10^{-4}$
40	6.059	60	$2.22X10^5$	$2.7X10^{-4}$
41	6.366	103	$1.88X10^5$	$5.5X10^{-4}$
42	6.681	63	$1.59X10^5$	$4.0X10^{-4}$
43	7.002	43	$1.36X10^5$	$3.2X10^{-4}$
44	7.332	66	$1.16X10^5$	$5.7X10^{-4}$
45	7.669	23	$9.99X10^4$	$2.3X10^{-4}$
46	8.014	23	$8.60X10^4$	$2.7X10^{-4}$
48	8.726	24	$6.44X10^4$	$3.7X10^{-4}$
60	13.634	30	$1.42X10^4$	$2.1X10^{-4}$
			Total Damage =	0.04041

*To convert to km/hr, multiply by 1.67.
**To convert to MPa, multiply by 6.895.

The expected fatigue life is 24.75 years. Note that all of the significant damage was due to wind speeds between 16 and 27 mph (26.72 and 43.45 km/hr). These winds correspond to the high end of the subcritical Reynolds number range, and also to synchronized vibration with the second natural frequency. The amplification of drag coefficient resulted in higher stresses, and thus lower available cycles to failure. The number of stress cycles experienced, while not the maximum, were still on the order of 10^4 cycles. The combination led to significant fatigue damage.

Analysis Using AASHTO Formula

A fatigue analysis method which uses the static pressure equation (see equation [11]) was also investigated. In the AASHTO method, drag coefficient is a function of Reynolds number, and is a constant in this example until wind speeds of about 55 mph (91.85 kmph). The gust factor was not used. The same histogram developed for the wind speed data (which included synchronization effects) and the same value of K_t resulted in an expected fatigue life of 36.1 years. This life increases to 524 years without using K_t in the analysis. Neglecting the vortex shedding effect, and using only the first fundamental frequency to develop the histogram results in an expected fatigue life of 277.9 years. These results show that static methods overestimate the expected fatigue life of a given detail by a significant margin.

Closure

Sample calculations of fatigue damage and expected fatigue life using both collected stress range-frequency data and analytical estimates of wind-induced stresses were presented in this chapter. The analytical procedure overestimated the expected fatigue life by about

25 percent compared to the strain gage data method. Results from static force methods were presented. These estimates of expected fatigue life were much higher (less conservative) than those previously calculated. This an indication that static methods are unsuitable for fatigue analysis of overhead sign and signal structures. As stated in the chapter introduction, the calculations are provided as examples. Other stress analysis methods are available, the goal of any method used is to derive a reasonable stress range-frequency histogram for use in the damage calculation procedure.

7. FACTOR OF SAFETY EQUATIONS FOR FATIGUE DESIGN

The purpose of this chapter is to discuss factor of safety equations for fatigue loaded details. Factor of safety equations are commonly used in machine design. The purpose for calculating a factor of safety in the context of fatigue of weldments is to determine susceptibility to fatigue failure during the design of a welded structure.

Factor of safety equations relate applied and mean stresses to material properties, typically fatigue strength and either yield or ultimate tensile strength. The need to incorporate mean stress effects into a factor of safety for welds may be questioned by some researchers who note that residual stresses at the weld are unpredictable, but are generally assumed to be at or near material yield strength. Further loading would not increase local stresses significantly due to the plastic nature of the stress-strain response after yield.

However, welds are only part of a total structure. Cracks must generally grow into unwelded parts of a structure in order to produce rupture. Outside the heat affected zone, fatigue behavior is comparable to unwelded specimens. Mean stress does affect the fatigue life of unwelded specimens and, therefore, will influence overall structural safety.

Factor of Safety Equations

The Goodman, Soderberg or Gerber fatigue failure equations are commonly used to calculate the safety factor in engineering fatigue and machine design.[30] The Goodman equation is conservative and is the

most widely used. The Gerber equation most accurately represents actual experimental fatigue data. The Soderberg equation is highly conservative. The Goodman and Gerber equations are presented below:

$$\text{Goodman: } N = \frac{1}{\left[\frac{S_a}{S_e}\right] + \left[\frac{S_m}{S_u}\right]} \qquad (19)$$

$$\text{Gerber: } N = \frac{1}{\left[\frac{S_a}{S_e}\right] + \left[\frac{S_m}{S_u}\right]^2} \qquad (20)$$

Where N = Safety factor,
S_a = alternating stress amplitude,
S_m = mean stress
S_e = fatigue strength of a given number of cycles, and
S_u = minimum specified ultimate tensile strength.

Welded structure design codes use a fatigue strength category for various details and stress ranges instead of alternating stress amplitudes. Mean stress is a combination of live load and dead load stresses. The Gerber equation may be modified to incorporate the detail fatigue strength and the applied stress range:[31]

$$N = \frac{1}{\frac{S_{LL}}{F_d} + \left[\frac{(S_{LL}+2S_{DL})/2}{S_u}\right]^2} \qquad (21)$$

Where S_{LL} = live load stress range,
S_{DL} = dead load stress in weld,
F_d = fatigue strength of detail at $2X10^6$ or 10^7 cycles,
S_u = minimum tensile strength of the steel specified.

In this equation, the live load stress range replaces the alternating stress amplitude, the detail fatigue strength replaces fatigue strength, and the mean stress component is replaced by a combination of dead load and live load stresses. Emphasis is placed on the relationship between the live load stress range and the detail fatigue strength. The

squared term is related to the ambient dead load stress in the structure, and is a measure of the remaining elastic-plastic strain capacity. The squared term becomes significant when ambient stresses start to approach code-allowable stresses. The squared term is also significant when steels with lower notch plasticity such as ASTM A514, A588, or A572 are used or for lower strength steels like ASTM A36 when used at lower temperatures.

For design purposes, a safety factor range of 1.40–1.60 is recommended when using 50% mean fatigue data. This range takes material and load variations into account. A safety factor as low as 1.20 may be used when using the more conservative AWS fatigue category data. In either case, a calculated factor of safety less than 1.00 indicates serious potential fatigue problems.

Closure

The use of a factor of safety provides an important, useful tool for the designer. With it, an estimate of the fatigue susceptibility of a structural detail may be made during the design process. This allows a fatigue-prone detail to be modified before it is placed in service. This capability for explicitly quantifying the factor of safety is absent from current design codes and specifications. Appropriate use of a factor of safety for fatigue design will result in improved fatigue life of overhead sign and signal structures because of the explicit relationship defined between live load stress range and the fatigue strength of the detail under consideration.

8. SUMMARY

The main purpose of this report was to combine pertinent wind loading and vibration theory, fatigue damage theory, and experimental data into a useable fatigue analysis method for overhead sign and signal structures.

Vibrations and forces induced by vortex shedding were studied analytically and measured experimentally. The force analysis methods are complex and approximate because vortex shedding is an aerodynamic behavior. Drag coefficients, generally assumed to be constants or simple functions of Reynolds number, actually depend on the amplitude of vortex shedding vibration. This is an outcome of the dynamic interaction of the fluid and the structure. The amplification of drag coefficients can have a significant effect on resulting forces. Although the analysis can be complex, it is preferred to static methods for fatigue analysis purposes because of greater expected accuracy.

Fatigue and the concept of fatigue damage quantification were discussed. Fatigue was described as a failure mode which results from cyclic application of stresses which may be much lower than the yield stress. The failure process, although not completely understood, can be regarded as having two phases; crack initiation and crack propagation. For the materials and stresses generally expected in overhead sign and signal structures, the crack initiation phase dominates the fatigue life. Fatigue damage was quantified using the Palmgren-Miner linear damage equation. This equation relates applied stress cycles to available stress cycles for each stress range encountered by the detail. Applied stress cycles are estimated by creating a stress

range-frequency histrogram either by analytical process or by strain gage instrumentation of a detail in question. Available stress cycles for each applied stress range are calculated by expressing published S-N fatigue data for welds or anchor bolts as N-S equations, where number of available cycles (N) is the dependent variable, instead of stress range. The total damage is the sum of the ratios of applied stress cycles to available stress cycles. If the total damage is calculated for a year, the inverse of the damage is the expected fatigue life in years. The remaining life of an in-service structure is the difference between expected life and years in service. The use and limitations of fracture mechanics methods were discussed. Stress concentrations were discussed as a vital parameter in fatigue analysis. Methods for estimating K_t for fillet welds and anchor bolt threads were extracted from the literature.

Experimental data were collected for a representative traffic signal structure. This data included stress range and frequency response for ambient wind loadings, dead load stresses, strain as a function of vertical tip deflection, vibration frequency and amplitude due to ambient winds, and strain response due to controlled-speed wind loads. Strain gages were installed at tube to base plate circumferential fillet welds and anchor bolts.

Wind speed data was collected at a traffic signal site in Springfield, Illinois for over a year. Portions of this data were presented in both histrogram and random daily graph formats. Inspection of this data showed that structures are subjected to variable wind loadings, and are experiencing fatigue-type loadings.

Factor of safety equations were discussed because the use of such design tools will improve the fatigue life and design of welded structures.

Sample fatigue life calculations using both strain gage-derived and analytically estimated stress range-frequency histrograms were performed as an example to the reader. Calculations using static assumptions were also performed. The results differed significantly from the other solutions.

9. CONCLUSIONS AND RECOMMENDATIONS

Based on the work conducted for this study, the following conclusions are made:

1. The nature of the forces on a structure due to wind is very complex, and is heavily influenced by the vortex shedding process. This complexity excludes the use of simple static methods of stress analysis for fatigue analysis purposes.

2. Wind speeds at a particular site vary continuously. This variation, in conjunction with the vortex shedding process, produces cyclic loading of the structure. This cyclic loading causes fatigue damage.

3. Stress range-frequency data collected for a representative structure indicate that the structure experiences several million stress cycles per year.

4. The actual behavior of an in-place structure can vary markedly from expected behavior. In particular, the cantilever assumption was seen to be very conservative for traffic signal mastarms.

5. Controlled-speed wind load testing showed that even constant velocity winds produce variable behavior.

6. The apparent drag coefficient of an in-place traffic signal decreases with increasing Reynolds number, similar to the behavior of a cylinder.

7. The histogram-linear damage method of computing fatigue damage is a quick, straightforward way to estimate expected fatigue life of a detail.

8. The analytical methods presented here, when used to build a stress range-frequency histogram from actual wind speed data, produce estimates of expected fatigue life which compare well to estimates calculated from experimental stress range-frequency data.

9. A comparison of the expected fatigue lives computed using static assumptions to the "dynamic methods" shown here indicated that the static methods considerably overestimate the expected fatigue life of a detail, and are thus non-conservative.

10. Although the examples considered a simple traffic signal structure, the fatigue analysis method is useable for any welded steel detail defined by AWS D1.1-84.

In addition, the following recommendations are made:

1. Factor of safety equations should be used by the designer to determine the susceptibility of design details to fatigue damage.

2. Because of the large difference between initiation life and propagation life of weld details, non-redundant structures located in areas of high winds, and which have working cracks, should be repaired or replaced quickly. Also, extreme care should be exercised during erection of such components in order to avoid "popping in" a crack.

3. The fatigue analysis methods should mainly be used for structures which are subjected to relatively larger proportions of higher wind speeds. Structures with long cantilevers should be analyzed carefully, since the length of cantilever affects both the vibration characteristics and the applied moment.

4. Structure Inspectors should pay particularly careful attention to welds in high stress areas. In welded traffic signal structures, this includes both mastarm to connection plate welds or other weld details which connect mastarm to standard, and standard to anchor plate welds. For overhead structures, fatigue critical weld details include welds in the middle one-third of simply supported space trusses and any areas which experience cantilever-type bending moments.

5. Major overhead sign and signal structures should be instrumented in the future 1) to determine their life span, 2) to identify fatigue susceptible designs and connections, and 3) to gather wind speed data for various locations which are remote from airports or weather stations.

REFERENCES

1. "Standard Specifications for Structural Supports for Highway Signs, Luminaires, and Traffic Signals", American Association of State Highway and Transportation Officials, Washington, D.C., 1985, p. 9.

2. Blevins, R., "Flow-Induced Vibrations", 2nd edition, Van Nostrand Reinhold, New York, 1990.

3. Blevins, p. 43.

4. Blevins, p. 45.

5. Blevins, p. 46.

6. Roshko, A., "On the Drag and Vortex Shedding Frequency of Two-Dimensional Bluff Bodies", National Advisory Committee for Aeronautics Report NACA TM 3159, 1954.

7. Roshko, A., "Experiments on the Flow Past a Circular Cylinder at Very High Reynolds Number", Journal of Fluid Mechanics, 10, 1961, pp. 345-356.

8. Griffin, D.M., "Universal Similarity in the Wakes of Stationary and Vibrating Bluff Structures", Journal of Fluids Engineering, 103, 1981, pp. 52-58.

9. Sarpkaya, T., "Vortex-Induced Oscillations", Journal of Applied Mechanics, 46, 1979, pp. 241-258.

10. Blevins, p. 51.

11. Blevins, p. 54.

12. Blevins, p. 56-58.

13. Blevins, p. 59.

14. Blevins, p. 63.

15. Blevins, p. 63.

16. Blevins, p. 72.

17. "Standard Specifications for Structural Supports for Highway Signs, Luminaires, and Traffic Signals", p. 10.

18. Blevins, p. 76.

19. "Standard Specifications for Structural Supports for Highway Signs, Luminaries, and Traffic Signals," p. 9.

20. "Mechanical Engineers' Handbook," Wiley, New York, 1968, p. 1525.

21. Hahin, C., South, J., "Accurate and Rapid Determination of Fatigue Damage in Bridge Superstructures," Physical Research Report Number 106, Illinois Dept. of Transportation, 1992.

References (Continued)

22. Palmgren, A., "Durability of Ball Bearings," 2DVDI, Vol. 68, No. 14, 1924, pp. 339-341 (in German).

23. Miner, M. A., "Cumulative Damage in Fatigue," Trans. ASME, J. Appl. Mech., Vol. 67, 1945, pp. A159-A164.

24. "Structural Welding Code - Steel", 8th edition, American Welding Safety, Inc., Miami, FL., ANSI/AWS D1.1-84, p. 167.

25. Barsom, J., Rolfe, S., "Fracture and Fatigue Control in Structures," 2nd edition, Prentice-Hall Inc., Englewood Cliffs, New Jersey, 1987.

26. Hahin, C., "Fatigue of Large Traffic Signal Structures", Illinois Department of Transportation, 1988, p. 7.

27. Barsom and Rolfe, p. 290.

28. Peterson, R. E., "Stress Concentration Factors," Wiley, New York, 1974.

29. "Standard Specifications for Structural Supports for Highway Signs, Luminaires, and Traffic Signals," p. 44.

20. Fuchs, H., Stephens, R., "Metal Fatigue in Engineering," Wiley, New York, 1980, p. 72.

31. Hahin and South, p. 46.